UNIVERSITY OF TRENTO - Italy

Department of Civil, Environmental and Mechanical Engineering

Doctoral School in Civil, Environmental and Mechanical Engineering

Curriculum "Modelling and Simulation" - XXXI cycle - 2016/2018

Doctoral Thesis – April 2019

Rocco di Filippo

Numerical and experimental methods for seismic risk assessment of civil and industrial structures

Supervisor

Prof. Oreste S. Bursi, University of Trento, Italy

To my family

Salus populi suprema lex esto.

Let the safety of the people be the highest law.

Marcus Tullius Cicero

ACKNOWLEDGMENTS

ABSTRACT

Due to high seismic vulnerability and severity of possible failure consequences, petrochemical installations are often considered as "special risk" plants. Although tanks, pipes, elbows and bolted flanges have been a major concern in terms of seismic design, generally, they have not been analysed with modern performance-based procedures. This thesis will explore some important themes in seismic risk assessment with a special focus on petrochemical plants and components.

In the first part of the thesis the case study of a probabilistic seismic demand analysis (PSDA) for a Refrigerated liquefied gas (RLG) subplant is presented. As a matter of fact, RLG terminals that are part of strategic facilities must be able to withstand extreme earthquakes. In detail, a liquefied natural gas (LNG, ethylene) terminal consists of a series of process facilities connected by pipelines of various sizes. In this study, the seismic performance of pipes, elbows and bolted flanges is assessed, and seismic fragility functions are presented within the performance-based earthquake engineering framework. Particular attention is paid to component resistance to leakage and loss of containment (LoC) even though several different limit states are investigated. The LNG tank, support structures and pipework, including elbows and flanges, are analysed with a detailed 3D finite element model. For this purpose, a mechanical model of bolted flange joints is developed, able to predict the leakage limit state, based on experimental data. A significant effort is also devoted to identification of a leakage limit state for piping elbows, and the level of hoop plastic strain was found to be an indicator.

The second part of the thesis describes an innovative methodology to evaluate seismic performances of a realistic tank-piping system with special focus on LoC from piping elbows. This methodology relies on a set of experimental dynamic tests performed throughout hybrid simulations where the steel storage tank is numerically modelled while, conversely, the physical substructure encompasses the coupled piping network. Besides, ground motions for dynamic tests are synthetized based on a stochastic ground motion model whose input parameters are derived from the results provided by a seismic hazard analysis. Then, based on output data from the experimental tests, both a high-fidelity and a low-fidelity FE model are calibrated. Furthermore, these models are used to run additional seismic analyses using a large set of synthetic ground motions. Moreover, in order to derive

the seismic response directly from inputs parameters of the stochastic ground motions model, the procedure to build a hierarchical kriging surrogate model of the tank-piping system is presented. Eventually, the surrogate model can be adopted to perform a seismic fragility analysis.

Along with the line of probabilistic analysis, another contribution to this research work is a probabilistic seismic demand model (PSDM) of a steel-concrete composite structure made of a novel type of high-strength steel moment resisting frame. According to the main topic of this thesis, the procedure that is here presented can be used either in a seismic risk assessment or a fully probabilistic performance-based earthquake engineering (PBEE) framework. In detail a 3D probabilistic seismic demand analysis was performed considering the variability of the earthquake incident angle, generally not taken in account in typical fragility analyses. Therefore, the fragility curves evaluated following this approach account for the uncertainty of both the seismic action and its direction.

PUBLICATIONS

As a result of the work conducted by the author during his years of doctorate, the following publications have been produced:

Journal publications

- Bursi, O. S.; **di Filippo, R**.; La Salandra, V.; Pedot, Reza, Md S, "Probabilistic seismic analysis of an LNG subplant", (2018), Pages 45-60, Risk Analysis in Process Industries: State-of-the-art and the Future, Edited by Genserik Reniers, Ankur Pariyani, Volume 53, Pages 1-148 (May 2018)

- **di Filippo R,** Abbiati G., Broccardo M., Abdallah I., Bursi O.S., "Seismic fragility assessment of a tank-piping system based on hybrid simulation and multi-fidelity modelling", Bulletin of Earthquake Engineering. In preparation.

- Tondini N., Zanon G., Pucinotti R., **di Filippo R**., Bursi O.S., "Seismic Performance and Fragility Functions Of A 3d Steel-Concrete Composite Structure Made Of High-Strength Steel", (2018), Engineering Structures, Volume 174, 1 November 2018, Pages 373-383.

Conference proceeding publications

- **di Filippo R**., Abbiati G., Sayginer O., Covi P., Bursi O.S., Paolacci F., "Numerical surrogate model of a coupled tank-piping system for seismic fragility analysis with synthetic ground motions", 2019, Proceedings of the ASME 2019 Pressure Vessels and Piping Conference, PVP2019, July 14-19, 2019, San Antonio, Texas, US. Under review.

- Pedot M., **di Filippo R**., Bursi O.S., "A Seismic Vulnerability Analysis of a Liquefied Natural Gas Subplant", (2018), Proceedings of the ASME 2018 Pressure Vessels and Piping Conference, PVP2018, July 15-20, 2018, Prague, Czech Republic

- V. La Salandra; **R. di Filippo;** O.S. Bursi; F. Paolacci; S. Alessandri, "Cyclic Response of Enhanced Bolted Flange Joints for Piping Systems" in Proceedings of the ASME 2016 Pressure Vessels & Piping Conference PVP. PVP2016, Vancouver, British Columbia, Canada, July 17-21, 2016

- G. Abbiati; O.S. Bursi; L. Caracoglia; **R. di Filippo;** V. La Salandra, "Probabilistic Seismic Response of Coupled Tank-Piping Systems" in Proceedings of the ASME 2016 Pressure Vessels & Piping Conference. PVP 2016, Vancouver, British Columbia, Canada, July 17-21, 2016

Contents

List of Abbreviations			
BFJ	Bolted flange joint	NPP	Nuclear power plant
CDF	Cumulative distribution function	NS	Numerical substructure
C_{LS}	Capacity limit state	OBE	Operating based earthquake
COV	Coefficient of variation	PBEE	Performance-based earthquake engineering
DM	Damage measure	PDF	Probability distribution function
DoF	Degree of freedom	PGA	Peak ground acceleration
DV	Decision variables	PGD	Peak ground displacement
EDP	Engineering demand parameter	PGV	Peak ground velocity
FE	Finite element	PRA	Probabilistic risk assessment
HF	High fidelity	PS	Physical substructure
HS	Hybrid Simulator	PSDA	Probabilistic seismic demand analysis
IDA	Incremental dynamic analysis	PSDM	Probabilistic seismic demand model
IM	Intensity measure	PSHA	Probabilistic seismic hazard analysis
IRF	Impulse response function	RLG	Refrigerated liquefied gas
LF	Low fidelity	R	Epicentral Distance
LNG	Liquified natural gas	SLS	Service limit state
LOC	Loss of containment	SSE	Safe shut-down earthquake
M	Magnitude	TES	Twice elastic slope
MCSs	Monte Carlo simulations	ULS	Ultimate limit state
MSA	Multi-Stripe analysis		

Introduction

Background and motivation

Industrial facilities like chemical, oil and gas plants can trigger severe environmental and human consequences when subjected to seismic action. Moreover, such consequences are not always limited to the facilities themselves but possibly affecting nearby communities, infrastructures and plants. As a matter of fact, earthquakes can cause exceptional human and economic losses in the case of natural-technological, or NaTech events (Cruz et al., 2006 and Steinberg, et al., 2008). Some recent examples of such events are petrochemical plant fires during the Izmint earthquake of 1999 (Sezen et al., 2006), environmental chemical contaminations following the Sichuan earthquake of 2008 (Krausmann et al., 2010) and the nuclear and radiation accident caused by the 2011 Fukushima earthquake (Lypscy et al., 2013).

In order to prevent the serious consequences of NaTech events, the European directive Seveso-III (Directive 2012/18/EU) explicitly states that safety reports for industrial plants involving hazardous substances should include "detailed description of the possible major-accident scenarios and their probability or the conditions under which they occur". The methodology of performance-based earthquake engineering (PBEE) can compute the probability of failure under seismic action and it is generally applied to quantify seismic risk of nuclear power plants. However, this framework is not so commonly adopted for petrochemical plants. This can be explained considering the several challenges that PBEE carries when applied to such facilities, such the high computational resources needed, several sources of uncertainties, the development of capable finite element models and the adoption of reliable experimental data. This thesis presents numerical and experimental methods to address the aforementioned issues together with their relevant application to realistic case studies.

The first part of the thesis presents a seismic risk assessment of a Liquified Natural Gas (LNG) plant carried out in the Performance-Based Earthquake Engineering (PBEE) framework. Refrigerated liquefied gas (RLG) terminals represent strategic infrastructure for energy supplies all over the world. They play an important role in the overall energy cycle, as their main purpose is to store and distribute RLG. For storage and transport by trains, ships and pipelines, natural gas like ethylene is liquefied. This is achieved by compression and cooling to low temperature. For these reasons, liquefied natural gas LNG terminals usually consist of a port and transport infrastructure, with all the systems related to both liquefaction and regasificationTogether with a clear strategic importance, LNG plants also carry a significant risk related to possible consequences of incidents caused by natural events. Moreover, leakage of hazardous or polluting substances can badly affect the local environment. The resulting hazard was evaluated in different situations by means of case studies (Cozzani et al. 2014, Baesi et al. 2013, and Young et al. 2005). The considerable variability of seismic events and the related domino effects were partly taken into account

in the overall hazard estimation by the application of complex methodologies (Campedel et al., 2008 and Antonioni et. al., 2007). Nevertheless, historic data shows that earthquakes can lead to severe losses due to the failure of different components of industrial plants; in this respect see Lanzano et al., (2015) and Krausmann et. al (2010). An industrial plant typically has many structural and mechanical components, with different resistance thresholds and different failure behaviours. One of the most dangerous failure effects is loss of containment (LOC) or leakage, which can lead to explosion, fire and environmental damage. An LNG plant includes a number of component types that can experience leakage, under certain conditions of stress and strain caused by a seismic event. Common vulnerable components of LNG pipelines are bolted flange joints (BFJs) and piping bends or elbows. With respect to BFJs, current European technical standards, like EN 1591-1,2 (2009), do not have tools to predict leakage. Moreover, studies whether focusing on leak-before-break, i.e. that concentrate on the steady growth of through-cracks in pipes (Xie, 1998) or tracing the plastic behaviour of elbows (Li and Mackenzie, 2006), do not predict leakage thresholds. To fill this gap, a practical predictive model based on EN 1591 (2009) was developed by La Salandra et al. (2016), also using experimental data found by Reza et al. (2014). As far as a probabilistic approach is concerned, the risk estimation of leakage events is usually based on historic evidence found in databases; for a review, see Barros da Cunha (2016). In order to quantify induced seismic risk in an LNG plant, a seismic Probabilistic Risk Assessment (PRA) approach suggested by IAEA (2009) for nuclear power plants (NPPs) is available. The procedure is as follows: i) Seismic hazard analysis; ii) Fragility analysis; iii) System analysis and consequence evaluation. The outcome of a seismic PRA includes seismic hazard of the site, the structural capacity of structures and equipment, incorporation of uncertainties in seismic hazard, structural fragility and response of components. Hoseyni at al., (2014) applied a variant of this approach to take into account soil-structure interaction effects. However, this approach is not directly applicable to (non-nuclear) LNG plants, because data on aleatory randomness and epistemic uncertainties in the capacity of LNG components is not available. As a viable alternative, to rationally quantify the seismic performance of civil facilities, the PBEE methodology has been proposed (Cornell and Krawinkler, 2000). Some examples of application of the PBEE approach can be found in civil engineering literature (Yang et al., 2009, Tondini and Stojadinovic, 2012). Along this line, application of the PBEE approach to petrochemical piping systems by means of codes can be found in Bursi et al. (2015a). Moreover, some applications based on the determination of fragility curves are available for piping systems of NPPs (Firoozabad et al., 2015) and boil-off gas compressors at LNG terminals (Park and Lee, 2015). In both cases, limit states related to leakage were not considered or quantified. Conversely, the selection of engineering demand parameters (EDPs) and corresponding damage levels for piping systems and tanks was carried out by Vathi et al. (2015). Nonetheless, a fragility analysis also requires the analysis of the effects of different intensity measures, e.g. peak ground acceleration (PGA), on the dispersion characteristics of a probabilistic seismic demand model. To the author's knowledge, this analysis has not yet been carried out for LNG plants.

The second part of the thesis presents a numerical and experimental procedure to perform seismic risk assessment of industrial system. Industrial plants can experience different types

of structural and non-structural failures when subjected to the effects of natural disasters, possibly resulting in Natech events (Cruz et. al, 2006 and Steinberg et al., 2008). Among natural disasters, earthquakes can badly affect industrial facilities causing severe damage and losses, as documented by Lanzano et al., (2015), and Krausmann et. al, (2010). For this reason, the European directive Seveso-III (Directive 2012/18/EU) demands the evaluation of the probability of Natech events for industrial plants that involve hazardous substances. In order to asses this type of probability two different actions are generally required: i) select the dangerous possible consequences associated to different types of failure, ii) evaluate the relevant probabilities of these failures related to the several possible causes. As a matter of fact, industrial plants often encompass numerous components with different associated risks and overall resistances to external actions. One of these components are pipelines, commonly adopted in petrochemical facilities and demonstrated to be vulnerable to seismic action. Among realistic failure scenarios, leakage or loss of containment (LoC) of hazardous substances is one of the possible effects of pipelines failure and can severely affect the environment and the nearby communities. Along with this line, this chapter investigates the seismic performances of a realistic piping network coupled to a steel tank with a special focus on LOC from bolted flange joints (BFJs), Tee joints and pipe bends, see for references, among others, Bursi et al, (2018). In this respect, seismic risk can be evaluated by means of fragility curves, see Baker, (2015), as a part of performance-based earthquake engineering (PBEE) methodology (Cornell and Krawinkler, 2000). In detail, a fragility curve can express the probability of exceedance of an engineering demand parameter (EDP) given - conditional- an intensity measure (IM). With reference to piping elbows, EDPs and relevant LOC limit states are selected after Vathi et al., (2015) and Pedot et al., (2018). Arguably, fragility curves and so the whole PBEE approach are affected by two main sources of uncertainty, i.e. ergodic and non-ergodic (Der Kiureghian, 2005). This categorization is useful in the case of time-variant reliability, see Der Kiureghian and Ditlevsen, 2009, where the categories of aleatory and epistemic uncertainty can be further classified. As a matter of fact, seismic action is an important source of aleatory uncertainty in seismic reliability evaluation. However, under the common hypothesis that both the occurrence and the intensity of earthquakes can be described by a Poisson process, this aleatory uncertainty is renewed at each seismic event. On the other hand, non-ergodic uncertainty is comprehensive of both aleatory uncertainties, as soil-structure interaction, and epistemic uncertainties, derived for model errors and approximations. Specifically, the variability of the seismic action and its characterization by the IM represents an ergodic uncertainty, and, for this reason, the more samples are involved, e.g. seismic records and relevant seismic response, the more accuracy we achieve. Nevertheless, it is not possible to increase the number of natural seismic record without scaling them and possibly involving additional errors; see for reference, among others, Bommer (2004) and Luco, (2007b). In this manuscript, we propose a methodology to address both ergodic and non-ergodic uncertainties. In detail, the epistemic part of non-ergodic uncertainty is managed with the support of experimental data obtained by means of components cyclic testing (La Salandra et al., 2016) and hybrid simulation on the system under study. As a matter of fact, Hybrid simulation (HS) is an effective technique to experimentally investigate the behaviour of structural systems not easily adaptable to

common testing laboratories. Specifically, the hybrid model of the system under study combines numerical (NSs) and physical substructures (PSs). Thus, the application of this approach to the coupled tank-piping system, being the steel tank the NS and the piping network the PS as showed in Abbiati et al., (2018a) is presented. Moreover, the testing campaigns provide the necessary background to properly calibrate FE models that represent the computational simulator (CS). In particular, two different CSs are presented, a refined high-fidelity (HF) FEM and a faster low-fidelity (LF) one

Conversely, we reduce the ergodic uncertainty with the implementation of synthetic ground motions based on the results of a site-specific probabilistic seismic hazard analysis (PSHA; Baker, 2008). In detail we calibrated the stochastic ground motion model as defined by Rezaeian and Der Kiureghian (2010) against a set of natural accelerograms compatible with the abovementioned PSHA. Furthermore, the space of the ground motion model parameters is reduced by means of a global sensitivity analysis (GSA) over the simulated coupled system response, see for reference Abbiati et al., (2015). In order to reduce the computational cost of the GSA, the polynomial chaos expansion (PCE, Xiu et al, 2002) is adopted to provide a surrogate model of the system response. Along this line, Sobol' indices (Sobol, 1993) are evaluated by post-processing PCE coefficients; see for reference Efron et al. (2006).

As another step of the procedure, the Kriging method is used to build a Multi-Fidelity (MF) surrogate model (Han and Görtz, 2012 and Abbiati et al., 2015) based on both the CS and HS results. Finally, the MF surrogate model of the coupled tank-piping system is adopted to perform a seismic fragility analysis with a cheap computational cost.

The last part of the thesis encompasses a seismic fragility analyses of a steel-concrete composite structure made of high-strength steel. In the last years, there has been a growing trend in the use of high-strength steel (HSS) in tubular structures thanks to the publication of EN1993-1-12, 2007, that extended the use of structural steel up to grades S690Q/S700MC. Nonetheless, EN1993-1-12 imposes many limitations at the material, structural and design level due to the limited knowledge of its actual behaviour. The use of HSS can be advantageous in seismic design when employing the capacity design philosophy for non-dissipative elements owing to its inherent overstrength. Thus, columns in moment-resisting frames (MRFs) designed in HSS and beams in mild steel can represent an effective solution for structures located in moderate seismic prone zones, when the limitation of lateral displacements is not dominant.

In the last fifteen years, the adoption of the probabilistic PBEE methodology has become popular (Cornell et al., 2000) and the availability of seismic fragility functions of a particular structural typology or components is fundamental both for risk assessment and/or a probabilistic PBEE application (Cornell and Krawinkler, 2000). Thus, the choice of interstorey drift ratio as global EDP can directly be assumed as a damage measure (DM)), see Cornell and Krawinkler, 2000. In this respect, the Hazus database, FEMA 2013, already contains a number of fragility functions for various structural typologies and components. However, if the structural typology/component is new, they have to be determined. The

computation of seismic fragility curves typically requires several nonlinear dynamic analyses with seismic input representative of the structure site. Due to the aleatory nature of ground motions a set of accelerograms has to be selected among: (1) artificial waveforms; (2) simulated accelerograms; and (3) natural records (Iervolino et al, 2008, and Bommer, 2004). for this analysis natural records are adopted. Generally, in design practice when plan regularity criteria are met, simplified 2D structural analyses are performed , as stated in EN1998-1, 2004. Conversely, when a non-symmetric irregular structure is examined, the dynamic behaviour becomes more complex and coupling between the two main directions owing to torsional effects is likely to occur; as a result, a more complex 3D model is required (Iervolino et al, 2008). Moreover, when a structure is made of two different lateral-force resisting systems in the two main directions, due to sensitive differences in dynamic properties the dynamic response of the whole system is less straightforward to predict. In fact, an increased dynamic complexity reduces considerably the intuitive understanding of structural response. As a result, for structures with a certain degree of irregularity or characterized by different lateral resisting systems in both directions, as composite structures, a separate analysis along the two main building directions may not suffice to accurately capture the dynamic behaviour; thus, a 3D analysis is needed.

The application of two horizontal components along the main building directions may not lead to the most unfavourable case, because the influence of the incidence angle of a seismic event can be significant. However, the analysis is rarely performed considering a variation of the incident angle of seismic motion. Works related to this topic were carried out by a few researchers. In detail, In detail, Lagaros, 2010a, proposed a procedure for performing multicomponent incremental dynamic analysis (MIDA) by taking into account incident angle. In particular, in accordance with MIDA, a sample of N pairs of record-incident angles was generated through the LHS method. Along this line, Sozonov et al., 2014, performed a probabilistic seismic demand analysis that relied on the cloud analysis method; it entailed the selection of a ground motion scenario representative of the Italian territory sorted according to magnitude and distance from the epicentre. The incident angle of the seismic event was deterministically considered with variations between 0 and 180 degrees.

Scope

In order to carry out a probabilistic seismic analysis for a real process plant, the first part of the thesis presents the application of the fully probabilistic PBEE approach to an LNG plant having a piping system coupled to a support structure and a relevant LNG tank. More precisely, limit states and engineering demand parameters related to damage of piping components, i.e. BFJs and elbows, are defined. Furthermore, among different damage levels, the correlation between the probability of leakage and the IM of the seismic event represented by the PGA and the spectral acceleration (Sa(T)) is evaluated. These correlations are then represented by the mean of fragility curves adopting the Cloud Analysis method (Baker, 2015).

The second part of the thesis focuses on the seismic risk assessment of petrochemical industrial plants. The PBEE methodology is affected by two main sources of uncertainties, ergodic, related to seismic action randomness, and non-ergodic, associated to errors and approximations in physical models. In order to cope with these issues, the authors present a rigorous procedure for deriving fragility curves of structural components based on multi-fidelity structural simulators calibrated against hybrid testing experiments and a stochastic model of the seismic input calibrated against real records. In particular, the seismic fragility analysis concerns a realistic tank-piping system with a special attention on LoC from vulnerable components.

The last part of the thesis shows a methodology to cope with the variability of the seismic action incident angle. In fact, even though numerous studies have dealt with the probabilistic seismic demand of structures subject to seismic loading, a few publications have been devoted to: i) analyses of representative realistic buildings characterized by different lateral-force resisting systems; ii) analyses that include input uncertainties, also in terms of earthquake incident angle. All together, they represent basic issues that are explored hereinafter. In detail, the aim is to provide seismic fragility functions to be used in a full PBEE framework of a 3D steel-concrete composite structure made of a novel type of high strength steel moment resisting frame in one direction and reinforced concrete shear walls in the other. They were set for the probability of exceeding an interstorey drift ratio equal to 1% -associated with the damage limit state (DLS)-, and the probability of exceeding an interstorey drift of 5% -associated with the collapse prevention limit state (CLS)- given different IMs, e.g. peak ground displacement. These fragility curves will serve as a means for practitioners to probabilistically assess/design structures made of this novel type of moment resisting frame. Moreover, it gives insight into the 3D dynamic performance and the influence of the earthquake incident angle on this structure that is representative of a realistic office building.

Structure of the thesis

This thesis it is organized as a collection of three journal publications which summarize the main research outcomes of the author. A brief summary of the relevant three chapters follows:

- Chapter 1 includes the publication titled "Probabilistic Seismic Analysis of an LNG Subplant". The manuscript analyses the seismic performance of a liquefied natural gas (ethylene) terminal, consisting in a series of process facilities connected by pipelines of various sizes, within the performance-based earthquake engineering framework. Particular attention is paid to component resistance to leakage and loss of containment even though several different limit states are investigated. The LNG tank, support structures and pipework, including elbows and flanges, are analysed with a detailed 3D finite element model. For this purpose, a novel mechanical model to predict the leakage limit state of generic BFJs is developed. Given the complexity of the FE model of the LNG plant, the Cloud method for probabilistic seismic

demand analysis is selected, due to its advantages in terms of consistency in the seismic input and of computational savings. In particular, in order to develop fragility curves of critical components such as elbows and BFJs, a set of 36 ground motions from a database of historic earthquake accelerations is selected and used for a series of nonlinear time history analyses.

- Chapter 2 includes the publication titled: "Seismic fragility assessment of a tank-piping system based on hybrid simulation and multi-fidelity modelling". This manuscript presents a seismic reliability analysis of a coupled tank-piping system. The novelty of this methodology lies in the implementation of artificial accelerograms, finite element models and experimental hybrid simulations to compute an accurate and fast surrogate meta-model of our coupled system. As the first step, to obtain the necessary input for a stochastic ground motion model able to generate synthetic ground motions coherent with the site-specific analysis, a disaggregation analysis of the seismic hazard is performed. Hence, the space of parameters of the stochastic ground motion model is reduced by means of an extensive global sensitivity analysis upon the seismic response of our system, evaluated with a simplified Matlab FEM. Based on the reduced space of parameters, a large set of artificial waveforms is so generated and, among them, a few signals to provide the input for experimental hybrid simulations are selected. In detail, the hybrid simulator is composed by a numerical substructure, able to predict the seismic sliding response of a steel tank, and a physical substructure made of a realistic piping network. Furthermore, these experimental results are used to calibrate a refined Ansys FEM with a special focus on the most vulnerable components, i.e. pipe bends More precisely, a special attention is given to tensile hoop strains in elbow pipes as a leading cause for leakage, monitoring them with conventional strain. Thus, we present the procedure to evaluate a numerical Kriging meta-model of the coupled system based on both experimental and finite element model results. This model will be adopted in a future development to carry out a seismic fragility analysis.

- Chapter 3 includes the publication titled "Seismic performance and fragility functions of a 3d steel-concrete composite structure made of high-strength steel". This manuscript provides insight into a probabilistic seismic demand analysis of a steel-concrete composite structure made of a novel type of high-strength steel moment resisting frame, to be used either in a seismic risk assessment or a fully probabilistic PBEE framework. Moreover, due to the dynamic complexity of the examined structure caused by irregularity in elevation and different lateral-force resisting systems in the two main directions -moment resisting frames and concrete shear walls- the seismic behaviour is not straightforward to foresee. Therefore, two separate 2D analyses along the building main directions may not suffice to identify the actual dynamic response and, consequently, a 3D comprehensive probabilistic seismic demand analysis is performed by taking into account the earthquake incident angle. A multiple incremental dynamic analysis is carried out with two groups of bespoke accelerograms characterized, on one hand, by large magnitude and large distance and, on the other hand, by near-source effects. The earthquake incidence

angle is also considered and, to decrease the number of simulations, the accelerogram-incident angle pairs are selected by means of the Latin hypercube sampling (LHS) method. The relevant seismic analyses highlight the need to include the incident angle to better characterise its dynamic behaviour. Hence, the seismic fragility functions are evaluated both for damage and collapse limit states considering both the maximum interstorey drift ratio as engineering demand parameter and different intensity measures as well as the incident angle randomness

Chapter 1

1. Probabilistic Seismic Analysis of an LNG Subplant

Abstract

Refrigerated liquefied gas (RLG) terminals that are part of lifeline facilities must be able to withstand extreme earthquakes. A liquefied natural gas (LNG, ethylene) terminal consists of a series of process facilities connected by pipelines of various sizes. Although tanks, pipes, elbows and bolted flanges have been a major concern in terms of seismic design, generally, they have not been analysed with modern performance-based procedures. In this study, the seismic performance of pipes, elbows and bolted flanges is analysed and seismic fragility functions are presented within the performance-based earthquake engineering framework. Particular attention was paid to component resistance to leakage and loss of containment even though several different limit states were investigated. The LNG tank, support structures and pipework, including elbows and flanges, were analysed with a detailed 3D finite element model. For this purpose, we developed a mechanical model of bolted flange joints, able to predict the leakage limit state, based on experimental data. A significant effort was also devoted to identification of a leakage limit state for piping elbows, and we found the level of hoop plastic strain to be an indicator. Given the complexity of the FE model of the LNG plant, we selected the Cloud method for probabilistic seismic demand analysis, due to its advantages in terms of consistency in the seismic input and of computational savings. Then, using a series of nonlinear time history analyses, we studied the behaviour of critical components such as elbows and bolted flange joints. In order to develop fragility curves, we selected a set of 36 ground motions from a database of historic earthquake accelerations. The results of seismic analysis show that bolted flange joints remain significantly below their leakage threshold whilst elbows at the top of the LNG tank are likely to show leakage. Moreover, fragility functions were computed, based on a linear regression approach, and we deduce that elbows located on the tank platform are relatively unsafe against earthquakes. Finally, the estimated probability of loss of containment was above the probability associated with ultimate limit states involved in structural Eurocodes.

1.1 Introduction

1.1.1 Background and Motivation

RLG terminals represent strategic infrastructure for energy supplies all over the world. They play an important role in the overall energy cycle, as their main purpose is to store and distribute RLG. For storage and transport by trains, ships and pipelines, natural gas like ethylene is liquefied. This is achieved by compression and cooling to low temperature. For

these reasons, liquefied natural gas LNG terminals usually consist of a port and transport infrastructure, with all the systems related to both liquefaction and regasification, as shown in Fig. 1. In this respect, LNG handles 10% of the global energy supply with 28 LNG terminals in Europe (GIE LNG Map, 2015).

Together with a clear strategic importance, LNG plants also carry a significant risk related to possible consequences of incidents caused by natural events. The Na-tech risk is a central aspect in different types of petrochemical plants due to possible damage to other nearby plant and communities, or to those who rely on them for energy or other needs. Moreover, leakage of hazardous or polluting substances can badly affect the local environment. The resulting hazard has been evaluated in different situations by means of case studies (Cozzani et al. 2014, Baesi et al. 2013, and Young et al. 2005). The considerable variability of seismic events and the related domino effects have been partly taken into account in the overall hazard estimation by the application of complex methodologies (Campedel et al., 2008 and Antonioni et. al., 2007). Nevertheless, historic data shows that earthquakes can lead to severe losses due to the failure of different components of industrial plants; in this respect see Lanzano et al., (2015) and Krausmann et. al (2010).

An industrial plant typically has many structural and mechanical components, with different resistance thresholds and different failure behaviours. One of the most dangerous failure effects is loss of containment (LOC) or leakage, which can lead to explosion, fire and environmental damage. An LNG plant includes a number of component types that can experience leakage, under certain conditions of stress and strain caused by a seismic event. Common vulnerable components of LNG pipelines are bolted flange joints (BFJs) and piping bends or elbows. With respect to BFJs, current European regulations, like EN 1591-1,2 (2009), do not have tools to predict leakage. Moreover, studies whether focusing on leak-before-break, i.e. that concentrate on the steady growth of through-cracks in pipes (Xie, 1998) or tracing the plastic behaviour of elbows (Li and Mackenzie, 2006), do not predict leakage thresholds. To fill this gap, a practical predictive model based on EN 1591 (2009) was developed by La Salandra et al. (2016), also using experimental data found by Reza et al. (2014). As far as a probabilistic approach is concerned, the risk estimation of leakage events is usually based on historic evidence found in databases; for a review, see Barros da Cunha (2016).

In order to quantify induced seismic risk in an LNG plant, a seismic Probabilistic Risk Assessment (PRA) approach suggested by IAEA (2009) for nuclear power plants (NPPs) is available. The procedure is as follows: i) Seismic hazard analysis; ii) Fragility analysis; iii) System analysis and consequence evaluation. The outcome of a seismic PRA includes seismic hazard of the site, the structural capacity of structures and equipment, incorporation of uncertainties in seismic hazard, structural fragility and response of components. Hoseyni at al., (2014) applied a variant of this approach to take into account soil-structure interaction effects. However, this approach is not directly applicable to (non-nuclear) LNG plants, because data on aleatory randomness and epistemic uncertainties in the capacity of LNG components is not available.

11

As a viable alternative, to rationally quantify the seismic performance of civil facilities, the Performance-Based Earthquake Engineering (PBEE) methodology has been proposed (Cornell and Krawinkler, 2000). This probabilistic framework is based on the prediction of structural behaviour under realistic seismic loadings that the structural system is likely to experience in its reference life. It is based on the combination of different quantities, such as seismic hazard, structural response, level of damage, and repair costs after cyclic loading.

Some examples of application of the PBEE approach can be found in civil engineering literature (Yang et al., 2009, Tondini and Stojadinovic, 2012). Along this line, application of the PBEE approach to petrochemical piping systems by means of codes can be found in Bursi et al. (2015a). Moreover, some applications based on the determination of fragility curves are available for piping systems of NPPs (Firoozabad et al., 2015) and boil-off gas compressors at LNG terminals (Park and Lee, 2015). In both cases, limit states related to leakage were not considered or quantified. Conversely, the selection of engineering demand parameters (EDPs) and corresponding damage levels for piping systems and tanks was carried out by Vathi et al. (2015). Nonetheless, a fragility analysis requires also the analysis of the effects of different intensity measures, e.g. peak ground acceleration (PGA), on the dispersion characteristics of a probabilistic seismic demand model. To the authors' knowledge, this analysis has not yet been carried out for LNG plants.

1.1.2   Scope

On these premises, this manuscript presents the application of the fully probabilistic PBEE approach to an LNG plant having a piping system coupled to a support structure and a relevant LNG tank. More precisely, we define limit states and engineering demand parameters related to damage of piping components, i.e. BFJs and elbows. Moreover, among different damage levels, we calculate the correlation between the probability of leakage and the IM of the seismic event represented by the PGA and the spectral acceleration (Sa(T)). We represent these by the mean of fragility curves adopting the Cloud Analysis method (Baker, 2015).

For clarity, the manuscript is organized as follows: Section 3.2 presents the methodology for the application of the PBEE method. A description of the LNG plant and the main components modelled by means of finite elements (FEs) is contained in Section 3.3. Section 3.4 presents a simple component-based mechanical model able to predict leakage of BFJs and a methodology to evaluate seismic performances of piping elbows. Successively, Section 3.5 presents a 3D non-linear stick model of the LNG terminal, fully developed in the ANSYS environment (ANSYS, 2015). This FE global model allows for evaluation of the seismic response of structural components of the plant by means of a non-linear analysis presented in Section 3.6. Thus, the demand model of the main components of the piping system is investigated in the spirit of the PBEE method. Finally, Section 3.7 draws the main conclusions and future perspectives.

Figure 1.1 Refrigerated liquefied gas plant overview

1.2 Performance-based earthquake engineering procedure

The PBEE procedure was mainly developed by the Pacific Earthquake Engineering Research (PEER) Center and estimates the probabilistic future seismic performance of buildings and bridges in terms of system-level decision variables (DVs), i.e., performance measures that are meaningful to the owner, such as repair cost, casualties, and loss of use - dollars, casualties and downtime-. It is based on four quantities:

•   Intensity Measure (*IM*), which represents a measure of the ground motion intensity. Several *IM* variables are available, such as PGA, Spectral Acceleration at the fundamental period (Sa(T)), etc.;

•   Engineering Demand Parameter (EDP), which describes the structural response in terms of global and local parameters such as deformation, forces, etc;

•   Damage Measure (DM), which identifies the most significant structural damage conditions;

•   Decision Variable (DV), which transforms the damage conditions into useful quantities for the risk management decision process.

Let's denote *G(x/y)=Pr(x<X/Y=y)* the complimentary cumulative distribution function of the considered variables and d*G(x/y)* the derivative of the conditional complementary cumulative distribution function, which is identical to the negative of the conditional probability density function. The evaluation of the mean annual rate λ of *DV* exceeding the threshold *dv* reads,

$$\lambda(dv < DV) = \int_{im} G(dv|im) \, |d\lambda(im)| \tag{1.1}$$

where the conditional probability $G(dv|im)$ can be obtained by use of total probability (Yang et al., 2009) as follows,

$$G(dv|im) = \int_{dm} \int_{edp} G(dv|im)dG(dm|edp)\, dG(edp|im) \qquad (1.2)$$

Substituting (1.2) in (1.1), we obtain the mean annual rate of a decision variable DV exceeding a threshold value *dv,*

$$\lambda(dv < DV) = \int_{im} \int_{dm} \int_{edp} G(dv|im)dG(dm|edp)dG(edp|im)\,|d\lambda(im)| \qquad (1.3)$$

It is evident that Equation (1.3) encompasses four components of performance assessment. Specifically, the quantification of *λ(im)* requires a site hazard analysis, usually performed by a probabilistic seismic demand analysis (PSDA); *G(edp|im)* needs a response analysis, usually performed by using numerical techniques, e.g. Cloud analysis, *G(dm|edp)* requires a damage analysis often based on experiments whilst *G(dv|dm)* requires cost-effective or loss analysis (Cornell and Krawinkler, 2000). Moreover, the quantification of Equation (1.3) requires a fully probabilistic approach. Given the scarcity of data, at this stage of the research, only the probability of exceeding of a certain *edp* will be quantified in Section 1.6. For this purpose, the following relationship is adopted:

$$P(edp) = \int_{im} P(EDP > edp|im)|d\lambda(im)|$$
$$= \int_{im} P(D > C_{LS}|IM = im)|\lambda(im)dim| \qquad (1.4)$$

where we introduce the structural demand *D* and C_{LS} , i.e. the capacity of the component/system associated with a prescribed limit state.

1.3 LNG Plant
1.3.1   Introduction

The case study investigated in this manuscript reproduces a realistic RLG plant, depicted in Fig. 1.1 and 1.2, i.e. the Case Study #2 analysed in the European research project INDUSE-2-SAFETY (Bursi et al., 2016b). Originally, this plant was designed for low seismic lateral loads; in stark contrast, in order to acquire additional information on the plant performance for extreme lateral loadings, we considered the LNG plant located in a high seismic-prone area of Priolo Gargallo in Sicily, in the south of Italy. The hazard curve for this site is depicted in Fig. 1.3 and was calculated within the activities of INDUSE-2-SAFETY (Bursi et al., 2015b). The main component of the plant is a 50 000 m^3 ethylene tank that supplies the LNG to the different process areas via a stainless-steel piping system.
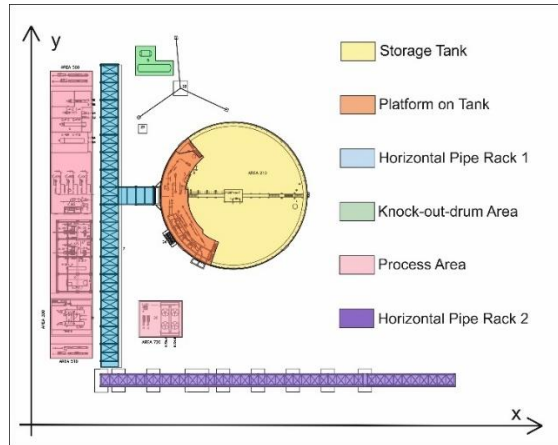
Figure 1.2 LNG plant layout
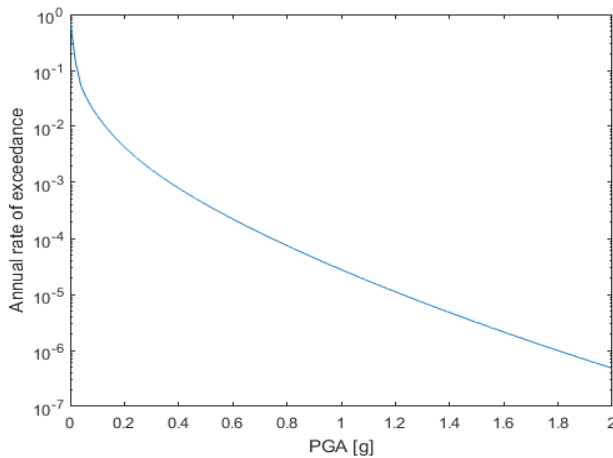
Figure 1.3 Hazard Curve of the high-seismic site of Priolo Gargallo (Sicily, Italy).

1.3.2 LNG Tank

Typically, LNG tanks are used to store LNG at very low temperatures, i.e. -100 °C. A relatively common kind of LNG tank is the full containment tank, where the inner steel tank encloses the LNG and the outer structure is generally thicker and of concrete and includes both an outer steel tank and the insulation material.

The tank of the LNG plant under study, depicted in Fig. 1.4, has two main different layers: i) the inner one has high resilience steel shells (X8Ni9) of thickness varying from 18 mm for the lower rings to 8 mm for the upper rings and of radius 23 meters; ii) the outer layer is concrete C30/37 with a total thickness of 650 mm. This concrete wall has an inner radius of

15

24.5 m and a height of 38 m. The roof is a concrete dome, with thickness ranging from 850 to 350 mm, reaching an overall height of 47.4 m.
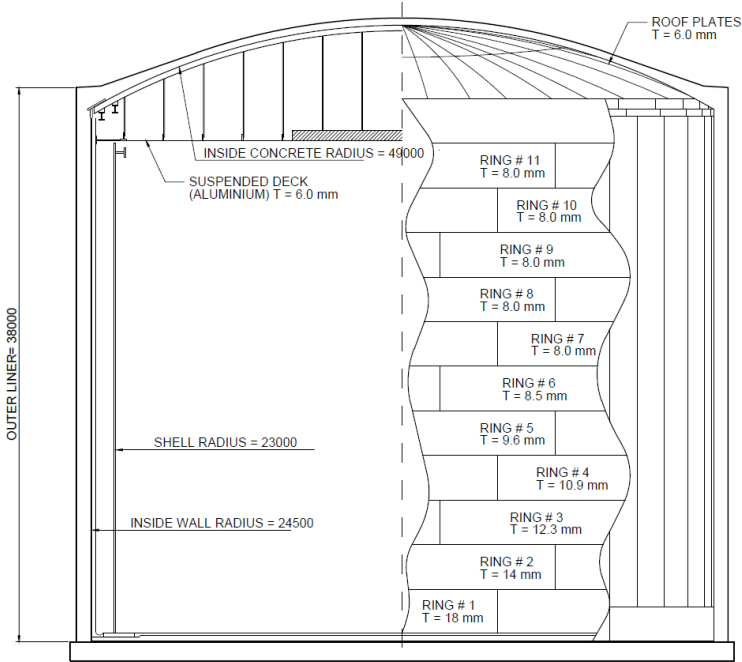
Figure 1.4 Main tank layout.

1.3.3   Substructures

Two different structures support the pipework: i) a steel platform located over the dome as shown in Fig. 1.5, and ii) a concrete structure placed at the base of the tank as in Fig. 1.6.
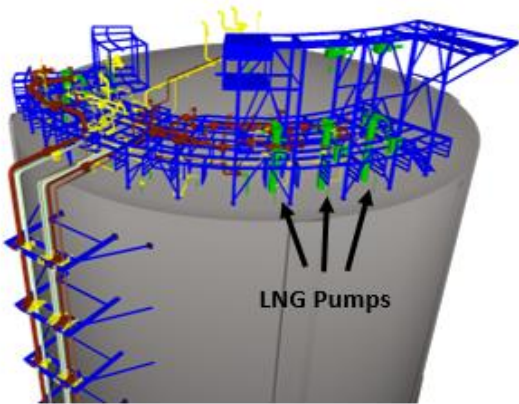
Figure 1.5 Steel platform and position of the three pump columns

The platform at the top of the tank is built with 17 different kinds of commercial steel profiles grade S235, arranged on three different levels, located respectively at 41, 45 and 48 m above ground. These steel profiles were selected in the range 100-280 for the HEB profiles and in the range 120-240 for the IPE profiles. Three pumps, located above the dome, transport the ethylene from the tank to the pipework.

At the base of the tank, the piping system distributes ethylene to the different process areas. The pipelines are supported by a concrete structure 102 m long, 6.5 m wide and 7.3 m high with an intermediate level placed 5.3 m above the ground. The span between the columns along the longest dimension is 6 m, whilst the span between the beams along the same direction is 3 m. The concrete compressive strength class is C50/40.
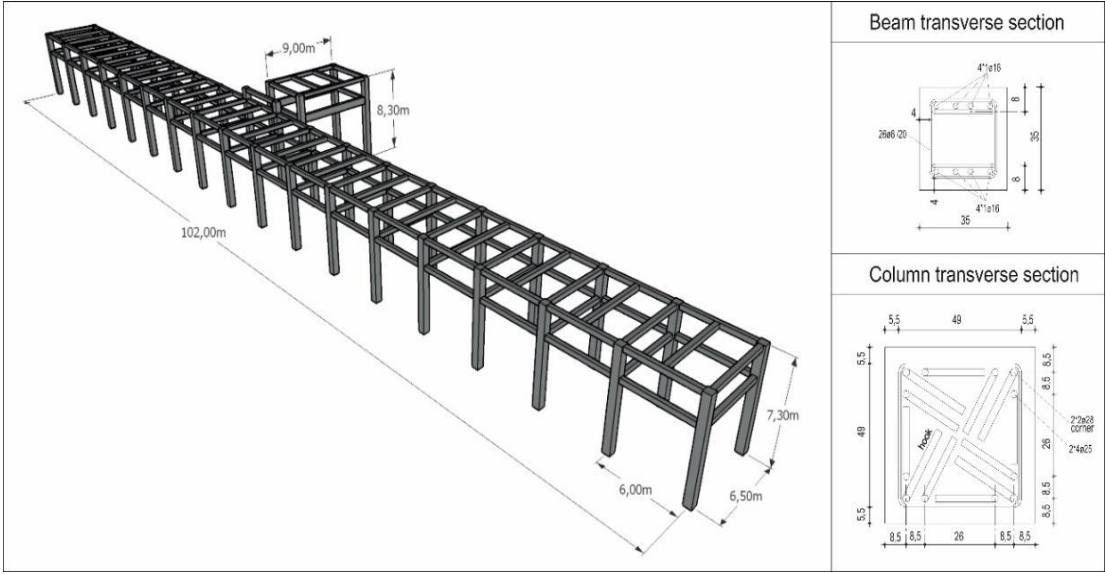
Figure 1.6 Concrete support structure

The columns have a 600 mm square section with 8 steel reinforcement bars $\phi25$ and 4 steel re-bars $\phi28$. The beams are 350 mm square section with 4 steel re-bars $\phi20$.

1.3.4   Knock-Out Drum Area

The knock-out drum process area, the function being to separate liquid from gas in the ethylene mixture, is located at the far end of the concrete support structure as shown in Fig. 1.2. Separation occurs in two stainless steel tanks, shown in Fig. 1.7, connected to the concrete support structure by a piping system for the ethylene supply. The tank considered in the analysis is named C608 and it is highlighted in red in Fig. 1.7. The vessel dimensions are in Table 1.1.
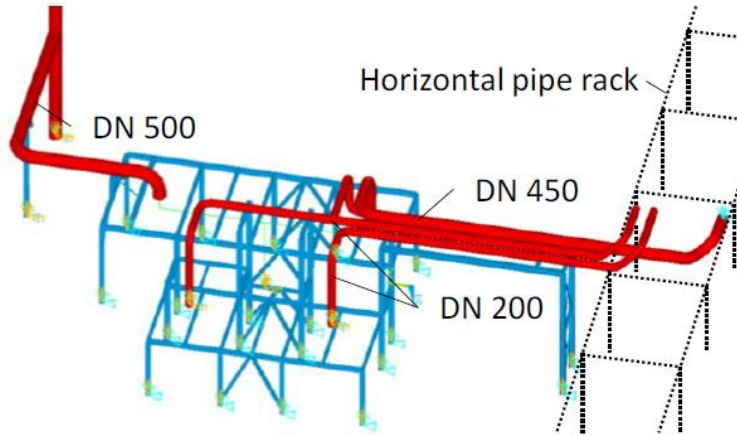
Figure 1.7 Knock-out drum process area

Table 1.1 Properties of Knock-out drum C608 tank

Knock-out drum C608 tank	
Capacity [m^3]	52
Diameter [m]	2.6
Length [m]	10.15
Wall thickness [mm]	8

The two tanks of the knock-out drum area are surrounded by a grade S235 steel support structure that is 17.5 m long, 9.2 m wide and 1.5 m high. The structural steel profiles are in the ranges 120-200 HEB and 160-220 IPE.

1.3.5 Piping System

The piping system, depicted in Fig. 1.5 and 1.8, is arranged into 8 different welded pipelines of stainless steel grade ASTM A312/TP304L.
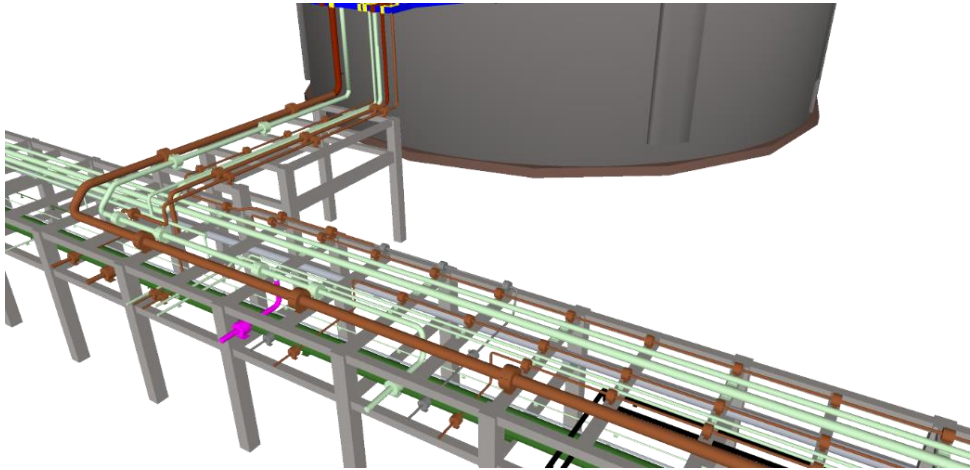
Figure 1.8 Pipelines layout on concrete support structure

The cross section properties of each pipeline are summarised in Table 1.2.

Table 1.2 Properties of Knock-out drum C608 tank

Cross section properties of the pipelines					
Pipeline number	Pipe specification	External radius [mm]	Wall thickness [mm]	Curvature radius [mm]	Max Operating Pressure [barg]
1	16''- SCH20	406.4	7.92	610	2.8
2	10'' - SCH10S	273.05	4.19	381	0.2
3	4'' - SCH10S	114.3	3.05	152	0.2
4	6'' - SCH10S	168.28	3.40	229	0
5	12'' - SCH10S	323.85	4.57	457	0.3
6	6'' - SCH10S	168.28	3.40	229	16.3
	8'' - SCH10S	219.08	3.76	305	16.3
7	6'' - SCH10S	168.28	3.40	229	1
8	18'' – SCH10S	457.2	4.78	686	0

The mechanical properties of the pipeline steel were defined during the INDUSE-2-SAFETY project, with experimental tests on metallographic samples of seamless pipes (Bursi et al., 2016a). In order to characterize the steel constitutive law for the operating conditions of the plant, tensile testing was done at room temperature and at -80°C. The relevant results are shown in Fig. 1.9 and Fig. 1.10.
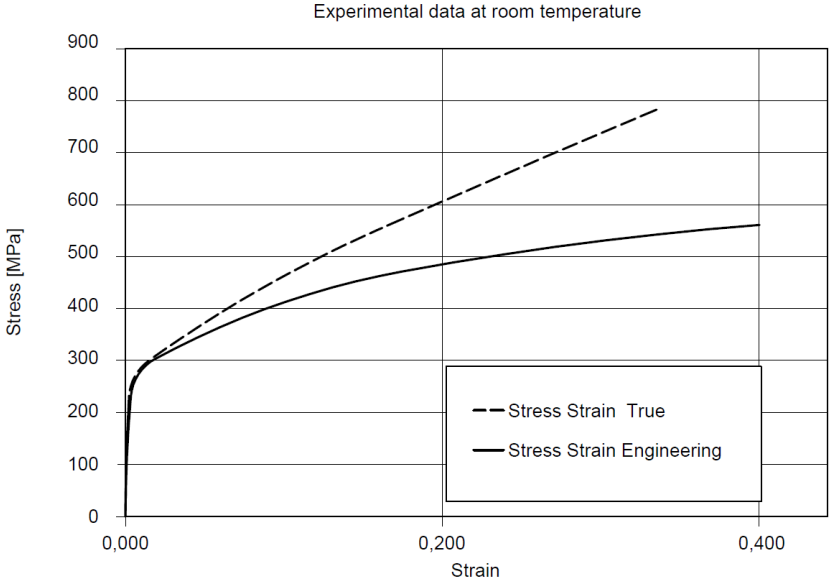
Figure 1.9 Stress-strain curve for A312/TP304L at room temperature
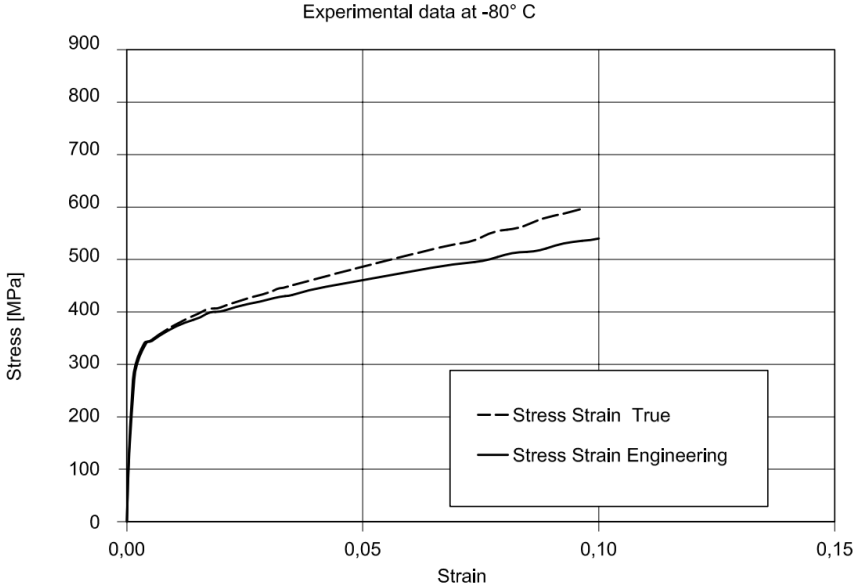
Figure 1.10 Stress-strain curve for A312/TP304L at -80°C

As expected for steel materials, the A312/TP304L showed a higher elastic modulus and a decrease in ductility at the lower temperature.

The connections between the piping system and other elements such as the pumps over the main tank or the nozzles in the knock-out drum area, are by BFJs. In particular, the connection between pipeline #6 and the three pump columns over the dome of the tank was made with a 6'' SCH10S CL300 welded neck flanges, as shown in Fig. 1.11. In addition, pipeline #8 and the knock-out drum tank were connected with an 18'' SCH10S CL150 welded neck flange as depicted in Fig. 1.12.
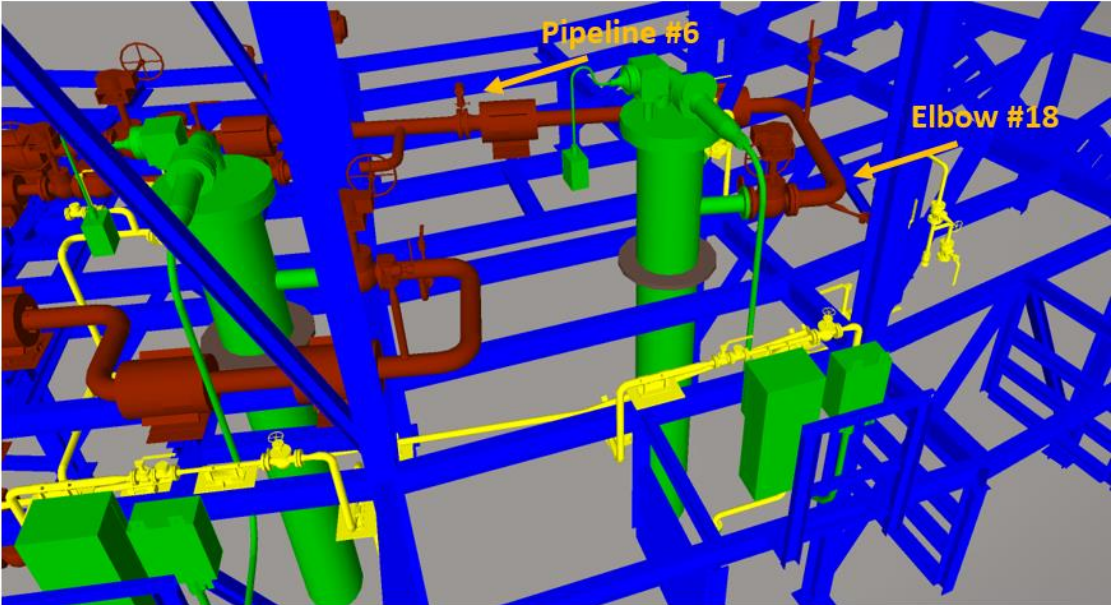
Figure 1.11 BFJs connecting the pumps to the piping system
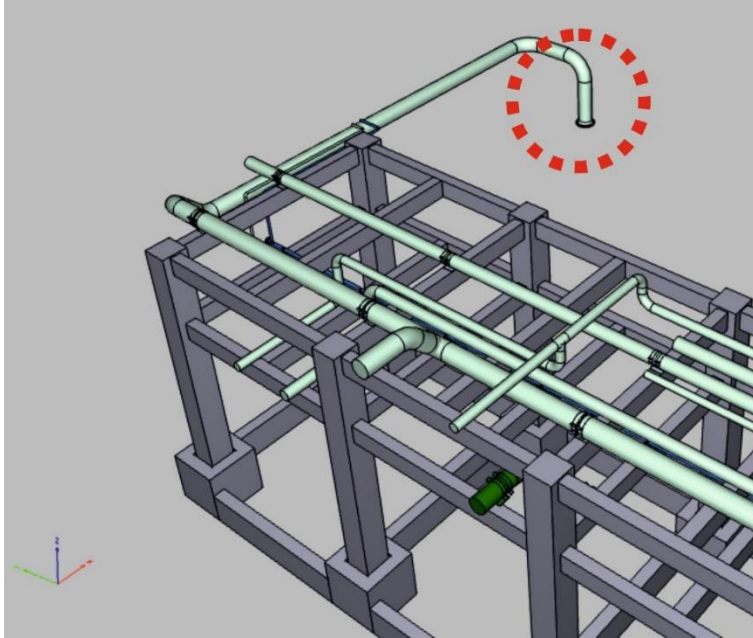
Figure 1.12 BFJ between the tank of the knock-out drum and the piping system

1.4 Critical components for leakage in the LNG plant

Pipelines and their components like BFJs, pipe bends and Tee joints are widely used in LNG plants including the one described in Section 1.3. With regard to BFJs, these joints are quite complex because they are highly confined statically indeterminate systems and also because they involve a high degree of non-linearity. As a result, it is difficult to correctly estimate their resistance and stiffness, as also the threshold of leakage. They have been investigated in Zerres and Guerot, (2004) and Reza et al., (2014), among others. Here we summarize the research work accomplished by La Salandra et al., (2016), see Subsection 1.4.1, whose results represent the basis for the mechanical model presented in Subsection 1.4.2. With reference to pipe bends, they are a vulnerable component of pipelines and we discuss their seismic performance evaluation in Subsection 1.4.3. Lastly, we do not explicitly mention Tee joints, since only one of them is encompassed into the pipelines. Nonetheless, the experimental campaign carried out allowed for its detailed modelling (Bursi, Reza et al., 2016b). More precisely, the Tee joint did not exhibit a significant stress level being located on the concrete rack, see Fig. 1.8, at a relatively low height.

1.4.1   Test campaign and main results

The mechanical model of BFJs was obtained by means of four experimental tests on two different BFJs, both for 8'' pipes, subjected to cyclic and monotonic loading. The two different types of BFJs had flanges of non-standard thickness; in greater detail, thicknesses of 18 and 27 mm (respectively Design 01 and Design 02) were employed, values less than those employed in industry, of the order of 35 mm. Therefore these flanges can be classified as non-standard flanges (Reza et al, 2014). During the test campaign, the BFJs specimens

were loaded in the testing equipment depicted in Fig. 1.13. In greater detail, the joints were located at 45° with respect to the vertical loading axis. The main reason for this choice was the fact that we had no data to predict whether the axial or the shear force would have most influenced the leakage threshold in BFJs. Therefore, we decided to adopt a testing configuration with equal intensity axial and shear forces.

<div align="center">(a)   (b)</div>
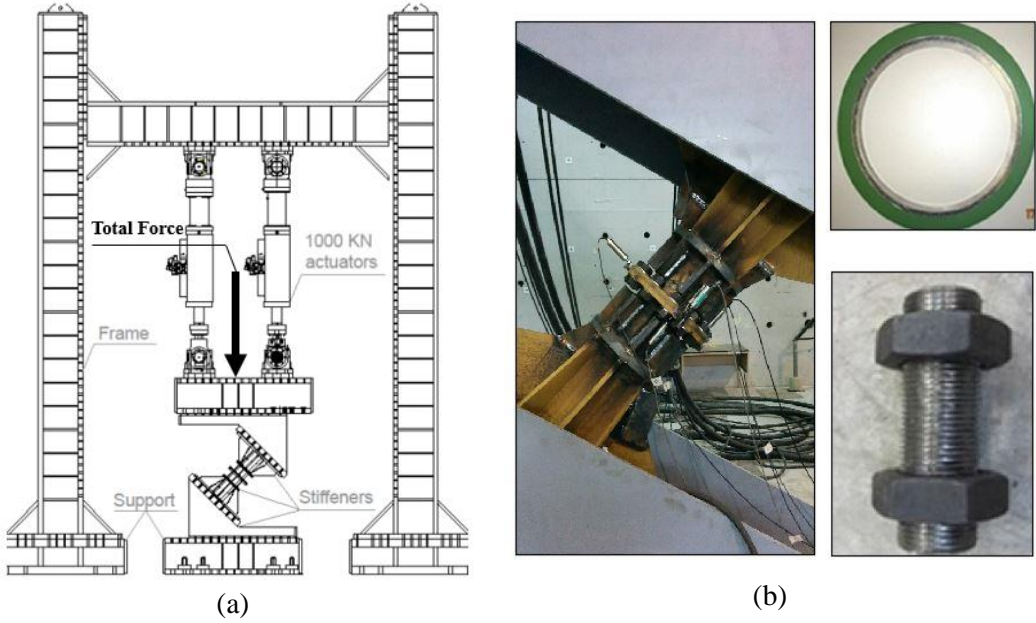
Figure 1.13 (a) BFJ setup. (b) Design 02 specimen, gasket, and a relevant bolt.

Both axial and shear force values corresponding to the onset of leakage are collected in Table 1.3.

Table 1.3 Leakage forces for the experimental tests

Specimen Flange Thickness and Loading Type	Leakage Axial Force [kN]	Leakage Shear Force [kN]
18 mm (Design 01) – Monotonic	1175	1175
18 mm (Design 01) – Cyclic	1100	1100
27 mm (Design 02) – Monotonic	1000	1000
27 mm (Design 02) – Cyclic	1470	1470

Although cyclic loading is more severe than monotonic loading for BFJ components, this is not reflected in the leakage forces of Design 02 joints. Moreover, it is worthwhile noting that

<div align="center">23</div>

the onset of leakage corresponds to an inside pressure of 32 bar which is far greater than the internal service pressure in the LNG pipelines, summarized in Table 1.2.

The corresponding force-displacement relationships are depicted in Figs 1.14 (a) and 1.14 (b) for monotonic and cyclic loading, respectively, where the Total Force shown in Fig. 1.13 (a), is equal to the sum of the forces exerted by the two actuators. These results show that the onset of leakage occurred after first yielding and before plastic collapse.

It is possible to notice that cyclic loading triggered leakage in Design 01 joints, with lower external forces compared to monotonic loading whilst the opposite happened for Design 02. This can be explained considering the differences between the deformation modes of Design 01 and 02. As a matter of fact, Design 01 experiences leakage through the bolts holes with a minimum involvement of flange plates; therefore, the bolts were the components that controlled leakage and similar leakage force levels were exhibited in both monotonic and cyclic loading. Conversely, in Design 02, leakage started from flange plates with a little involvement of bolts. As a result, cyclic loading pre-compressed flange plates increasing their leakage resistance and making the BFJ less vulnerable than that subjected to monotonic loading.
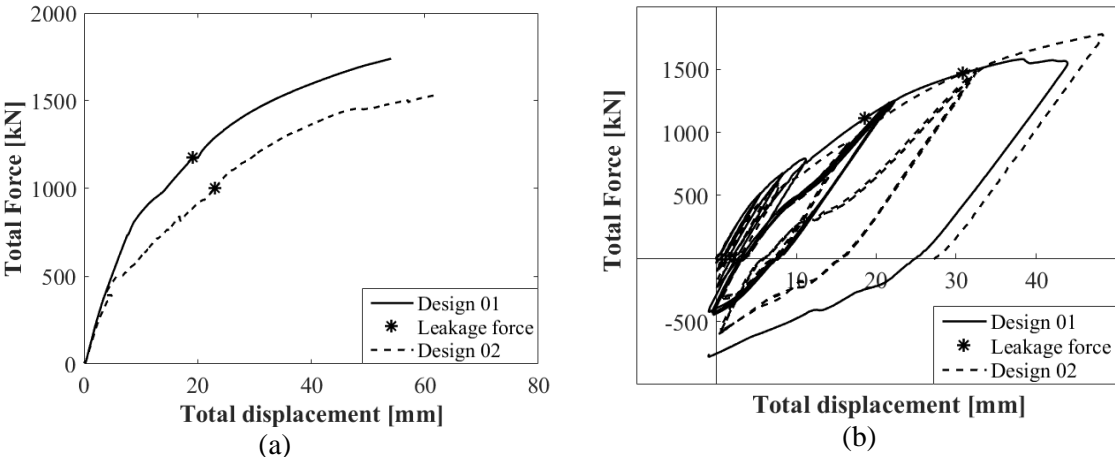
Figure 1.14 Load-Displacement diagrams for 18 mm (Design 01) and 27 mm (Design 02) BFJs: (a) Monotonic loading and (b) Cyclic Loading.

1.4.2 Predictive model for leakage and mechanical model of BFJs

Because pipelines and relevant BFJs of the LNG plant under study are characterized by a variety of diameters, from 4'' to 18'', as listed in Table 1.2, a mechanical model is needed to predict the onset of leakage for the remaining diameters. To this end, the experimental work of La Salandra et al. (2016) provides the basis for the predictive mechanical model summarized here.

The proposed mechanical model is based on the framework of EN 1591 standard (2009). More precisely, the model considers the BFJ as composed of three main components: bolts, flange and gasket, as reported in Fig. 1.15, where F_{BI} and F_{GI} define the tensile bolt and the gasket compressive axial forces, respectively; F_{QI} equals the force due to internal pressure whilst F_{RI} represents the resulting external force acting on the joint. Additionally, all these forces are referred to a generic design load condition I.
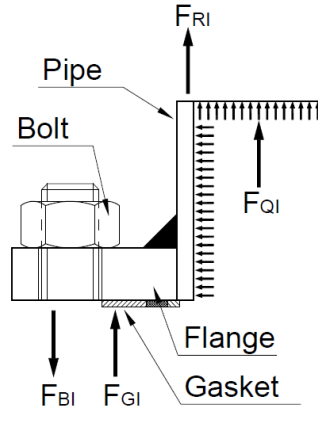
Figure 1.15 Bolt, flange and gasket components and force balance in the mechanical model of a BFJ proposed in EN 1591-1 (2009).

This model is based on the assumption that the flange is infinitely stiff in bending, see in this respect Fig. 1.17, differing from bolts and gasket which can exhibit axial deformation. Moreover, we assume that leakage occurs when the compressive stress on the gasket σ_{GI} is lower than a certain threshold $Q_{s,min,I}^{(L)}$ (EN 1591-1 standard, 2009). Starting from these hypotheses, the proposed model employs the following equation of the joint compliance at the load condition I:

$$F_{GI}Y_{GI} + F_{QI}Y_{QI} + F_{RI}Y_{RI} + \Delta U_I = F_{G0}Y_{G0}P_{QRI} \tag{1.5}$$

where, F_{G0} defines the gasket compressive force at the initial state 0 - the assembly condition - due to the bolt force tightening, i.e.

$$F_{G0} = \sigma_{G0}A_{Ge} = \sum_{n° \; bolts} F_{tor}$$
$$= \sum_{n° \; bolts} \frac{M_{torq}}{0.18 * d} \tag{1.6}$$

After some algebraic manipulations, the pressure on the gasket at the load condition I can be calculated and compared to the limit provided by the standard, i.e.

$$\sigma_{GI} = \frac{\sum F_{tor} Y_{G0} P_{QRI} - \frac{\pi}{4} d_{Ge}^2 F_{QI} Y_{QI} - F_{RI} Y_{RI}}{Y_{GI} A_{Ge}} \leq Q_{s,min,I}^{(L)} \qquad (1.7)$$

If Eq. (7) is satisfied, then the leakage limit state does not occur. As a result, by working out Eqs. (5-7), we can derive the external force F_{RI},

$$F_{RI} \geq \frac{\sum F_{tor} Y_{G0} P_{QRI} - \frac{\pi}{4} d_{Ge}^2 F_{QI} Y_{QI} - Q_{s,min,I}^{(L)} Y_{GI} A_{Ge}}{Y_{RI}} \qquad (1.8)$$

that corresponds to the leakage onset. Further details of this derivation and relevant symbols can be found in La Salandra et al. (2016).

This model seems to predict satisfactorily the experimental results of the testing campaign by Reza et al. (2014), where BFJs were loaded only axially. Nonetheless, BFJs present in the piping system under study are subjected to multiple actions, in agreement with the experimental testing presented in Subsection 1.4.1. As a result, the mechanical model takes into account the possible interaction between axial and shear loading. More precisely, the leakage force for a BFJ subjected only to the shear loading is supposed equal to the bolt shear strength T_u provided by EN 1993-1-8 (2005), i.e.,

$$T_u = n * \frac{0.6 * f_u * A_{res}}{\gamma_{M2}} \qquad (1.9)$$

Additionally, based on the aforementioned test campaign, the relation between the combined axial and shear leakage loading is approximated as linear,

$$T = (N_u - N)\rho, \text{ where } \rho = {}^{T_u}/{}_{N_u}. \qquad (1.10)$$

Eq. (1.10) is presented graphically in Fig. 1.16 and the reader can appreciate the favourable agreement between model and test data.
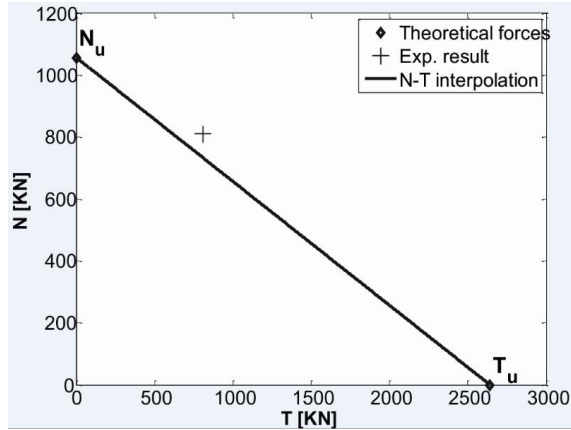
Figure 1.16 Comparison between axial and shear leakage forces from the predictive model and experimental results.

Therefore, it is possible to calculate both axial and shear leakage forces of relevant BFJs under study, i.e. both 6'' and 18'' weld neck flanges, and relevant values are summarized in Table 1.4.

In order to accomplish the FE analysis presented in Subsection 1.6.3, we also needed to characterize BFJs in terms of axial and shear stiffness. With reference to the axial stiffness, we start from the mechanical model proposed in EN 1591 (2009). In particular, the mechanical model – sketched in Fig. 1.17 - considers the joint axial deformation δ_s due to an external force F_R as:

$$\delta_s = u_{an} + v_{an}.$$

(1.11)

where, u_{an} defines the bolt axial elongation and v_{an} identifies the axial deformation due to rigid flange rotation.
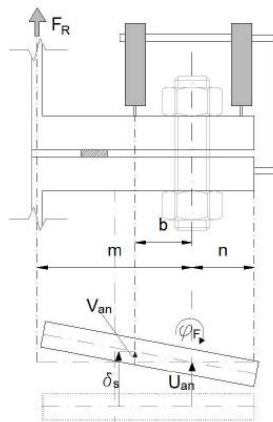
Figure 1.17 Axial deformation model for BFJs.

Moreover, the equivalent shear stiffness K_s is estimated considering two plates of equal thickness t and joined by means of one bolt, i.e.

$$\frac{1}{K_s} = \frac{10t^3}{24E_b I_b} + \frac{4t}{3A_b G_b} + \frac{2tE_f}{t^2 E_f^2} \tag{1.12}$$

where the first and the second term on the right hand side refer to bending and shear compliance of the bolt, respectively; whilst the third term is related to the bearing compliance of plates. Finally, linear stiffness values for BFJs under study are collected in Table 1.4. As a result, BFJs add stiffness to the whole piping system under study.

Table 1.4 Axial and shear stiffness and leakage forces of BFJs.

	6'' Weld Neck Flange CL300	**18'' Weld Neck Flange CL150**
Axial stiffness [kN/mm]	14400	26000
Shear stiffness [kN/mm]	1270	4700
Axial leakage force [kN]	939	1034
Shear leakage force [kN]	2228	6097

With regard to leakage forces, one can notice that their values are significant; moreover, leakage due to shear needs greater force values.

1.4.3   Elbows performances

Piping elbows are critical component in a piping system and are characterized by a high flexibility, relevant level of stresses and strains and a significant cross-sectional deformation. Since the goal of this study was the investigation of the onset of leakage triggered by seismic action, particular attention was paid to pipe bends due to their vulnerability. Therefore, we focused on the identification of reliable EDPs related to leakage. Present regulations such as ASME BPVC (2004) do not explicitly treat leakage but consider "gross plastic deformation" instead. In particular, they are defined by means of the twice elastic slope (TES) method. In addition, very few papers are available on the topic; see Karamanos (2016) and Brinnel et

al., (2016). A useful tool to classify the performance of piping elbows was developed by Vathi et al. (2015), which defines a set of damage levels, see in this respect Table 1.5, and the related limit states associated with several failure modes and relevant EDPs: they are collected in Table 1.6.

Table 1.5 Performance levels (after Vathi et al., 2015)

Level	Description
0	No damage
I	Minor (non-severe) damage
II	Major damage, but no loss of containment
III	Major damage with loss of containment

As stated before, our main interest was the LOC that corresponds to the Level III of damage.

Table 1.6 Failure modes with relevant EDPs and limit states (after Vathi et al., 2015)

Failure mode	EDP	Performance level and corresponding range	
Tensile fracture	Tensile strain ε_T	$\varepsilon_T < \varepsilon_\gamma$	0
		$\varepsilon_\gamma < \varepsilon_T < 0.5\%$	I
		$0.5\% < \varepsilon_T < \varepsilon_{Tu}$	II
		$\varepsilon_T \geq \varepsilon_{Tu}$	III
Local buckling	Compressive strain ε_C	$\varepsilon_C < \varepsilon_\gamma$	0
		$\varepsilon_\gamma < \varepsilon_C < \varepsilon_{Cu}$	I
		$\varepsilon_{Cu} < \varepsilon_C < 5\varepsilon_{Cu}$	II
		$\varepsilon_C \geq 5\varepsilon_{Cu}$	III
Low-cycle fatigue cracking failure	Damage factor $D = \sum_i \frac{n_i}{N_i}$	$D < 0.5$	0
		$0.5 < D < 0.8$	I
		$0.8 < D < 1$	II
		$D > 1$	III

In particular, the threshold for tensile strain ε_{Tu} suggested by Vathi et al. is equal to 2%; conversely, to compute the same limit state for compressive strains, i.e. $5\varepsilon_{Cu}$, we adopted the following relationship,

$$\varepsilon_{Cu} = 0.5 \left(\frac{t}{D}\right) - 0.0025 + 3000 \left(\frac{\sigma_h}{E}\right)^2 \tag{1.13}$$

where t is the thickness of the pipe walls, D is the diameter, σ_h the internal pressure and E the Young's modulus.

The leakage compressive strains for pipeline #1 and #6 are calculated by means of Table 1.2, where no internal pressure is considered to simulate the worst conditions. The resulting strain values are 3.6% for pipeline #1 and 4.7% for pipeline #6, significantly higher than the leakage tensile strain assumed to be 2%.

With regard to low-cycle fatigue defined in Table 1.6, we relied on the design low-cycle fatigue curves proposed by Otani et al., (2017), based on data derived from several experimental campaigns. Therefore, on the basis of the records 007162 and 006277, see Table 1.8, characterized by PGA of 1.04 g and 0.86 g, respectively, the seismic analysis on the plant was carried out. The corresponding time histories of elbow hoop strains were treated by means of a rainflow analysis. The subsequent application of the Palmgren-Miner rule entails damage values corresponding to D=8.52 10-5 and 8.89 10-5, respectively. On this basis and also in the case of some strong aftershock event, one can exclude LOC of elbows due to low-cycle fatigue failure.

In sum, the tensile strain can be considered the most important indicator of leakage in seismic assessment. This is also confirmed by the extensive test campaign conducted by the Japan Nuclear Energy Safety Organization and the Nuclear Power Engineering Corporation of Japan (JNES/NUPEC, 2008); and we recall the experimental work of Karamanos and co-workers that produced an overview of the mechanical behaviour of elbows, reporting analytical solutions, numerical results and experimental data. (Karamanos, 2016). As a result, we assume that piping elbows experience the onset of leakage when tensile hoop strains reach values of about 2% at the outer surface, in agreement with experiments. Indeed, studies by Singh and co-workers confirm that fatigue crack growth appears on the inside as well as the outside surface of the flank region (Singh et al., 2014).

1.5 FE modelling of LNG plant components and preliminary analyses
After the design of the BFJ mechanical model, FE modelling of other components in the LNG plant is reported in this section. For this purpose, the FE software ANSYS was employed.

1.5.1   LNG Storage Tank
The outer concrete layer of the storage tank was modelled by means of 4-node SHELL181 elements. In this respect, the design of the mesh was conceived with 34 elements along the circumference section, 19 elements along the wall height and 11 elements along the radius of the dome, as depicted in Fig. 1.18 (a). Moreover, the outer tank was fixed to the ground by means of rigid constraints. On the other hand, the inner steel tank was modelled by assigning the total mass of the LNG content when filled at the maximum capacity, i.e. 290,000 tons, to a single MASS21 element placed in the middle of the tank and connected

to the concrete tank by means of 4 MPC184 Rigid Link elements; see Fig. 1.18 (b) in this respect.

Internal tank content
mass - rigidly connected
to the base of the
external tank walls

Rigid connections

Fixed base

(a)   (b)
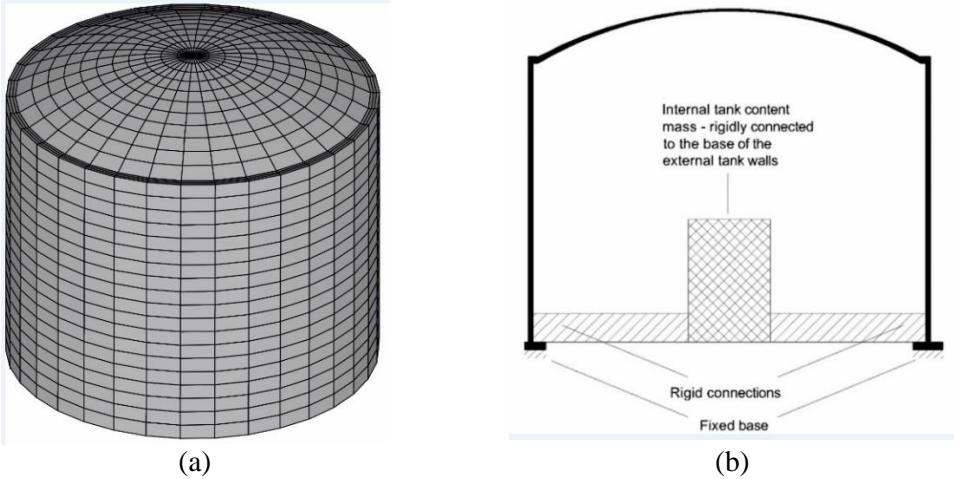
Figure 1.18 (a) Mesh design for the outer tank; (b) FE model of the inner tank.

The assumption of rigid walls is mainly due to the large outer tank thickness. Then, since forces generated by liquid modes (Malhotra et al., 2000) on the structure did not produce significant effects, we decided not to monitor local stresses on tank walls. Thus, from a dynamic point of view, we only take into account inertial effects of the LNG content in the calculation of reaction forces at the tank base.

1.5.2   Support Structures

The steel platform supporting piping systems and pumps, is on the top of the tank, as depicted in Fig. 1.19 (a). It is modelled by means of the BEAM4 and LINK180 elements for beams and axial members, respectively. All these elements are modelled with a linear constitutive law. On the other hand, the concrete support structure at the base of the tank is modelled with the same BEAM4 elements used for the steel platform. Moreover, it is rigidly constrained to the ground. In agreement with the Seismic Italian Standards (Norme Tecniche, 2008), the elastic modulus of concrete was reduced by 50 percent to account for cracking at the ultimate limit state. Nonetheless, during seismic analyses stress levels never

exceeded plastic limits in reinforced concrete elements. Therefore, a linear elastic constitutive law was considered also for this substructure.

(a)

(b)
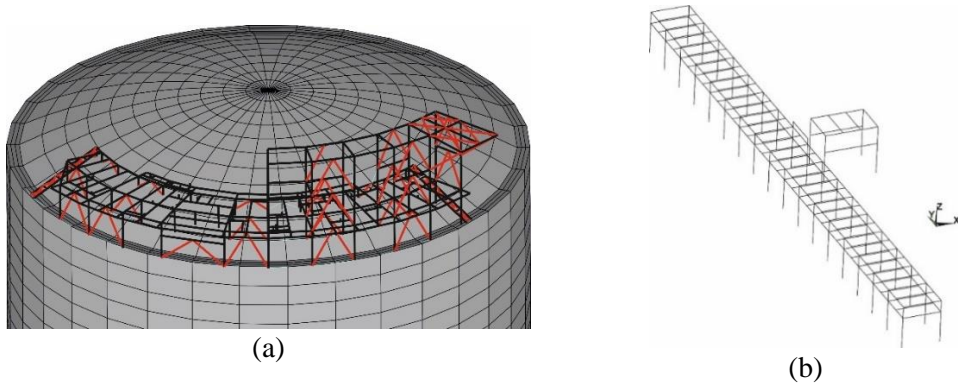
Figure 1.19 ANSYS FE model: (a) steel platform; (b) concrete support structure.

1.5.3   Piping System and Knock-Out Drum Area

The piping system was modelled by means of PIPE289 and ELBOW290 elements; these are both 3-node 3D elements with 6 DoFs per node. Lateral walls were modelled with SHELL181 elements with the shell thickness equal to the real pipe thickness. The design of the mesh was conceived with 20 shell elements along the circumference section. Furthermore, in order to correctly model the elbow constitutive law, the A312/TP304L stress-strain curve depicted in Fig. 1.20 (a) was reproduced with a bilinear relationship accounting for kinematic hardening.

Due to their complexity, only two of the seven pipelines on the steel platform on the tank dome were entirely modelled in ANSYS, i.e. pipeline #1 – the largest - and #6 – the smallest - as reported in Fig. 1.20 (b). Given the relevant involved weights, the unmodeled pipelines did not influence the dynamic response of the system. According to design requirements, two types of constraints were applied in modelling the contact between the piping system and the two support structures: i) a fixed constraint and ii) a roller allowing the piping to slide in its longitudinal direction.

(a)   (b)
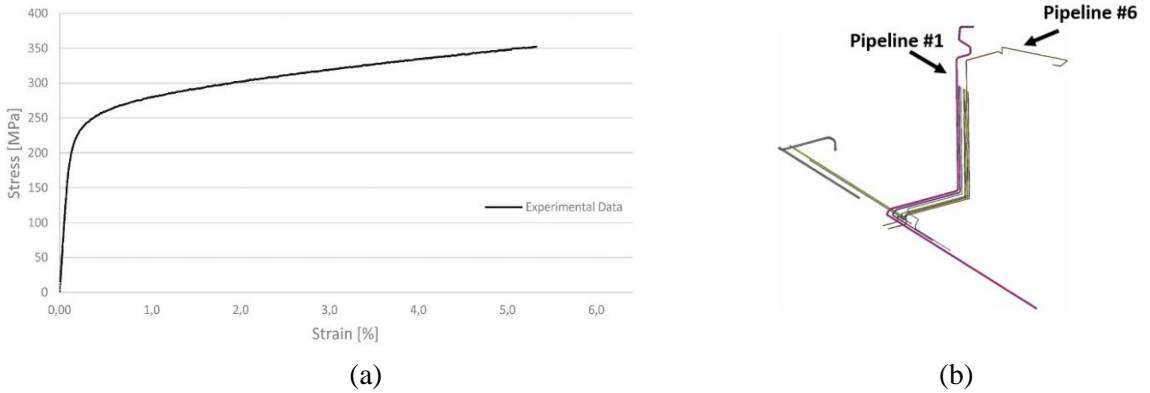
Figure 1.20 (a) Experimental results for A312/TP304L steel (b) FE model of the piping layout.

On the other hand, BFJs were modelled by means of a longitudinal and two transversal springs as presented in Subsection 1.4.2. To this end, and to take into account the different responses for tensile and compression forces, the COMBIN39 element was used for the axial spring. The values of both longitudinal and shear stiffness for BFJs modelling are in Table 1.4. Finally, the knock-out drum area is placed on the ground, close to the LNG storage tank, see Fig. 1.2 in this respect. The FE model developed by Kondorfer et al. (2016) was used for modelling both the pressure vessel C608 and the relative steel support structure. In particular, the support structure was modelled by means of BEAM4 elements, whilst the pressure vessel C608 was simplified with a mass-spring model, as depicted in Fig. 1.21.
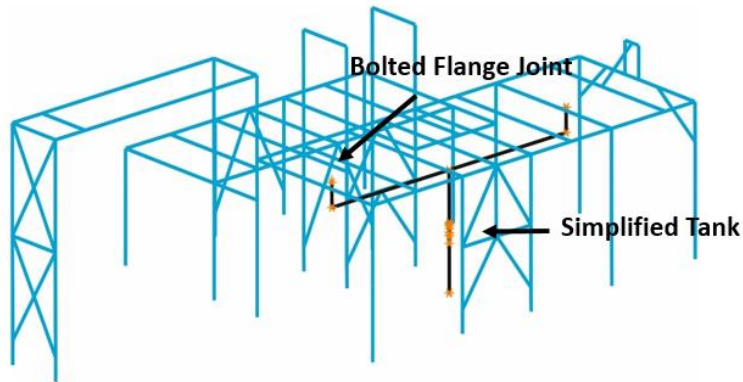
Figure 1.21 FE model of Knock-out drum process area.

1.5.4 The whole ANSYS model

Once each single component was modelled, they were assembled to build up the complete FE model of the plant, as depicted in Fig. 1.22.
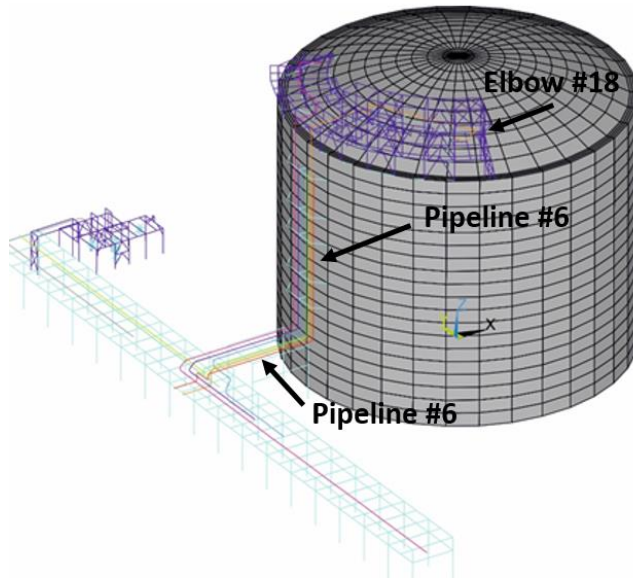
Figure 1.22 ANSYS complete FE model of the LNG plant.

The complete model is highly complex, with totals of 19568 DoFs, 1338 BEAM4 elements, 159 PIPE289, 95 ELBOW290 and 1122 SHELL181.

1.5.5 Preliminary seismic analyses for boundary conditions and mesh sizes.

In order to assemble a FE model of the plant, a sensitivity analysis was conducted on important elements like tanks and elbows. As a result, the proper number of FE for the tank was set to 1122 shell elements; also, the number of integration points along the wall thickness of elbows was selected equal to 2. The FE model was assembled considering the relative boundary conditions between the different components. In a greater detail we had to model the connections between: i) the knock-out drum area and the concrete support structure; ii) the steel platform and the dome of the LNG tank; iii) the two different sections of the concrete rack and the LNG tank; iv) the pipelines and the support structures. The first connection was made only by means of the pipelines that, coming from the support rack, were connected to the 18'' BFJs of the knock-out drum vessel; see, in this respect, both Fig. 1.7 and Table 1.4. The second connection was accomplished with rigid links coupling base nodes of the steel platform with nodes of the LNG tank dome. This was done to simulate a fixed constraint between the tank and the platform. The third coupling, like the first one above, was realised by the set of pipelines running through the different components. With regard to the last set of links, it is well known that pipeline supports are not frictionless (Peng, 1989). For this reason, we employed two different types of constraint: fixed supports

with all displacement blocked in the *FIXED* case; roller supports with free axial displacements in the *FREE* case.

Once assembled the entire FE model of the plant, we needed to define important parameters, such as the amounts of fluids in pipelines and the types of constraint on support structures. For the first parameter, two cases were defined: i) the "LNG" case, in which the mass of the fluid was included in the pipelines, ii) the "EMPTY" case where the liquid mass was neglected. Finally, some preliminary seismic analyses were carried out with different scenarios; the results are reported in Table 1.7.

Table 1.7 Comparison between preliminary simulations.

Earthquake	Record ID	PGA	Pipelines content	Constraints	Max Axial Strain Detected
South Iceland (aftershock)	006334	3.84	EMPTY	FREE	0.32% - Pipeline #6 Elbow 15
South Iceland (aftershock)	006334	3.84	LNG	FIXED	0.32% - Pipeline #6 Elbow 15
L'Aquila Mainshock	IT0792	5.35	EMPTY	FREE	0.45% - Pipeline #6 Elbow 11
L'Aquila Mainshock	IT0792	5.35	LNG	FREE	0.45% - Pipeline #6 Elbow 11
L'Aquila Mainshock	IT0792	5.35	LNG	FIXED	0.45% - Pipeline #6 Elbow 11
South Iceland	006277	5.08	EMPTY	FREE	3.25% - Pipeline #6 Elbow 18
South Iceland	006277	5.08	LNG	FIXED	3.25% - Pipeline #6 Elbow 18

It can be seen that there are no large differences between simulations with the same earthquake input and different pipeline conditions; hence, in order to obtain fragility curves for elbows, all required simulations were carried out considering the same conditions, i.e. the "LNG" case for the pipeline content and the "FREE" condition for pipeline constraints.

1.6 Probabilistic Seismic Analysis

In order to evaluate the probability of exceeding a certain *EDP i.e. P(EDP)* from Eq. (1.4), the conditional probability of exceeding a prescribed *EDP* given the intensity measure, *IM, i.e. $P(EDP > C_{LS}|IM = im)$* must be estimated. There are several alternative non-linear dynamic analysis procedures available in the literature for characterizing the relationship between *EDP* and *IM* based on recorded ground motion waveforms, such as: i) Incremental Dynamic Analysis (IDA, see Vamvatsikos & Cornell, (2004)); ii) Multiple-Stripe Analysis (MSA, see Jalayer & Cornell, (2009)); and iii) the Cloud Method (Cornell et al. 2002). Both

IDA and MSA are suitable for evaluating the relationship between *EDP* and *IM* for a wide range of *IM* values; however, their application is time-consuming in our context of the LNG plant, about three days per run, as nonlinear dynamic analyses are repeated -usually for scaled ground motions- for increasing levels of *IM*. Moreover, the Cloud method does not require any amplitude scale factor. In fact, scaling can entail incoherencies in the probabilistic model, especially when all three -X, Y and Z- different components of each waveform are used for seismic demand analysis (Mackie and Stojadinović, 2005). Therefore, a *Cloud Analysis* will be applied in the sequel.

1.6.1 Cloud analyses and seismic input

As a first step, we consider only one scalar *IM* in the *Cloud Analysis, i.e.* the PGA. In particular, we decided to avoid, in the initial phase of the study, the adoption of any spectral quantity because of the heterogeneity in the modal frequencies of the LNG plant substructures. However, the Cloud Analysis was later performed by considering as additional IM the spectral acceleration Sa(T). Accordingly, the LNG plant described in Section 1.5 is subjected to a suite of 36 ground-motion waveforms shown in Table 1.8, and the associated structural response parameters, as anticipated in Subsection 1.2., are denoted as D = {D_i, i = 1:n}. In particular, the *Cloud Analysis* is based on two main hypotheses: i) D is characterized by a lognormal distribution; ii) the expected D is modelled as a linear relationship in the logarithmic space of D versus the candidate *IM*, i.e.

$$E[lnD|IM] = a + bln(IM) \tag{1.14}$$

In particular, *a* and *b* are regression coefficients estimated with the least square method. Then, *a* and *b* let us set the main parameters of the probabilistic seismic demand model (PSDM), i.e.

$$\sigma_{lnD|IM} = \beta_{D|IM} = \sqrt{\frac{\sum_{i=1}^{n}[ln(D_i) - ln(a(IM_i)^b)]^2}{n-2}} \tag{1.15}$$

$$m_D = \left(\frac{C_{LS}}{a}\right)^{1/b} \tag{1.16}$$

$$\beta_D = \frac{1}{b}\beta_{D|IM} \tag{1.17}$$

where:

β_D and m_D are the dispersion and the median of *D* values that exceed the limit state level, indicated as C_{LS}.

Thus, the conditional probability that the demand D exceeds the limit state capacity C_{LS}, which is known as fragility function, reads,

$$P[D \geq C_{LS}|IM = im] = \Phi\left[\frac{ln(im/m_D)}{\beta_D}\right] \tag{1.18}$$

In order to cover different values of magnitude M_w and PGA, we chose the suite of ground motions from different European databases (ESM and ITACA). All three components, two horizontal and one vertical, were applied during the seismic analysis. In particular, we applied the strongest of the components along the X axis, as depicted in Fig. 1.2, since we required a more demanding load in the preliminary analyses. The record names and relevant characteristics are collected in Table 1.8.

Table 1.8 Natural records used for Cloud analysis.

Record Name	Record ID	Date	M_w	PGA [m/s^2]
L'Aquila Mainshock	IT0792	06/04/2009	6.3	5.352
L'Aquila Mainshock	IT0789	06/04/2009	6.3	3.947
South Iceland (aftershock)	006334	21/06/2000	6.4	4.123
L'Aquila Mainshock	IT0790	06/04/2009	6.3	4.793
Northern Italy	IT0049	17/06/1976	4.5	0.811
Friuli	IT0077	11/09/1976	5.8	2.29
Southern Italy	IT0231	16/01/1981	5.2	1.069
Umbria-Marche 3rd shock	IT0491	14/10/1997	5.6	0.435
Garfagnana	IT0157	07/06/1980	4.6	0.595
App. Lucano	IT0607	09/09/1998	5.6	0.427
Ancona	IT0009	21/06/1972	4.0	4.025
South Iceland (aftershock)	006349	21/06/2000	6.4	8.218
Ancona	IT0002	14/06/1972	4.8	5.309
Firuzabad	007162	20/06/1994	5.9	10.444
Gazli	000074	17/05/1976	6.7	7.065
Erzincan	000535	13/03/1992	6.6	5.028
South Iceland	006277	17/06/2000	6.5	5.083
Racha (aftershock)	000501	03/05/1991	5.6	4.989
Pyrgos	000558	26/03/1993	5.4	4.256
Kalamata (aftershock)	000419	15/09/1986	4.9	3.275
NE of Banja Luka	005651	13/08/1981	5.7	3.551
Ionian	006131	24/04/1988	4.8	2.705

Bovec (aftershock)	006247	06/05/1998	4.3	2.801
Kozani (aftershock)	006093	19/05/1995	5.2	2.601
Patras	001932	14/07/1993	5.6	3.337
Faial	007329	09/07/1998	6.1	4.12
Oelfus	005030	13/11/1998	5.1	1.439
Mt. Hengill Area	005149	24/08/1997	4.9	1.691
Mouzakaiika	000566	13/06/1993	5.3	1.428
Holt	005237	23/04/1991	4.7	1.212
Kremidia (aftershock)	002025	25/10/1984	5.0	1.766
Friuli (aftershock)	000707	11/09/1976	5.3	1.931
Valnerina	000246	19/09/1979	5.8	0.870
Izmit (aftershock)	006440	07/11/1999	4.9	3.449
Ancona	000030	14/06/1972	4.3	3.972
Strait of Gibraltar	000878	04/01/1994	4.9	0.596

The response spectrum of the strongest components of the natural records is depicted in Fig. 1.23.
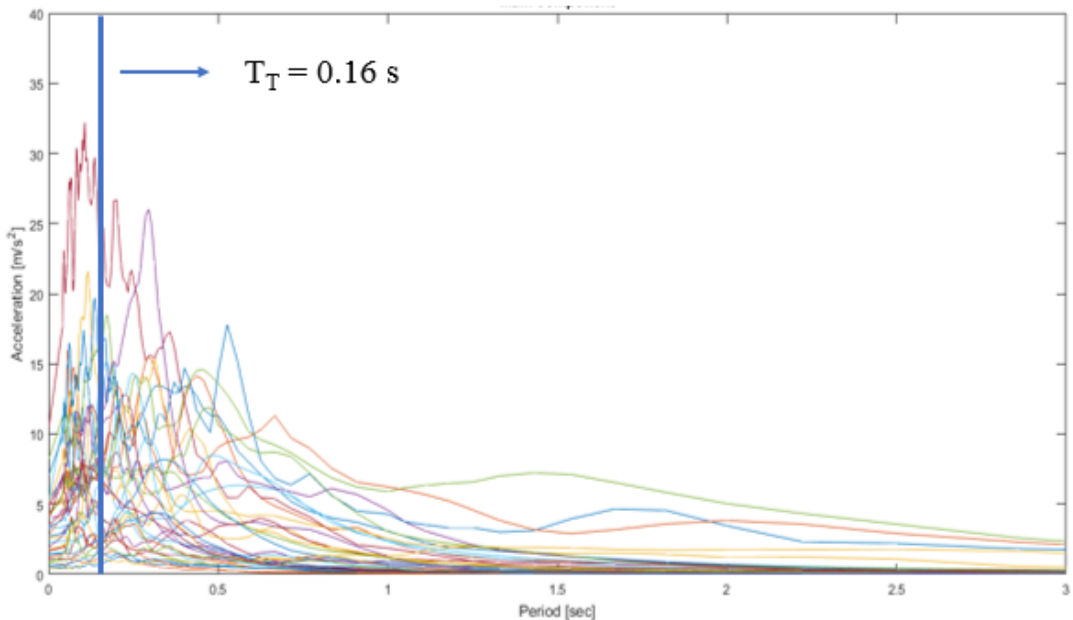
Figure 1.23 Response spectra of the strongest components of natural records employed.

We can see the high variability of spectral acceleration; for instance, the values cover a wide range, from near zero to 3g. This wide range lets us evaluate and improve the efficiency of the PSDM accomplished in Subsection 1.6.4.

1.6.2 EDPs and Limit States

As anticipated in Subsection 1.1.1., because LNG is a hazardous material due to its flammability after vaporization, we must prevent component leakage under environmental hazards: i.e. earthquakes, in our particular case. Therefore, we focused our attention on leak-prone elements like BFJs and piping elbows. In this respect and in agreement with the PBEE framework described in Section 1.2, three EDPs, i.e. demands D in Eq. (1.4), were selected as listed in Table 1.9.

Table 1.9 EDPs description

EDPs Number	Parameter Description
1	BFJs Max Axial Force
2	BFJs Max Shear Force
3	Elbow Max. Tensile Hoop Strain

With regard to EDP1 and EDP2, leakage thresholds were discussed and defined in Subsection 1.4.2 and Table 1.3. Conversely, the onset of leakage in elbows was directly defined relating EDP3 to a value of tensile hoop strain according to the literature review and the analyses presented in Subsection 1.4.3. Relevant C_{LS} values − see Eq. (1.4)- associated with leakage thresholds are reported in Table 1.10 and EDP3 reads 2 percent for elbows. As a result to reach the LOC, piping elbows experienced several limit states corresponding to the different damage levels thresholds reported in Table 1.6. Nonetheless and in agreement with EN 1473 (2016), LOC is the most critical limit state for risk assessment and hazard tolerability classification of LNG plants, and therefore, we decided to perform a fragility analysis only for the LOC limit state.

Table 1.10 EDPs leakage limit states

	6" Flange [kN]	18" Flange [kN]
EDP1	939	1034
EDP2	2228	6097
	6" Elbows (%)	
EDP3	2	

1.6.3 Main results of FE analyses

With reference to BFJs and EDP1 and EDP2 values set in Table 1.10, the results of seismic analysis reveal that axial and shear forces do not approach leakage thresholds. Relevant values are shown in Fig. 1.24 for 6" and 18" flanges, respectively. A careful reader can notice that force values experienced by BFJs are substantially lower than limit leakage

domains. Other limit states like yielding have not experienced both by flanges and bolts of FBJs.
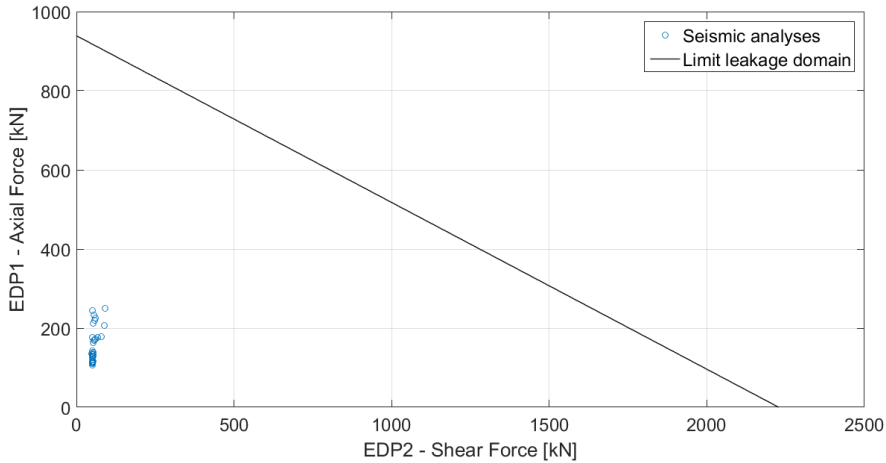
(a)
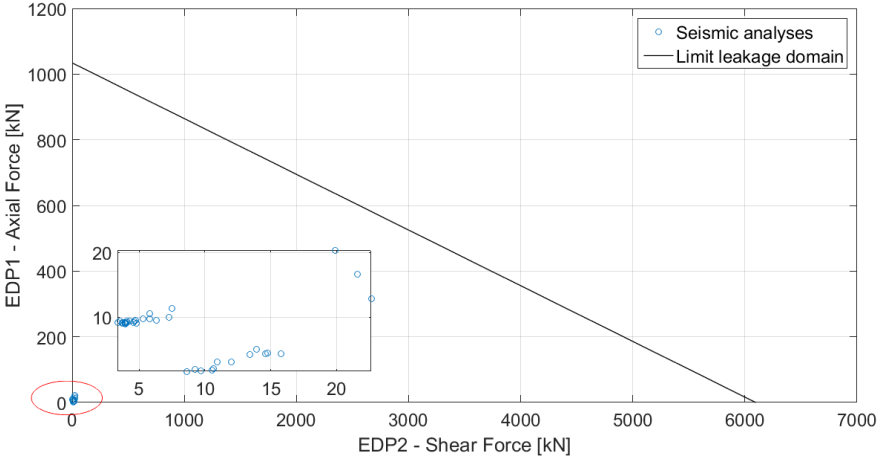
(b)

Figure 1.24 Seismic analysis results for: a) 6" BFJs; b) 18" BFJs.

With regard to EDP3, both maximum and minimum absolute values of tensile hoop strains collected in Table 1.11 were detected for the Elbow #18 shown in both Fig. 1.11 and in Fig. 1.22.

Table 1.11 Maximum and minimum absolute values of EDP3

Record Name	Record ID	EDP3 - Elbow Tensile Hoop Strain [%]
Firuzabad	007162	4.77
Mt. Hengill Area	005149	0.106

These values are justified by the fact that Elbow #18 is located at about 40 m above ground on the steel platform that is built above the dome of the LNG tank; and relevant seismic forces are clearly significant. Therefore, we decided to introduce as additional IM, the spectral acceleration Sa(T) at the main vibration period of the LNG tank, i.e. $T_T = 0.16$ s, since we expect a stronger influence upon the EDP3 compared to the PGA. The values of $Sa(T_T)$ can be observed in Fig. 1.23. Moreover, only one of three pipelines associated with pumps was modelled; other non-modelled elbows will likely be subject to similar seismic forces. However, we will consider these effects in the forthcoming subsection.

1.6.4   Efficiency analysis and fragility curves

According to Baker (2015), a PSDM is defined as efficient when the variance of the estimators is low; and in our particular case, the estimator is represented by *lnD* of Eq. (1.14). Given the results of the previous Subsection 1.6.3, only EDP3 was worthy of attention and, therefore, it was associated with the demand parameter *D*. Hence, we rearranged the seismic results as shown in both Fig. 1.25 and 1.26, and computed the coefficient of variation (COV) and the R^2 associated with (1.12). The PSDM based on the PGA achieved values of COV and R^2 equal to 0.6 and 0.6, respectively. These figures show that the correlation between PGA and EDP3 is relatively weak and associated with high dispersion (Mackie and Stojadinović, 2005, and Ebrahimian et al., 2015). On the other hand, the adoption of Sa(T) as IM, with COV and R^2 equal to 0.33 and 0.88, respectively, led to a very efficient PSDM involving a strong correlation on EDP3.
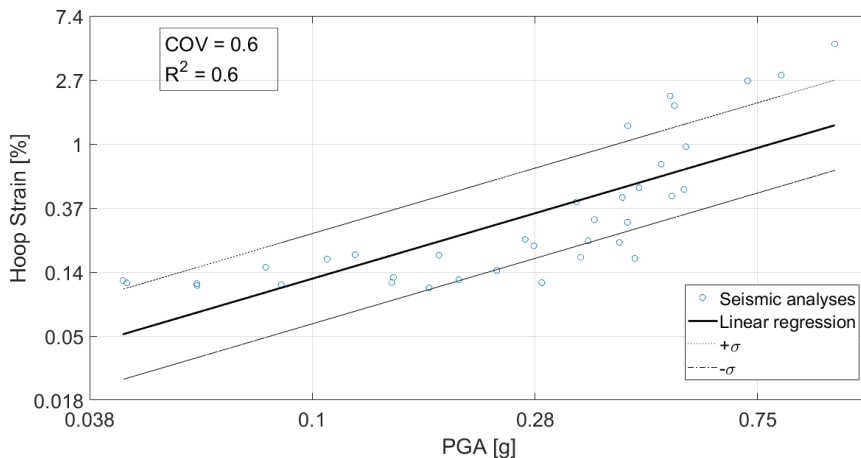
Figure 1.251 Seismic analysis results and linear regression for EDP3 and PGA as IM.
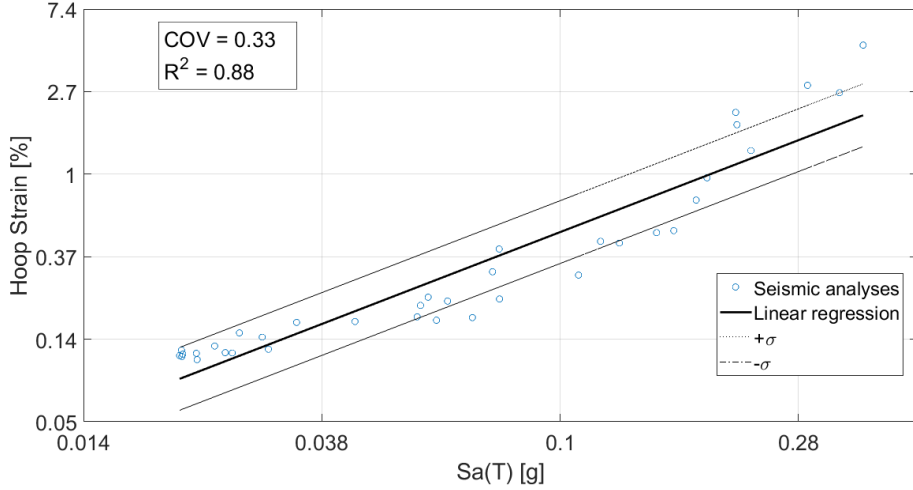
Figure 1.26 Seismic analysis results and linear regression for EDP3 and Sa(T) as IM.

In order to proceed with a fragility analysis, we computed the fragility functions $F_D(IM)$, i.e. the probability of the demand D exceeding C_{LS} as,

$$F_D(IM) = P[D \geq C_{LS}|IM = im] = \Phi\left[\frac{ln(im/m_D)}{\beta_D}\right] \qquad (1.19)$$

We note that $F_D(IM)$ was expressed using a lognormal cumulative distribution function (Baker, 2015). Both $F_D(PGA)$ and $F_D(Sa(T))$ of EDP 3 are reported in Fig. 1.27 and 1.28, respectively, whilst their parameters are listed in Table 1.12.
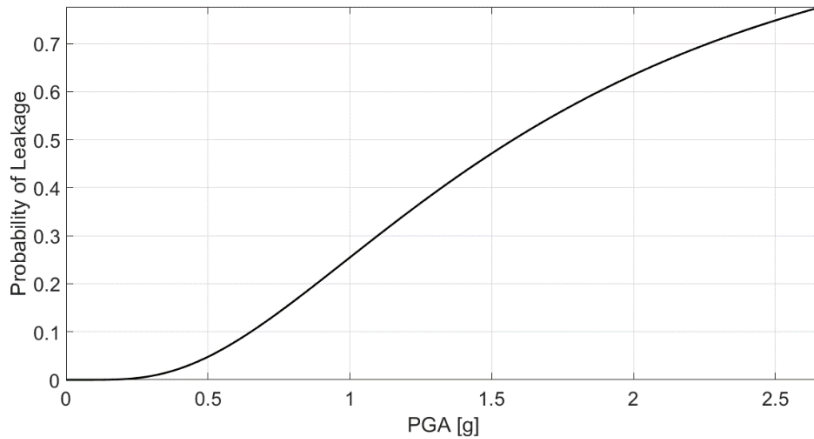
Figure 1.27 Fragility curves for EDP 3 and PGA as IM.

42
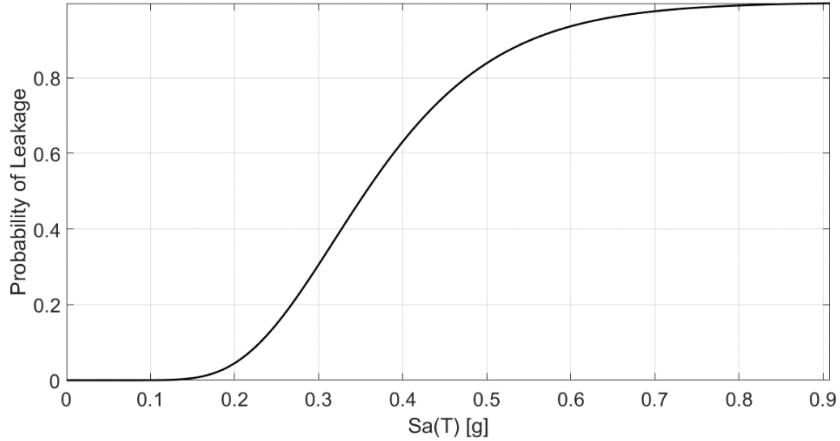
Figure 1.28 Fragility curves for EDP 3 and Sa(T) as IM.

Table 1.121 Fragility function parameters

EDP	IM	Parameters	
		m_D	β_D
3	PGA	1.62	0.71
3	Sa(T)	0.345	0.342

As a result, both $F_D(PGA)$ and $F_D(Sa(T))$ exhibit a substantial vulnerability at low PGA levels even though $F_D(Sa(T))$ is significantly more severe. Moreover, the different values of the dispersion β_D expressed by (1.17), reflect the greater value of COV associated to PGA. Given the fragility function $F_d(PGA)$ and the probability of failures involved in structural regulations EN 1990 (2002), i.e. $P_d = 7.2 \times 10^{-5}$ for ultimate limit states and $P_d = 6.7 \times 10^{-2}$ for serviceability limit states, it is important to estimate the relative annual probability *P(edp)* by means of Eq. (1.4): this read 1.38 × 10⁻⁵. Nonetheless, we also calculated the leakage probability $P_n(edp)$ over the reference life of the LNG plant, i.e. 100 years by means of

$$P_n(edp) = 1 - (1 - P(edp))^n \tag{1.20}$$

where *n* defines the number of years. $P_n(edp)$ reads 1.4 × 10⁻³ and, compared to the aforementioned probability of failure values involved in EN 1990 (2002), we deduce that $P_n(edp)$ appears to be relatively high for LOC. It is worth noting that $P_n(edp)$ refers to the elbow of the pipeline connected to the pump column and located on the tank platform shown in Fig. 1.5. However, as stated in Subsection 1.3.5, the tank platform is characterized by 3 identical pump columns, each connected to one pipeline fitted with elbows. As a result, it is

43

reasonable to assume that the leakage probability $\widetilde{P_n}(edp)$ referred to all three pipelines must be higher than $P_n(edp)$. In particular, if one assumes that LOC is considered as an independent event in each pipeline, then it follows that $\widetilde{P_n}(edp) = 3\,P_n(edp)$.

1.7 Conclusions

In this manuscript, we present a probabilistic seismic demand analysis of an LNG plant following the Performance-Based Earthquake Engineering procedure. In particular, first we evaluate the non-linear response of the whole LNG plant. Then we express the leakage risk of the most critical components of its pipeline network, i.e. elbows, by means of fragility functions. For this, we developed a mechanical model of bolted flange joints for leakage prediction, then calibrated by monotonic and cyclic joint testing. With regard to the seismic response of LNG plant components, we found that bolted flange joints are relatively safe under seismic action, whilst elbows exhibit a significant degree of vulnerability. Due to the complexity of LNG plant and the high computation demand by the FE model, we used the Cloud method for probabilistic seismic demand analysis. With regard to elbow response, we found that the maximum tensile hoop strain represents a suitable function for fragility analysis. Moreover, we show that fragility can be expressed as a function of peak ground acceleration of natural records. Nonetheless, the spectral acceleration evaluated at the period of the tank is more efficient due to the lower dispersion involved. The results of fragility functions of elbows, i.e. the probability of leakage over the reference life of the plant of about 1.4×10^{-3}, demonstrates that the examined plant characterized by a reference life of 100 years would be at risk. Therefore, an adequate pipework design for LNG plants subjected to strong earthquakes is needed, especially for piping components on top of tall tanks.

Finally, given the limited number of leakage data of elbows and the two unmodeled pipelines connected to the LNG pump columns, both the effects of uncertainty in leakage thresholds and the correlation among damage levels of critical elbows on fragility functions deserve further investigation.

Chapter 2

2. Seismic fragility assessment of a tank-piping system based on hybrid simulation and multi-fidelity surrogate modelling

Abstract

Seismic risk assessment of coupled systems of industrial plants often needs the implementation of complex finite element models able to take into account their multicomponent nature and the relevant coupling effects. These models typically rely on an extensive consumption of computational resources. Moreover, the relationships between seismic action, system response and relevant damage levels are often characterized by a high level of nonlinearity, thus requiring a solid background of experimental data. Furthermore, both fragility and reliability analyses depend on the adoption of a significant number of seismic waveforms that are generally not available when the seismic risk evaluation is strictly site-specific. With the aim to propose a methodology able to manage the above-mentioned issues, this manuscript presents a seismic reliability analysis of a coupled tank-piping system. The novelty of our approach lies in the adoption of synthetic ground motions, finite element models and experimental hybrid simulations to evaluate a reliable and surrogate model of our system. As the first step, to obtain the necessary input for a stochastic ground motion model able to generate synthetic ground motions coherent with the site-specific analysis, a disaggregation analysis of the seismic hazard is performed. Hence, we reduce the space of parameters of the stochastic ground motion model by means of an extensive global sensitivity analysis upon the seismic response of our system, evaluated with a simplified Matlab FEM. Based on the reduced space of parameters, we generate a large set of a synthetic ground motions and select, among them, a few signals to provide the input for experimental hybrid simulations. In detail, the hybrid simulator is composed by a numerical substructure, able to predict the seismic sliding response of a steel tank, and a physical substructure made of a realistic piping network. Furthermore, we use these experimental results to calibrate a refined Ansys FEM with a special focus on the most vulnerable components, i.e. pipe bends. More precisely, we focus on tensile hoop strains in elbow pipes as a leading cause for leakage, monitoring them with conventional strain gauges. Thus, we present the procedure to evaluate a numerical Kriging meta-model of the coupled system based on both experimental and finite element model results. This model will be adopted in a future development to carry out a seismic fragility analysis.

2.1 Introduction

2.1.1   Background and motivation

Industrial plants can experience different types of structural and non-structural failures when subjected to the effects of natural disasters, possibly resulting in Natech events (Cruz et. al, 2006 and Steinberg et al., 2008). Among natural disasters, earthquakes can badly affect industrial facilities causing severe damage and losses, as documented by Lanzano et al., (2015), and Krausmann et. al, (2010). For this reason, the European directive Seveso-III (Directive 2012/18/EU) demands the evaluation of the probability of Natech events for industrial plants that involve hazardous substances. In order to asses this type of probability two different actions are generally required: i) select the dangerous possible consequences associated to different types of failure, ii) evaluate the relevant probabilities of these failures related to the several possible causes. As a matter of fact, industrial plants often encompass numerous components with different associated risks and overall resistances to external actions. One of these components are pipelines, commonly adopted in petrochemical facilities and demonstrated to be vulnerable to seismic action. Among realistic failure scenarios, leakage or loss of containment (LoC) of hazardous substances is one of the possible effects of pipelines failure and can severely affect the environment and the nearby communities. Along with this line, the following manuscript investigates the seismic performances of a realistic piping network coupled to a steel tank with a special focus on LOC from bolted flange joints (BFJs), Tee joints and pipe bends, see for references, among others, Bursi et al, (2018). In this respect, seismic risk can be evaluated by means of fragility curves, see Baker, (2015), as a part of performance-based earthquake engineering (PBEE) methodology (Cornell and Krawinkler, 2000). In detail, a fragility curve can express the probability of exceedance of an engineering demand parameter (EDP) given - conditional- an intensity measure (IM). With reference to piping elbows, EDPs and relevant LOC limit states are selected after Vathi et al., (2015) and Pedot et al., (2018).

Arguably, fragility curves and so the whole PBEE approach are affected by two main sources of uncertainty, i.e. ergodic and non-ergodic (Der Kiureghian, 2005). This categorization is useful in the case of time-variant reliability, see Der Kiureghian and Ditlevsen, 2009, where the categories of aleatory and epistemic uncertainty can be further classified. As a matter of fact, seismic action is an important source of aleatory uncertainty in seismic reliability evaluation. However, under the common hypothesis that both the occurrence and the intensity of earthquakes can be described by a Poisson process, this aleatory uncertainty is renewed at each seismic event. On the other hand, non-ergodic uncertainty is comprehensive of both aleatory uncertainties, as soil-structure interaction, and epistemic uncertainties, derived for model errors and approximations.

Specifically, the variability of the seismic action and its characterization by the IM represents an ergodic uncertainty, and, for this reason, the more samples are involved, e.g. seismic records and relevant seismic response, the more accuracy we achieve. Nevertheless, it is not

possible to increase the number of natural seismic record without scaling them and possibly involving additional errors; see for reference, among others, Bommer (2004) and Luco, (2007b).

In this manuscript, we propose a methodology to address both ergodic and non-ergodic uncertainties. In detail, the epistemic part of non-ergodic uncertainty is managed with the support of experimental data obtained by means of components cyclic testing (La Salandra et al., 2016) and hybrid simulation on the system under study. As a matter of fact, Hybrid simulation (HS) is an effective technique to experimentally investigate the behavior of structural systems not easily adaptable to common testing laboratories. Specifically, the hybrid model of the system under study combines numerical (NSs) and physical substructures (PSs). In this manuscript we show the application of this approach to the coupled tank-piping system, being the steel tank the NS and the piping network the PS as showed in Abbiati et al., (2018a). Moreover, the testing campaigns provide the necessary background to properly calibrate FE models that represent the computational simulator (CS). In particular, two different CSs are presented, a refined high-fidelity (HF) FEM and a faster low-fidelity (LF) one

Conversely, we reduce the ergodic uncertainty with the implementation of synthetic ground motions based on the results of a site-specific probabilistic seismic hazard analysis (PSHA; Baker, 2008). In detail we calibrated the stochastic ground motion model as defined by Rezaeian and Der Kiureghian (2010) against a set of natural accelerograms compatible with the abovementioned PSHA. Furthermore, the space of the ground motion model parameters is reduced by means of a global sensitivity analysis (GSA) over the simulated coupled system response, see for reference Abbiati et al., (2015). In order to reduce the computational cost of the GSA, the polynomial chaos expansion (PCE, Xiu et al, 2002) is adopted to provide a surrogate model of the system response. Along this line, Sobol' indices (Sobol, 1993) are evaluated by post-processing PCE coefficients; see for reference Efron et al. (2006).

As another step of the procedure presented in this manuscript, the Kriging method is used to build a Multi-Fidelity (MF) surrogate model (Han and Görtz, 2012 and Abbiati et al., 2015) based on both the CS and HS results. Finally, the MF surrogate model of the coupled tank-piping system is adopted to perform a seismic fragility analysis with a cheap computational cost.

2.1.2   Scope

The PBEE methodology is affected by two main sources of uncertainties, ergodic, related to seismic action randomness, and non-ergodic, associated to errors and approximations in physical models. In order to cope with these issues, the authors present a rigorous procedure for deriving fragility curves of structural components based on multi-fidelity structural simulators calibrated against hybrid testing experiments and a stochastic model of the seismic input calibrated against real records. In particular, the seismic fragility analysis concerns a realistic tank-piping system with a special attention on LoC from vulnerable components.

For the sake of clarity, the manuscript is organized as follows: Section 2 contains a description of the coupled tank-piping system under study together with the model of the seismic input and the relevant experimental campaigns: In Section 3 both a low-fidelity and a high-fidelity FE model are described together with their calibration against the experimental results. Thus, Section 4 presents the procedure to evaluate the multi-fidelity Kriging surrogate model and to derive the relevant seismic fragility curves. Finally, in Section 5 the main conclusions are drawn, and future developments are proposed.

2.2 Description of the case study

The following subsection provides insight about the coupled tank piping system understudy, alongside with the model of the seismic input and the experimental campaigns.

2.2.1   Tank-piping system

The coupled tank piping system is composed by a steel slender tank and a piping network connected through a BFJ. In detail, the piping network consists of 8" (outer diameter: 219.08mm; thickness: 8.18mm) and 6" (outer diameter: 168.28mm; thickness: 7.11mm) schedule 40 straight pipes and contains several critical components, i.e. two elbows, a bolted flange joint and a Tee-joint. Moreover, the piping material is a API 5L X52 steel, equivalent to the European P355 steel. On the other hand, the steel tank is 14 meters high with a diameter of 8 meters and supposed to be filled with oil. Moreover, the steel tank is placed unanchored on a concrete foundation, in this respect Fig. 2.1 depicts the coupled system.
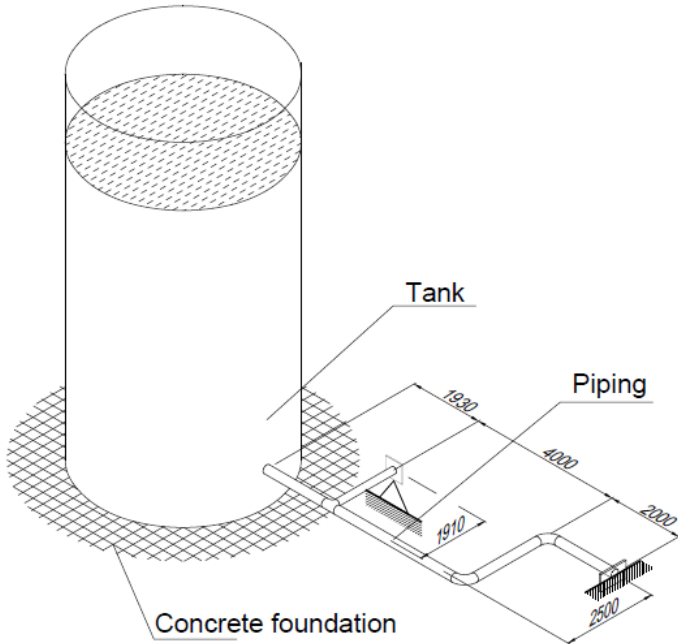
Figure. 2.1: Realistic tank-piping system, measures in mm.

In addition, being the tank unanchored it is supposed to slide if subjected to a sufficient external action.

2.2.2   Seismic input

As a matter of fact, the variability of the seismic action and its characterization by a generic intensity measure (IM) are a source of uncertainty and error in fragility analyses. Nevertheless, these intensity variables (Der Kiureghan, 2005) are ergodic, i.e. statistically independent in the time domain, and, for this reason, the more samples are used, e.g. more seismic waveforms, the more accuracy will be obtained.

However, while it is possible to lower the uncertainty of seismic input by studying a large set of accelerograms, the availability of natural records is clearly limited. For this reason, with the aim of adopting a number of seismic signals higher than the available set of coherent natural accelerograms, we decided to use artificial ones. In detail we implemented a multi-step procedure to calibrate a stochastic ground motion model and generate coherent artificial seismic signals.

The first step of this procedure is performing a probabilistic seismic hazard analyses (PSHA), Cornell (1968) and Baker (2017), of a hypothetical geographical location where our case study would be placed, i.e. Hanford in California (US). We relied on the United States Geological Survey (USGS) database and the relevant PSHA results are depicted in Fig. 2.2 and 2.3.
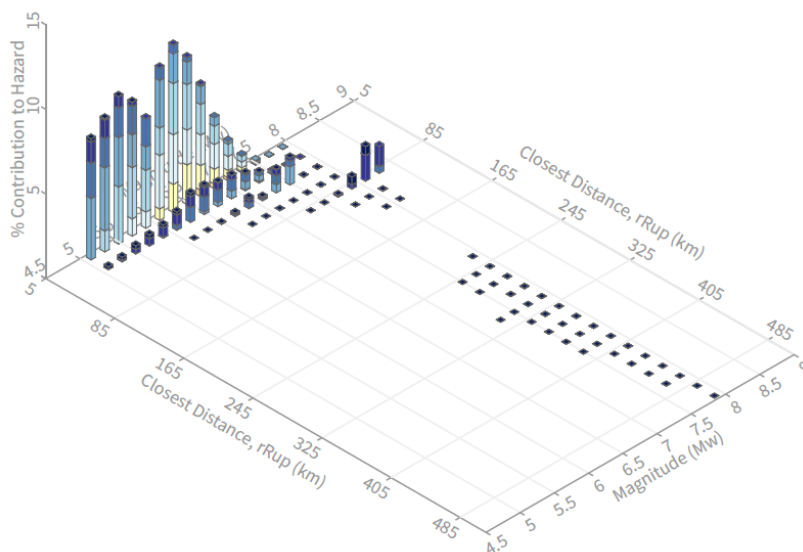
Figure. 2.2: Probabilistic seismic hazard deaggregation analysis for Hanford, California (US).
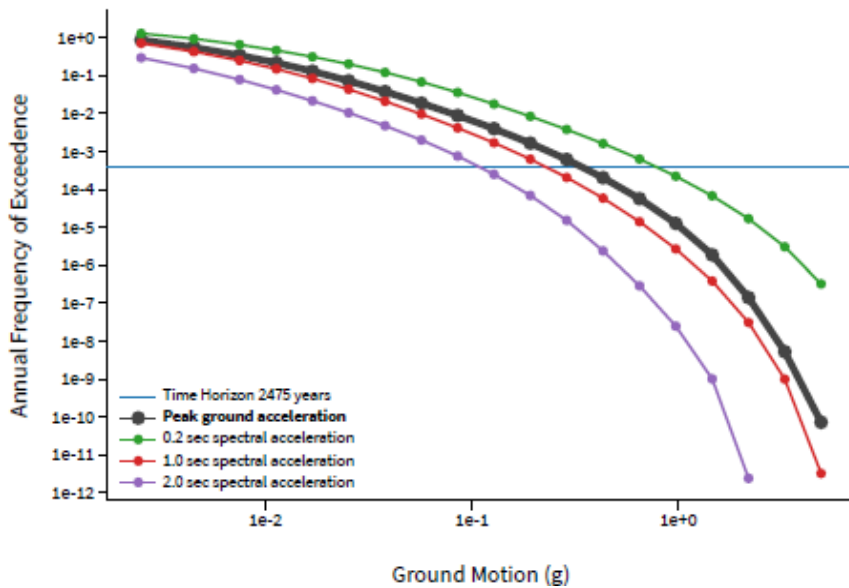
Figure. 2.3: PSHA for Hanford, California (US).

From the deaggregation analysis, see Fig. 2.2, we obtain the mode values for magnitude (M) and distance from the fault (R), which read 6.3 and 10.75 km respectively. Thus, based on these two values, a set of 7 compatible accelerograms is selected, as reported in Table 2.1.

Table 2.1: Set of compatible accelerograms.

Earthquake Name	Year	Station Name	Magnitude	Distance (km)
"Northridge-01"	1994	"Canoga Park - Topanga Can"	6.69	14.7
"Northridge-01"	1994	"Canyon Country - W Lost Cany"	6.69	12.44
"Northridge-01"	1994	"N Hollywood - Coldwater Can"	6.69	12.51
"Northridge-01"	1994	"Northridge - 17645 Saticoy St"	6.69	12.09
"Northridge-01"	1994	"Simi Valley - Katherine Rd"	6.69	13.42
"Northridge-01"	1994	"Sun Valley - Roscoe Blvd"	6.69	10.05
"Northridge-01"	1994	"Sunland - Mt Gleason Ave"	6.69	13.35
"Northridge-02"	1994	"Pacoima Kagel Canyon"	6.05	11.34

As it is possible to notice from Table 1, all the different signals are related to the same event, i.e. Northridge earthquake. Though this earthquake is clearly compatible with the geographical location, we decide to rely on a single event in order to limit the variability of the calibration input. In fact, the stochastic ground motion model, that we adopt in this work is already capable of taking into account a sufficient level of variability. In detail, the model

was developed by Razaeian and Der Kiureghian (2010) and generates synthetic ground motions processing 6 different parameters, listed in Table 2.2, by means of the following expression:

$$a_g(t) = q(t, \boldsymbol{\alpha}) \left[\frac{1}{\sigma_f(t)} \int_{-\infty}^{t} h(t - \tau, \boldsymbol{\lambda}(\tau)) \omega(\tau) d\tau \right] \tag{2.1}$$

Table 2.2: Stochastic ground motion model parameters.

I_a	Arias intensity
$D_{5\text{-}95}$	Time interval of 95% of the I_a
t_{mid}	Time at which 45% of the I_a is reached
ω_{mid}	Filter frequency at t_{mid}
ω'	Rate of change of the filter frequency with time
$\zeta_f,$	Filter damping ratio (constant).

Eq. (2.1) can be considered as the combination of three different factors, being the first of them $(t, \boldsymbol{\alpha})$, i.e. the time modulating function (TMF), given as following:

$$\begin{cases} q(t, \boldsymbol{\alpha}) = 0 & \text{if } t \leq 0 \\ q(t, \boldsymbol{\alpha}) = \alpha_1 t^{\alpha_2 - 1} exp(-\alpha_3 t) & \text{if } t < 0 \end{cases} \tag{2.2}$$

where $\hat{\boldsymbol{\alpha}}$ is defined by means of:

$$\hat{\boldsymbol{\alpha}} = arg \min_{\boldsymbol{\alpha}} \left(\left| I_a(t_{45}) - \hat{I}_a(t_{45}) \right| + \left| I_a(t_{95}) - \hat{I}_a(t_{95}) \right| \right) \tag{2.3}$$

with:

$$I_a(t) = \frac{\pi}{2g} \int_0^t a_g^2(\tau) d\tau : \text{Arias intensity of the real record} \tag{2.4}$$

$$\hat{I}_a(t) = \frac{\pi}{2g} \int_0^t q^2(t, \boldsymbol{\alpha}) d\tau : \text{Arias intensity from the time modulating function} \tag{2.5}$$

The second factor in Eq. (2.1) is $h(t - \tau, \boldsymbol{\lambda}(\tau))$, i.e. the Impulse Response Function (IRF) of a linear time-varying filter, expressed as follows:

$$\begin{cases} h(t-\tau, \boldsymbol{\lambda}(\tau)) = \dfrac{\omega_f(\tau)}{\sqrt{1-\zeta_f^2(\tau)}} exp[-\zeta_f(\tau)\omega_f(\tau)(t-\tau)]sin\left[\omega_f(\tau)(t-\tau)\sqrt{1-\zeta_f^2(\tau)}\right] & if\ \tau \leq t \\ h(t-\tau, \boldsymbol{\lambda}(\tau)) = 0 & if\ \tau > t \end{cases} \quad (2.6)$$

where:

$$\omega_f = \omega_{mid} + \omega'(t - t_{mid}) \quad (2.7)$$

Eq. (2.6) can also be used to compute $\sigma_f(t)$, by means of:

$$\sigma_f^2(t) = 2\pi S \int_{-\infty}^{t} h^2(t-\tau, \boldsymbol{\lambda}(\tau))d\tau \quad (2.8)$$

The last of the three factors, $\omega(\tau)$, is the baseline noise. It is possible to notice that the parameters listed in Table 2 influence both the TMF and the IRF while $\omega(\tau)$ is only affected by the baseline noise variability.

Following the calibration process described by Razaeian and Der Kiureghian (2010), we evaluate the model parameters able to generate a set of accelerograms similar to those listed in Table 2.1. Once we get these values we make two hypotheses in order to define a statistical distribution for each of the model parameters. The first hypothesis is considering the parameters as statistically uncorrelated. With reference to this, the actual linear correlations between the different parameters are shown in Fig. 2.4. The second hypothesis is the choice of uniform distributions to describe the probability distributions of all the parameters, with the only exception of ω' that we consider constant with a value of -0.568 rad/s^2. With regard to the uniformly distributed parameters, their lowest and highest boundaries, set to encompasses all the values retrieved from the aforementioned calibration process, are listed in Table 2.3.

Table 2.3: Distributions of stochastic parameters

Name	Distribution	LB	UB	Units
I_a	Uniform	0.019	3.992	m^2/s^3
D_{5-95}	Uniform	5.083	16.810	s
T_{45}	Uniform	1.596	5.664	s
ω_{mid}	Uniform	14.620	31.000	rad/s
ζ	Uniform	0.074	0.557	-
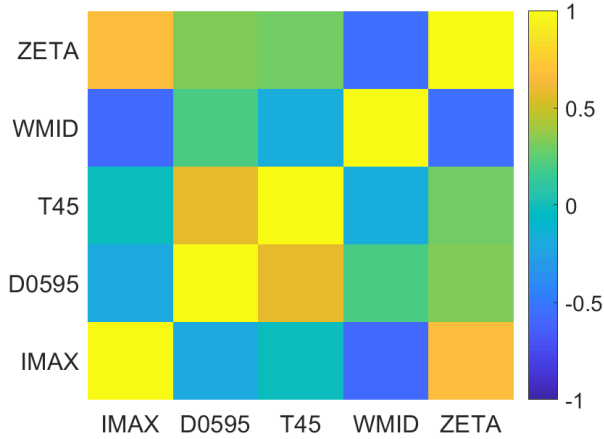
Figure. 2.4: Linear correlation of stochastic parameters.

It is worthwhile to notice from Table 2.3 that the degree of variability among the different parameters is not uniform. As a matter of fact, while I_a and ζ exhibit wide distributions, the other three parameters are encompassed in a narrower range of values. Moreover, as shown in Fig. 2.4, the hypothesis of uncorrelated parameters is not so dissimilar from the reality. Finally, with the above-mentioned parameters distributions and the model described by Eq. 2.1, it is possible to generate synthetic ground motions coherent with the seismic hazard characteristics of our geographical site.

Nevertheless, to prepare the experimental campaign, we have to select the proper seismic input taking into account the limited number of tests practically manageable. On the other hand, we need to guarantee a certain variability of the parameters listed in Table 2.2 to properly calibrate the surrogate model. For this reason, a preliminary step is that to reduce the space of these parameters selecting those with the highest influence on the system seismic response. In order to select a simple parameter to identify the seismic response with, the maximum sliding displacement of the steel tank, see Fig. 2.5 for reference, is chosen. As a matter of fact, it is straightforward that the sliding displacement a reliable benchmark of the external load on the piping system.
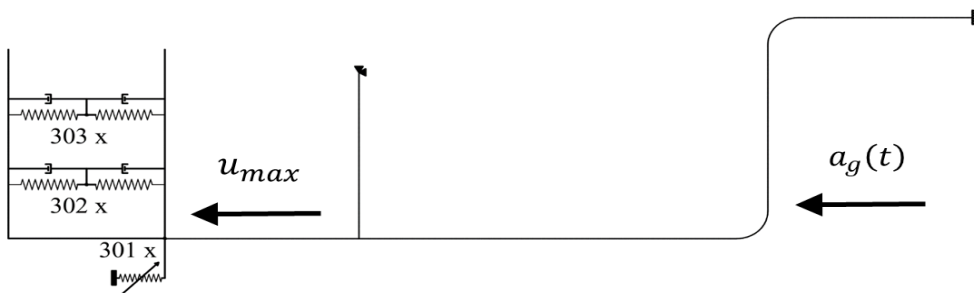
Figure. 2.5: Scheme of system input/output.

Once the choice of inputs and outputs, respectively x and y, is done, it is possible to formalize them by means of:

$$x \in X_{ED} = \{I_a, D_{5-95}, T_{45}, \omega_{mid}, \zeta\} \qquad (2.9)$$

$$y \in Y_{ED} = u_{max}^{80\%} \qquad (2.10)$$

Thus, a set of 2e2 stochastic ground motion model parameters is generated according to the distributions defined in Table 2.3, in order to perform a Monte Carlo (MC) analysis with a simplified MATLAB model. However, this set is expanded to a total of 4e4 artificial accelerograms combining each of the 2e2 parameters realizations with 2e2 different baseline noises, $\omega(\tau)$. A preliminary analysis on a smaller set is realized with a convergence check upon the 80% percentile of the maximum displacements, as depicted in Fig. 2.6 while the complete distribution of u_{max} is shown in Fig. 2.7.
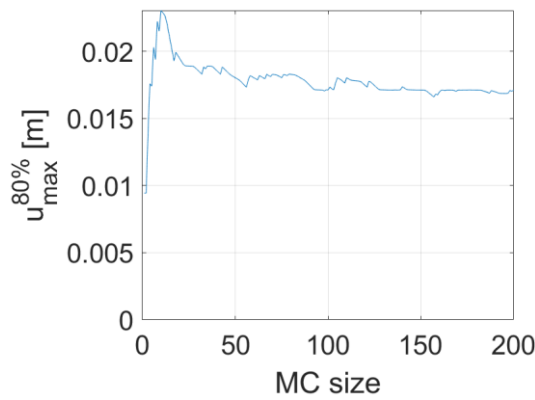
Figure. 2.6: Convergence of the 80th percentile of maximum sliding displacement.
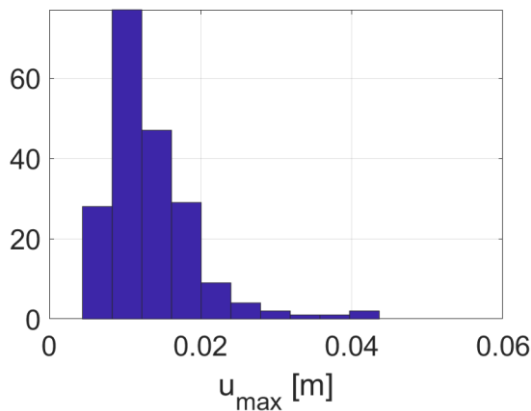
Figure. 2.7: Distribution of maximum sliding displacements.

Therefore, a global sensitivity analysis (GSA) is performed to assess the individual contributions of each of the input variables to the variance of the model response. A GSA

can be carried out with Sobol' decomposition (also called general ANOVA decomposition) of the computational model, which allows one to decompose a full model response in submodels, according to Sobol, 1993. As stated in Marelli and Sudret, 2014, polynomial chaos expansion (PCE) methodology provides an effective way to estimate the Sobol' indices, by post-processing the polynomial coefficients. The analytical formulation of PCE method can be written as follows:

$$\hat{y}(x) = \mathcal{M}^{PC}(x) = \sum_{\alpha \in \mathcal{A}^{M,p}} y_\alpha \Psi_\alpha(x)$$

(2.11)

Where Ψ_α is a multivariate polynomial with multi-index vector α, y_α is the coefficient of a single multivariate polynomial and $\mathcal{A}^{M,p} = \{\alpha \in \mathbb{N}^M : |\alpha| \le p\}$ is the truncated set of multi-indices. In particular Ψ_α, can be written as:

$$\Psi_\alpha(x) \stackrel{\text{def}}{=} \prod_{i=1}^{M} \phi_{\alpha_i}^{(i)}(x_i)$$

(2.12)

where $\Psi_{\alpha_i}^{(i)}(X_i)$ is a univariate polynomial of degree α_i orthonormal with respect to the distribution of the input variable X_i. With respect to this, Table 2.4 summarizes the usual pairs of polynomial families with their associated PDFs.

Table 2.4: Classical families of orthogonal polynomials and the related PDFs.

Probability density function	Orthogonal polynomials
Uniform	Legendre
Gaussian	Hermite
Gamma	Laguerre
Beta	Jacobi

Furthermore, the expected value and the relevant variance can be written as:

$$E[\mathcal{M}^{PC}(x)] = y_0$$

(2.13)

$$Var[\mathcal{M}^{PC}(x)] = \sum_{\substack{\alpha \in \mathcal{A}^{M,p} \\ \alpha \neq 0}} y_\alpha^2$$

(2.14)

In order to proceed with Sobol' decomposition of the computational model M and according to the procedure reported in Abbiati et. al, 2015, we can write:

$$M(x) = M_0 + \sum_{i=1}^{M} M_i(x_i) + \sum_{1 < i < j \leq M} M_{ij}(x_i, x_j) + \cdots + M_{12\ldots M}(x) \tag{2.15}$$

Where M_0 is a constant, $\{M_i(x_i), 1 \leq i \leq M\}$ are univariate functions, $\{M_{ij}(x_i, x_j), 1 \leq i < j \leq M\}$ are bivariate functions. With the definition of a multi-index $\boldsymbol{u} = \{i_1, \ldots, i_s\} \subset \{1, \ldots, M\}$, the Sobol' decomposition can be rewritten as:

$$M(x) = M_0 + \sum_{\substack{\boldsymbol{u} \subset \{1,\ldots,M\} \\ \boldsymbol{u} \neq \emptyset}} M_{\boldsymbol{u}}(x_{\boldsymbol{u}}) \tag{2.16}$$

Partial variances can be defined as follows:

$$D_{\boldsymbol{u}} \stackrel{\text{def}}{=} \mathrm{Var}\big(M_{\boldsymbol{u}}(X_{\boldsymbol{u}})\big) \tag{2.17}$$

By taking into account the orthogonality of the elements of the decomposition, total variance of the model output can accordingly be defined as the sum of the partial variances over all the possible subsets:

$$D \stackrel{\text{def}}{=} \mathrm{Var}\big(M(X)\big) = \sum_{\substack{\boldsymbol{u} \subset \{1,\ldots,M\} \\ \boldsymbol{u} \neq \emptyset}} D_{\boldsymbol{u}} \tag{2.18}$$

The Sobol' index for each subset of input variables $\boldsymbol{u}$ can be written as follows:

$$S_{\boldsymbol{u}} = \frac{D_{\boldsymbol{u}}}{D} \tag{2.19}$$

On the other hand, *first-order* Sobol' indices are defined as:

$$S_i = \frac{D_i}{D} \tag{2.20}$$

These indices measure the contribution of each single variable (without interactions with others) to the total variance. Conversely, Total Sobol' indices quantify the entire contribution of each variable, both singularly and in interaction with others, to the total variance:

$$S_i^T = \sum_{\mathbf{u} \ni i} S_{\mathbf{u}} \tag{2.21}$$

By means of (2.14) we can rewrite (2.20) and (2.21) as:

$$\hat{S}_i^{PC} = \frac{\sum_{\boldsymbol{\alpha} \in \mathcal{A}_i} \hat{y}_{\boldsymbol{\alpha}}^2}{\sum_{\substack{\boldsymbol{\alpha} \in \mathcal{A} \\ \boldsymbol{\alpha} \neq \mathbf{0}}} \hat{y}_{\boldsymbol{\alpha}}^2}, \quad \mathcal{A}_i = \{\alpha \in \mathcal{A} : \alpha_i > 0, \ \alpha_{j \neq i} = 0\} \tag{2.22}$$

and

$$\hat{S}_i^{T,PC} = \frac{\sum_{\boldsymbol{\alpha} \in \mathcal{A}_i^T} \hat{y}_{\boldsymbol{\alpha}}^2}{\sum_{\substack{\boldsymbol{\alpha} \in \mathcal{A} \\ \boldsymbol{\alpha} \neq \mathbf{0}}} \hat{y}_{\boldsymbol{\alpha}}^2}, \quad \mathcal{A}_i^T = \{\alpha \in \mathcal{A} : \ \alpha_i > 0\} \tag{2.23}$$

Finally, the results of GSA with the relevant values of Sobol' indices are shown in Fig. 2.8.
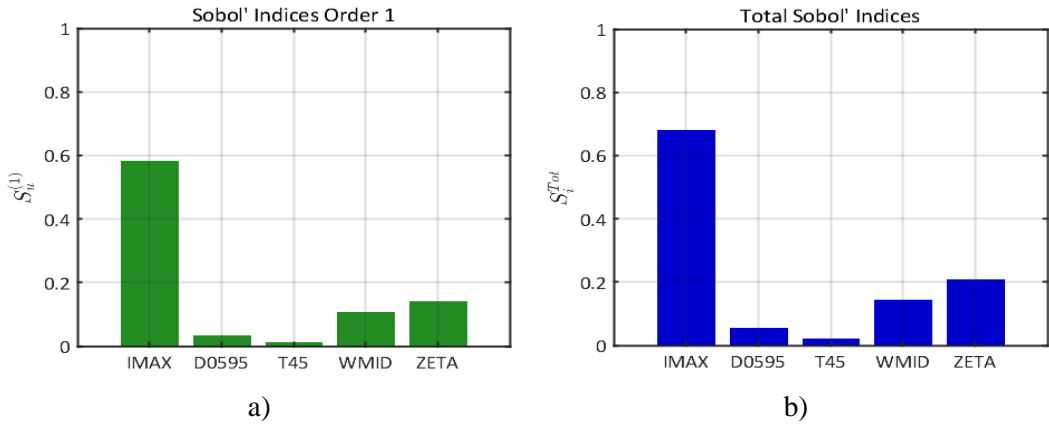
Figure. 2.8: a) first-order and b) total Sobol' indices.

From Fig. 2.8 it is possible to notice that three parameters generate most part of the output variance, i.e. I_a, ω_{mid} and ζ. This is somehow expected since they represent the most significant part of the intensity of accelerograms physical effects. Besides, based on GSA results these three parameters are chosen to vary according to the statistical distributions defined in Table 2.3, while the remaining three are fixed at their average value as reported in Table 2.5.

Table 2.5: Constant parameters.

Name	Value	Units
D_{5-95}	10.441	s

T_{45}	3.700	s
ω'	-0.568	rad/s^2

According to these modified distributions, a new set of 4e4 artificial accelerograms is so generated combining 2e2 parameters realizations with 2e2 different baseline noises. Thus, from this set of artificial accelerograms, seven signals are selected to be tested with HS. Among them, 4 are chosen to keep the system in the linear regime, equivalent to service limit state (SLS), and 3 to go slightly in the non-linear regime, to investigate ultimate limit state (ULS). This categorization is made upon u_{max} value, by setting $u_{max} < 0.04\ m$ for SLS signals and $u_{max} > 0.06\ m$ for ULS ones. Spectral accelerations and displacements of these 7 accelerograms are depicted in Fig. 2.9 and 2.10 respectively with SLS signals in blue and ULS in red.
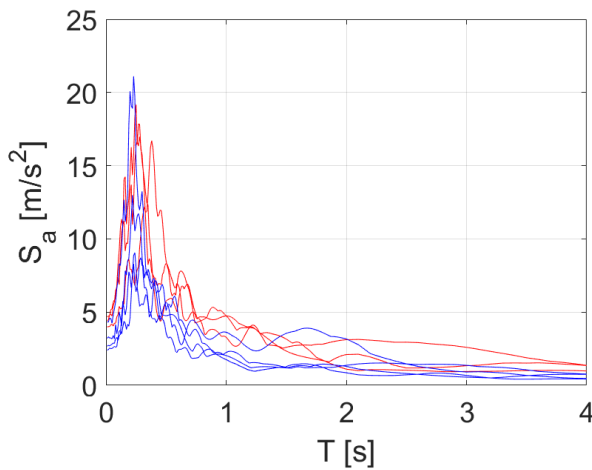
Figure. 2.9: Spectral accelerations of ULS (red) and SLS (blue) synthetic ground motions
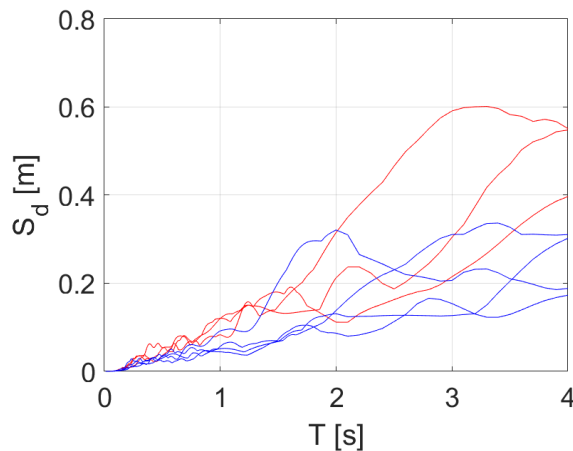
Figure. 2.10: Spectral displacements of ULS (red) and SLS (blue) synthetic ground motions

58

2.2.3 Cyclic and hybrid-testing campaign

Two different experimental campaign are carried out, the first aims at investigates tee joint behavior and their LOC limit states while the second one is performed with hybrid simulations and concerns the whole coupled system.

2.2.3.1 Cyclic and monotonic tests on tee joints.

Among industrial piping system components, tee joints are one of the most critical due to stress concentration. For this reason, several different design solutions are employed to make these joints more resistant. Considering the specific case of petrochemical plants, the event of loss of containment (LOC) in tee joints can generate severe consequences. Earthquakes are certainly a highly demanding external action, and, for this reason, seismic risk assessment is a very important part of plant design. However, tee joints seismic resistance is poorly investigated and, consequently, related regulations prescriptions lack of detail and precision which can lead to an inefficient design and incorrect safety assessment. In addition, there are very few experimental data on tee joints making difficult the development of FEM models.

In this experimental campaign two different sets of tee joints are considered:

- connection with a fitting, denoted as TJ_NR and reported in Fig. 2.11 (left) and

- T-joint with a welded reinforcement plate, denoted as TJ_YR and shown in Fig. 2.11 (right).

The pipes are made of P355 steel (Grade X52) with a yield stress of 380 MPa while the fitting steel has a nominal yield stress of 355 MPa. More in detail, the relevant geometric and mechanical characteristics of the specimens are reported in Table 2.6.

Table 2.6: Geometrical and mechanical properties of tee joints (dimensions in mm).

Design	Diameter	Thickness	Length	Material
Main pipe	219.1 (8'')	8.2	1568	P355N steel fy = 380 MPa
Branch pipe	168.3 (6'')	7.1	678	P355N steel fy = 380 MPa
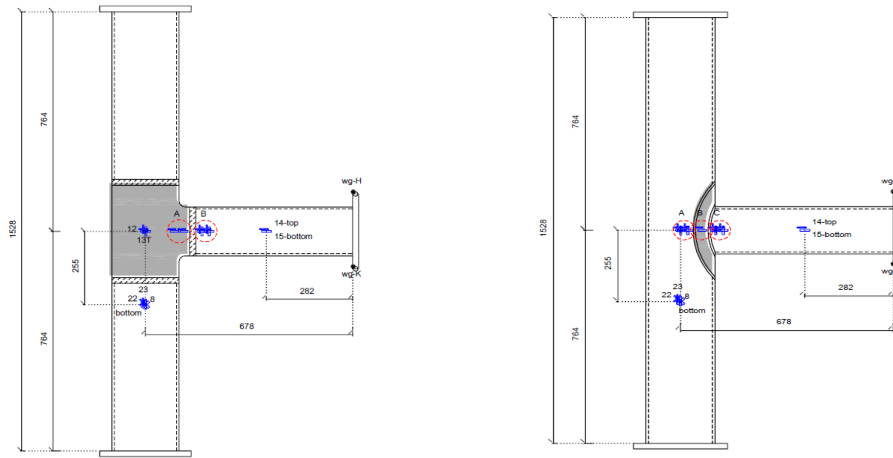
Figure. 2.11: Two types of tee joint branch connection studied: (left) fitting, TJ_NR; (right) welded reinforcement ring-plate, TJ_YR.

With reference to external load, monotonic and cyclic (ECCS 45, 1983) loadings are applied by means of a 100 tons MTS actuator, see Fig. 2.12, and a value of 3.2 MPa is chosen for internal pressure in order to investigate if this could affect the mechanical properties of the joints. A total of four tests are carried out, whose results allow the definition of two separate force-deformation curve with yielding and LOC points.

Specifically, the experimental investigation consists of four tests on tee joint pipe connections. Moreover, two types of branch to main pipe connections are considered: i) connection with a fitting, denoted as TJ_NR and ii) tee joint with a welded reinforcement plate, denoted as TJ_YR. These specimens are subjected to monotonic and low cycle fatigue tests until a LOC occurred. In Table 2.7 the actual test program is reported while in Fig. 2.12 the test set-up is shown. For all tee joints tests, strain gauges are placed at critical locations to determine the strain distribution in the region of the joint studied. In addition, a wire position transducer is used for the load-point displacement (LPD) measurements.
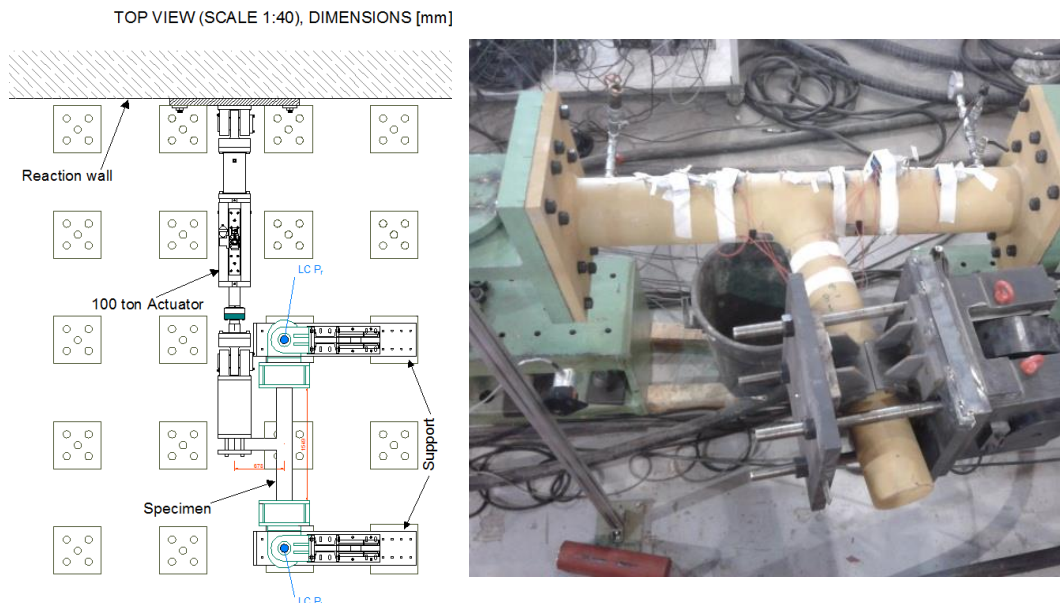
Figure. 2.12: Experimental set-up for in-plane bending tests: (left) top view; (right) the TJ_NR_Mo specimen during test.

Table 2.7: Test program of tee joints.

No.	Test type	Test name	Loading protocol
1	Bending (In-plane)	TJ_NR_Mo	Monotonic
2	Bending (In-plane)	TJ_NR_Cy	Cyclic (ECCS45)
3	Bending (In-plane)	TJ_YR_Mo	Monotonic
4	Bending (In-plane)	TJ_YR_Cy	Cyclic (ECCS45)

Finally, results are depicted in Fig. 2.13 showing both the crack and buckling detection on the Tee joint without reinforcement under monotonic loading (TJ_NR_Mo), while in Fig. 2.14 the leakage occurrence instant, during the test of the reinforced specimen under monotonic loading (TJ_YR_Mo), is reported as well. Moreover, a comparison between the moment-rotation curves of different specimens is presented in Fig. 2.15 for both the monotonic and cyclic loading. Furthermore, it is worthwhile to notice that tests have been conducted until the LOC is reached so that the leakage conditions correspond to the maximum values on the moment-rotation curves. Finally, in Table 2.8 the relevant results in terms of moments, rotations and ductility are reported.
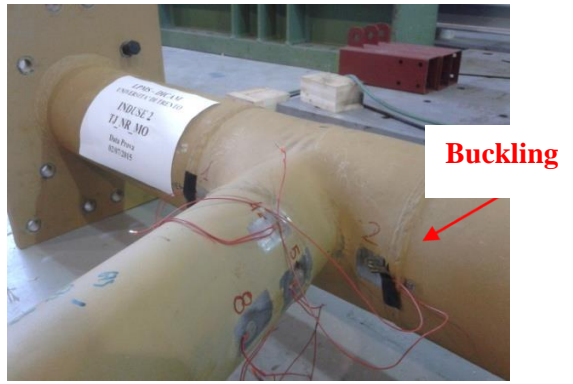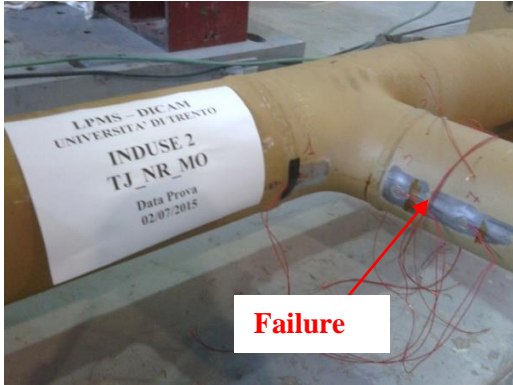
Figure. 2.13: The tee joint without reinforcement subjected to monotonic loading after the test: (left) crack detection; (right) buckling phenomena in compressive zone.

Figure. 2.14: Leakage detection during the test of the reinforced specimen under monotonic loading.
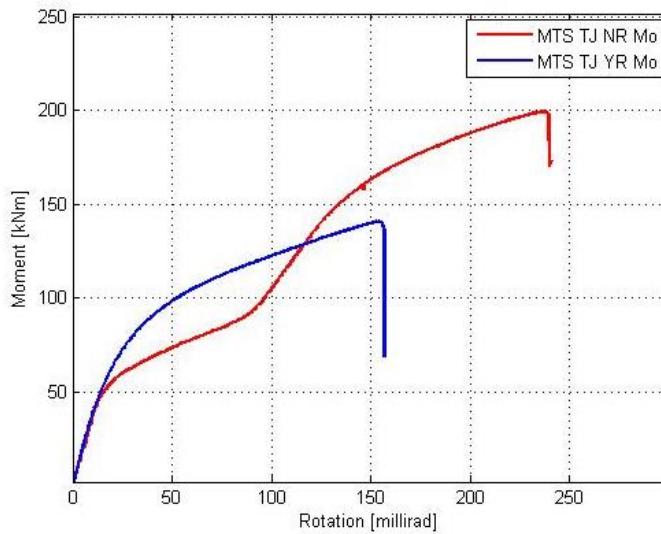
(a)
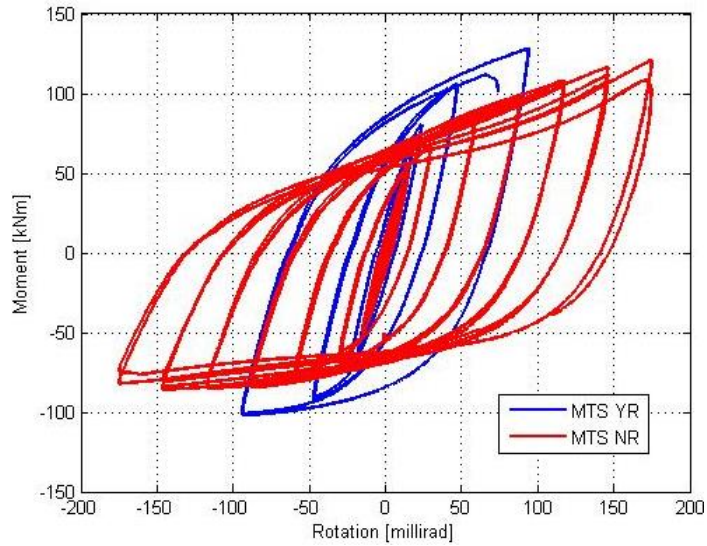
(b)

Figure. 2.15: Comparison of moment-rotation curves: (a) monotonic loading; (b) cyclic loading.

Table 2.8: Main results from tee joint tests.

Test	M_y [kNm]	φ_y [mrad]	M_{max} [kNm]	φ_{max} [mrad]	μ_φ [-]
TJ_NR_Mo	56.5	15.0	199.5	237.1	15.8
TJ_YR_Mo	89.4	25.1	153.4	140.9	5.61
TJ_NR_Cy	76.5	19.2	121.0	174.7	9.1
TJ_YR_Cy	89.3	20.6	127.2	93.8	4.6

According to Table 2.8 tee joints without reinforcing pad are found to have a higher resistance, both under monotonic and cyclic loading. Besides, these findings suggest that the reinforced pad increase the joint stiffness leading to a non-ductile fracture without a beneficial exploitation of steel ductility properties. In addition, due to a more brittle failure, the intensity of the leakage event is noticed to be more severe in reinforced tee-joints. This phenomenon could be explained with the differences in stiffness and ductility between tee joints; and it can play an important role in the overall seismic vulnerability of piping systems. As a result, the stiffness data are adopted to model the tee joint of the piping network understudy as an equivalent rotational spring.

2.2.3.2 Hybrid simulations campaign

The second campaign of experimental tests is performed by means of hybrid simulations, with a numerical substructure (NS), i.e. the unanchored tank, replaced by a MTS actuator

and a physical substructure, i.e. the piping network, as in Abbiati et al., 2018a. The numerical substructure of the hybrid simulator (HS) is modelled with a simplified model based on Malhotra et al., 2000, as showed in Fig. 2.16 while the relevant parameters are reported in Table 2.9. For reference, the main scheme of HS is shown in Fig. 2.17.
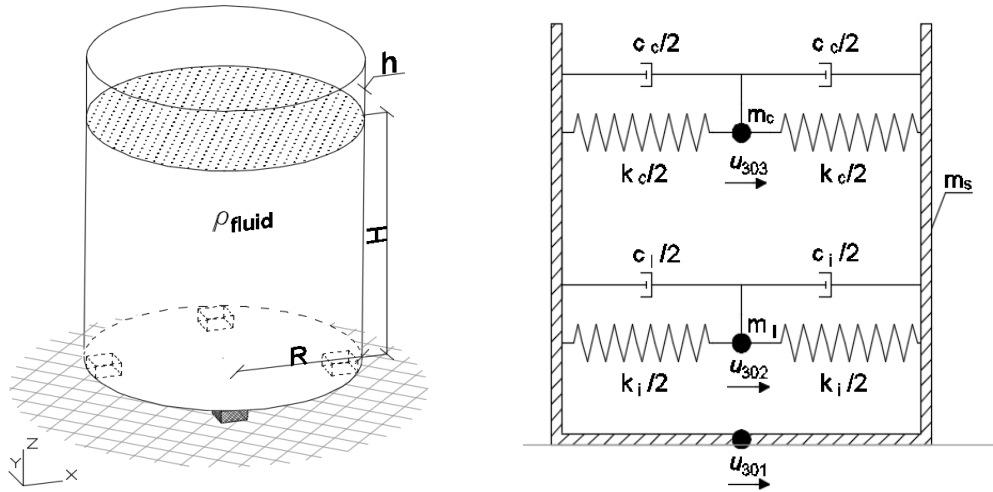
Figure. 2.16: Simplified tank model after Malhotra et al., 2000.

Table 2.9: Simplified tank model parameters.

Parameter	Value	Unit
E	210	GPa
ρ_{fluid}	900	kg/m³
ρ_{tank}	7850	kg/ m³
c_c	1.69e3	Ns/m
c_i	1.93e6	Ns/m
H	14	m
R	4	m
m_t – steel tank mass	1.65e4	kg
m_l – liquid mass	6.33e5	kg
m_c – convective mass	7.98e4	kg
m_i – impulsive mass	5.47e5	kg
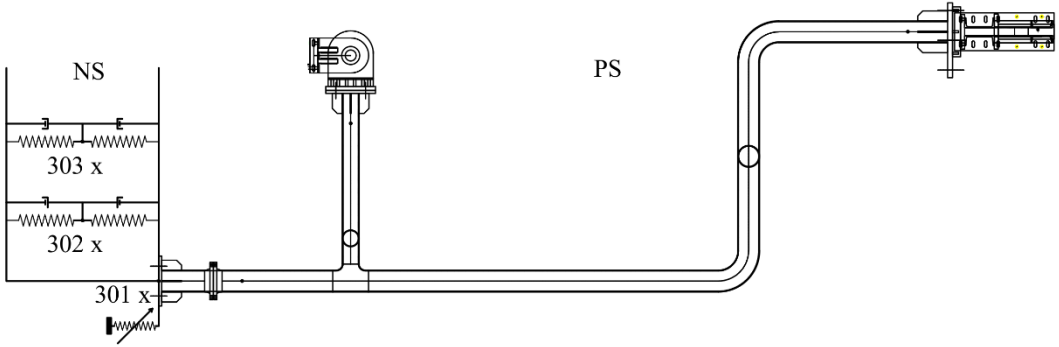
Figure. 2.17: Hybrid simulator scheme.

Furthermore, the sliding effect at the base of the tank is set to replicate the friction interaction between the tank steel bottom and a concrete foundation. In detail, this effect is implemented into the NS trough a static friction model analytically described by a non-linear hysteretic model after Mostaghel, 1999. The model is shown in Fig. 2.18 while its analytical formulation follows:

$$\begin{cases} \dot{r} = \left(\alpha_{MST}k_{MST} + (1 - \alpha_{MST})k_{MST}\big(\bar{N}(v)\bar{M}(s - \delta_{MST}) + M(v)N(s + \delta_{MST})\big)\right)v \\ \dot{u} = v \end{cases} \quad (2.24)$$

with,

$$s = \frac{r - \alpha_{MST}k_{MST}u}{(1 - \alpha_{MST})k_{MST}} \quad (2.25)$$
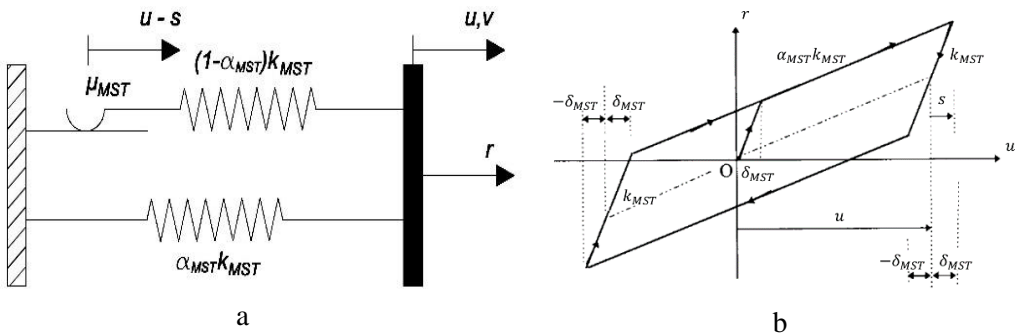
a

b

65

The remaining functions $N, M, \bar{N}$ and $\bar{M}$ read,

$$N(v) = 0.5\big(1 + sgn(v)\big)\Big(1 + \big(1 - sgn(v)\big)\Big)$$

$$M(v) = 1 - N(v)$$

$$\bar{N}(v) = M(-v) \tag{2.26}$$

$$\bar{M}(v) + N(-v)$$

where $sgn(\cdot)$ is the sign function.

Specifically, we made the hypothesis of a static friction coefficient for the interaction steel-concrete equal to $\mu = 0.1$ after Gorst et al., 2003. The parameters k_{MST}, α_{MST} and δ_{MST} represent initial stiffness, post-yielding stiffness reduction factor and yielding displacement of the idealized spring system. These parameters are set in order to replicate the static friction phenomenon as follows:

$$\delta_{MST} = \Delta = 1e - 3 \, m$$
$$\alpha_{MST} = 1e - 3$$
$$k_{MST} = \frac{\mu(m_l + m_t)g}{\Delta} = 2.18e + 8 \frac{N}{m} \tag{2.27}$$

With reference to the PS, the piping network consists of 8" (outer diameter: 219.08mm; thickness: 8.18mm) and 6" (outer diameter: 168.28mm; thickness: 7.11mm) schedule 40 straight pipes and contains several critical components, i.e. two elbows, a bolted flange joint and a tee joint. In this respect, see Fig. 2.19 and 2.20. Moreover, the piping network is filled with water at a pressure of 15 bar.

Figure. 2.19: Experimental setup, physical substructure of hybrid simulator.
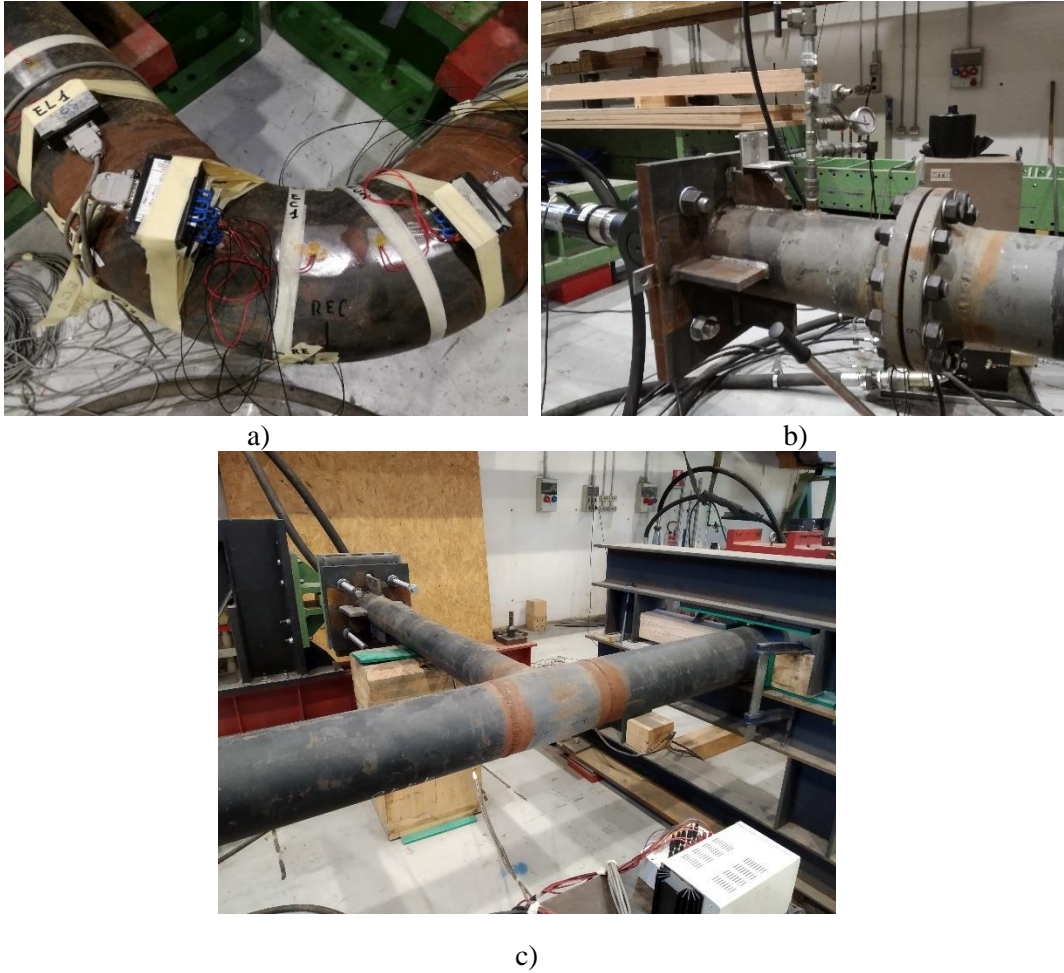
Figure. 2.20: a) piping elbow, b) bolted flange joint and c) tee joint .

A set of different sensors, specifically strain gauges (SGs) and linear transducers (LVDTs), is placed on the experimental setup. In detail, three SGs are positioned on both the elbows (named E81 and E82) in order to detect hoop strain levels, while four LVDTs are placed on the first of the two elbows. With respect to this see Fig. 2.21 for additional details.
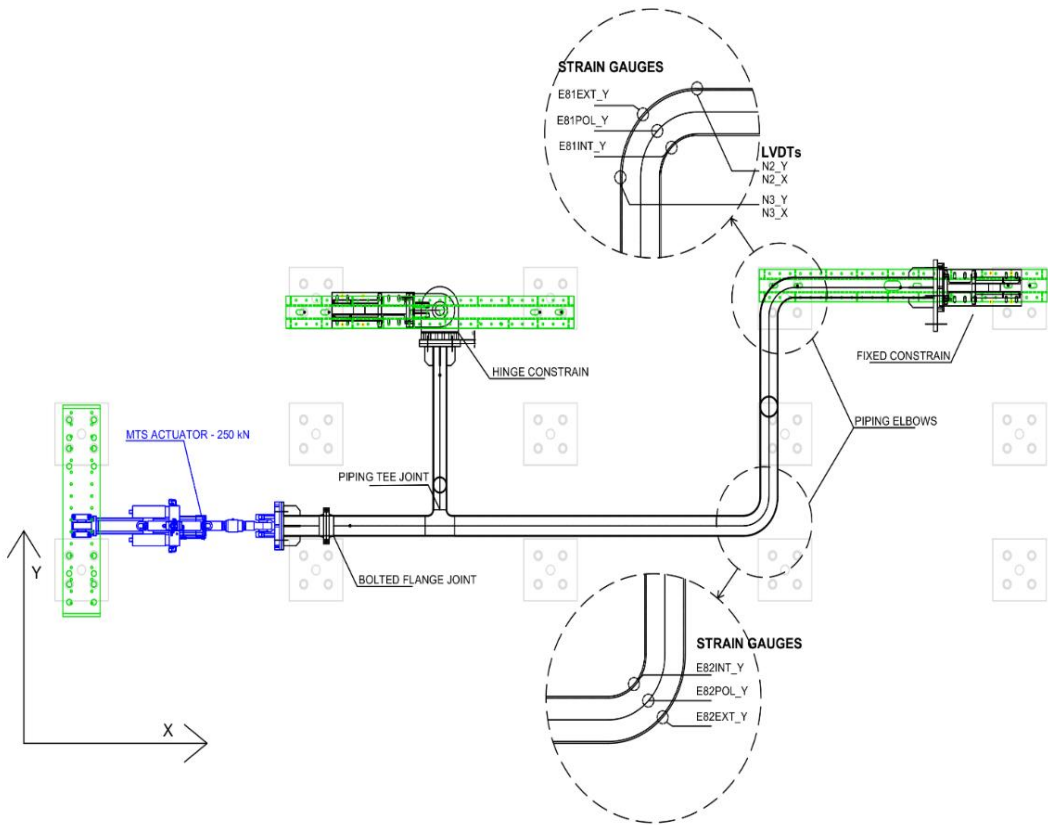
Figure. 2.21: Experimental setup and sensor placement.

Thus, the aforementioned 7 synthetic ground motions are experimentally tested with HS, performing the simulation 64 times slower than the actual signal rate. As a result, two examples of strain values detected in one of the elbows together with hysteresis loops of the actuator are depicted in Fig. 2.22- 2.25.
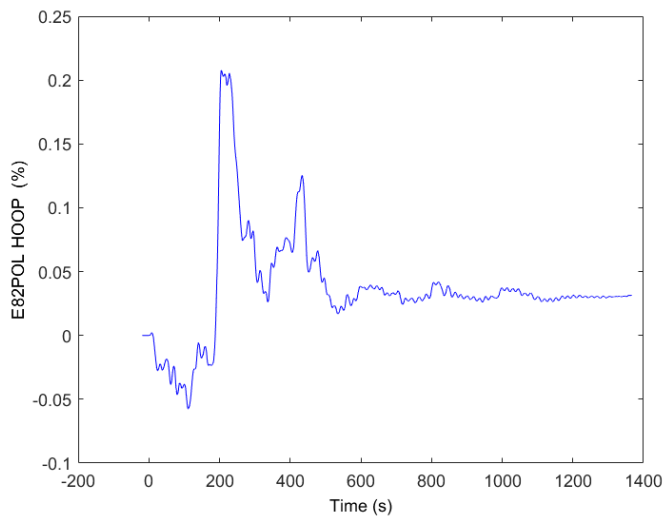
Figure. 2.22: Elbow 82 hoop strain - ULS seismic signal
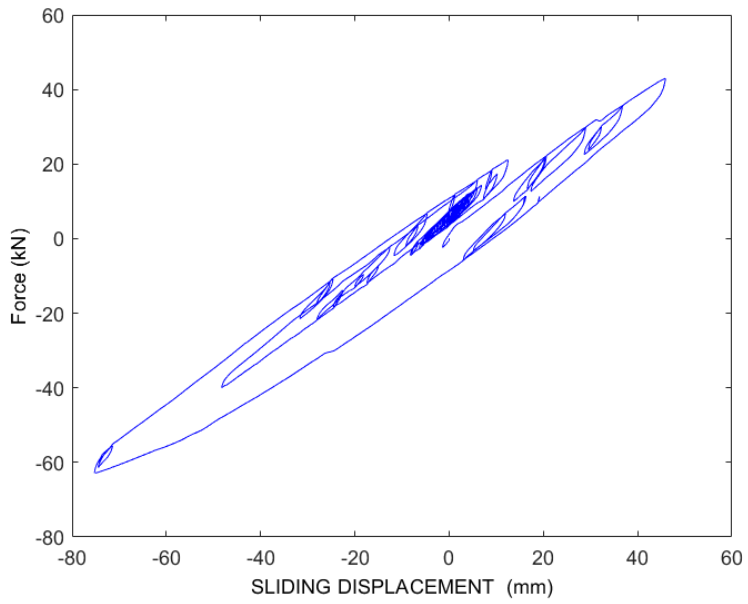
Figure. 2.23: MTS force versus sliding displacement – ULS seismic signal
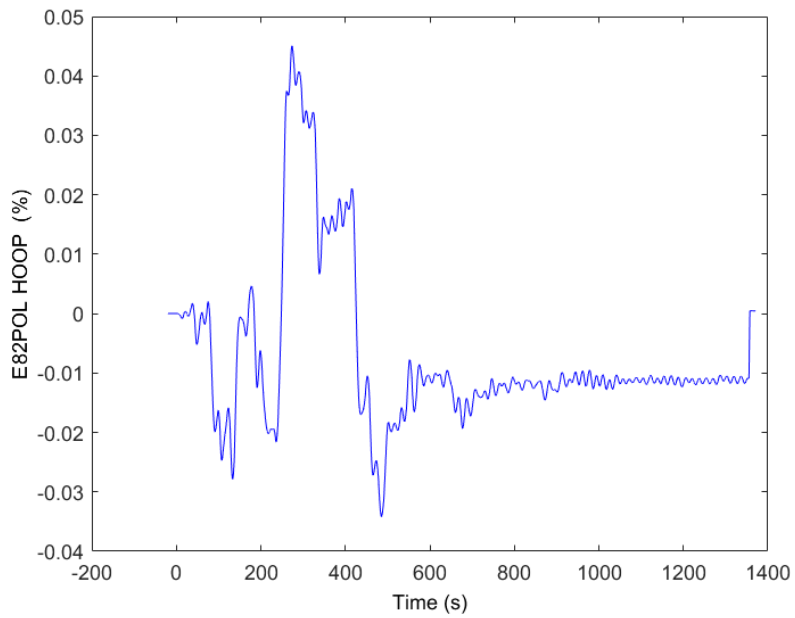
Figure. 2.24: Elbow E82 hoop strain - SLS seismic signal
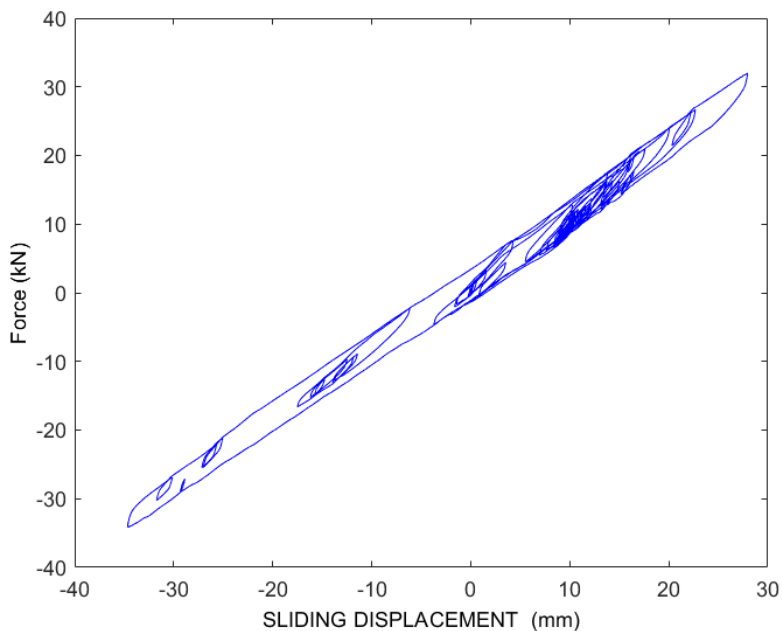
Figure. 2.25: MTS force versus sliding displacement – SLS seismic signal

As it is possible to notice from both hysteresis loops and strains values, the system response for SLS signals mostly remain in linear regime while, for ULS ones, it exhibits a certain degree of nonlinearity. Hereafter, outputs from experimental tests are adopted to better calibrate HF model with a special focus on strain level in the elbows.

2.3 Multi-fidelity modelling of the tank piping system

A multi-fidelity approach to the finite element modelling of the system understudy is shown in this section. Along this line, two models are built capable of a different degree of fidelity when compared to the experimental HS. In particular, in the following subsections we present low-fidelity and a high-fidelity model, both of them realized with ANSYS software (ANSYS, 2015).

2.3.1   Low-fidelity model calibrated against cyclic tests

The steel tank of the LF model is implemented with a 3 dofs system based on the work of Malhotra et al., 2000, as depicted in Fig. 2.16. Moreover, the relevant parameters of the system are the same adopted in the NS of the hybrid simulator and listed in Table 2.9. In detail we adopt the linear spring-damper elements COMBIN14 and mass elements MASS21 to realize the spring-mass dofs. Moreover, the sliding effect is simulated with a non-linear spring element COMBIN39, following the scheme depicted in Fig. 2.18 after Mostaghel, 1999, and formalized in Eq. (2.26) and Eq. (2.27).

Besides, the piping network is modelled with 3D equivalent beams, i.e. BEAM4 A element, with an adjusted density to consider additional weight from the water content. Moreover, the tee joint depicted in Fig. 2.9c, is modelled with a rotational spring according to the experimental results for the T-joint without reinforcement listed in Table 8. In addition, the BFJ that connects the piping network, see for reference Fig 2.9b, is realized with two springs, axial and rotational, calibrated following the experimental procedure of Bursi et al., 2018. The relevant scheme of the LF model is depicted in Fig. 2.26
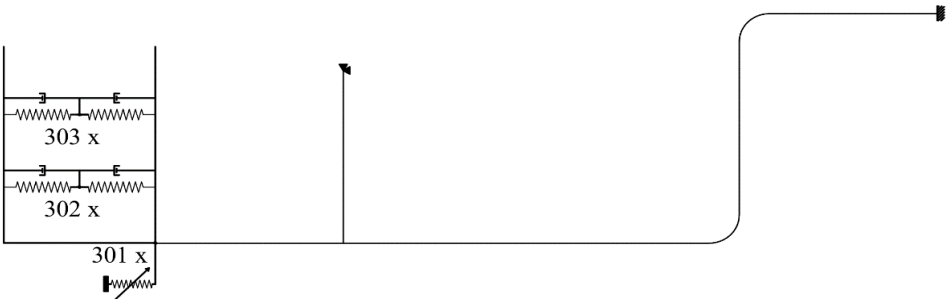
Figure. 2.26: Scheme of the low-fidelity model.

After this process of calibration against experimental results, the performances of the LF model are assessed against the unbiased experimental results from the HS. In order to make this comparison. we select as output the strain level in one of the piping elbows, as it is shown in Fig. 2.27 and 2.28.
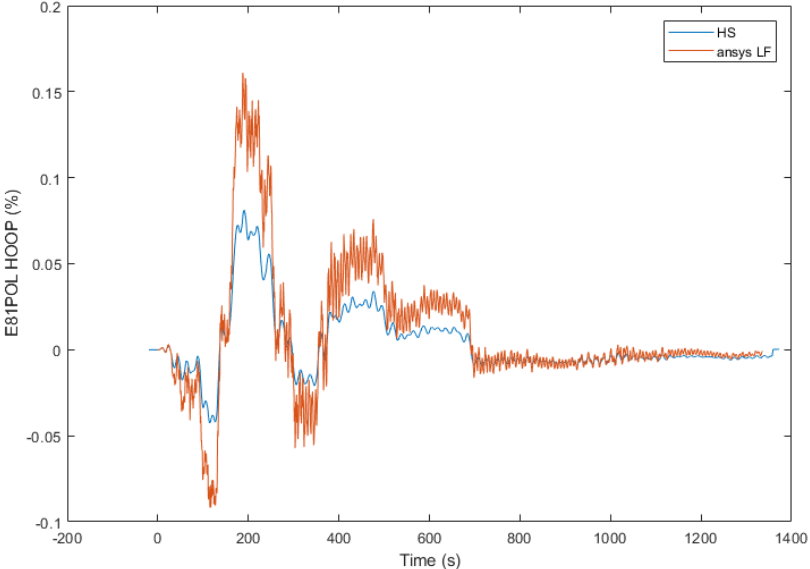
Figure. 2.27: Comparison between HS and LF model elbow E81 strain outputs - SLS seismic signal.
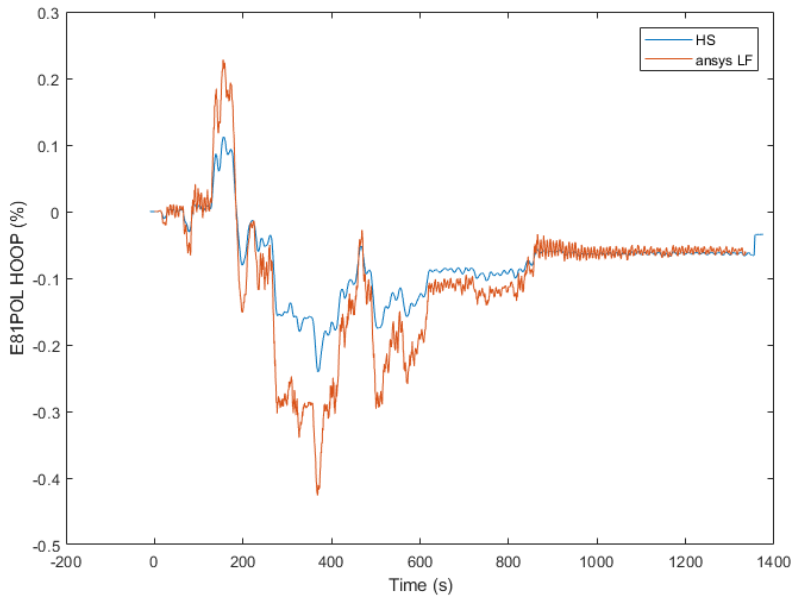
Figure. 2.28: Comparison between HS and LF model elbow E81 strain outputs - ULS seismic signal.

It is possible to notice that the LF model is capable of predict the general trend of the experimental strain even though a clear offset in present. However, considering the simplified nature of the linearized beam elements, the performances of this model are assessed as acceptable taking into account also the low computational cost of this kind of analyses. In fact, each LF model simulation lasts for a few seconds on a normal personal computer.

2.3.2 High-fidelity model calibrated against hybrid tests

Differently from the LF model, dedicated shell elements are implemented in the HF model to represent piping elbows. In detail, we adopt ELBOW290 elements that are depicted in Fig. 2.29 and the HF model scheme is shown in Fig. 2.30
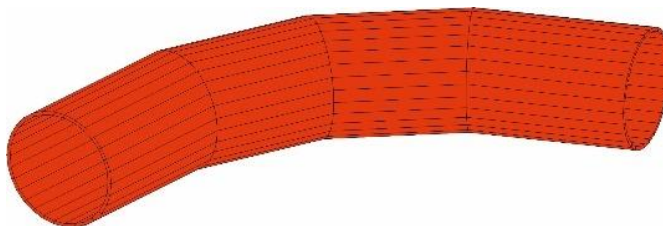
Figure. 2.29: ELBOW290 shell element
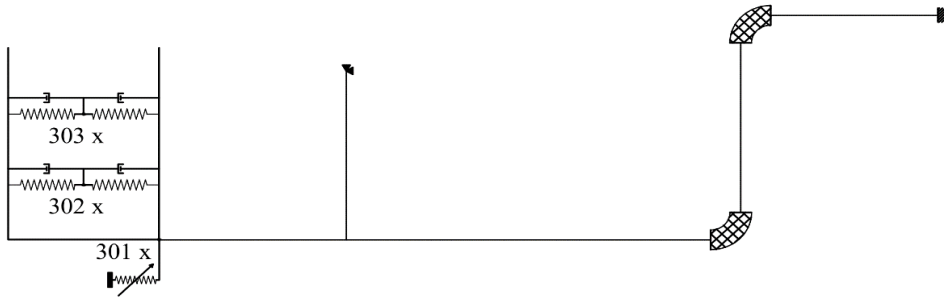
Figure. 2.30: Scheme of the high-fidelity model.

Furthermore, in order to take into account the possible yielding of pipe bends under ULS seismic signals, we implement a non-linear constitutive law for their steel material, i.e. an API 5L X52 steel. Specifically, some tensile tests are carried out on piping specimens and a multilinear kinematic hardening model is so defined. The relevant constitutive law is depicted in Fig. 2.31.
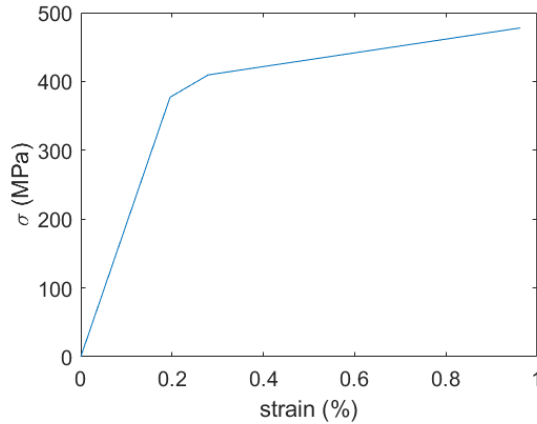
Figure. 2.31: Multi-linear constitutive law of elbows piping steel material

As a result, the HF model.is capable of predicting possible non-linear behavior of the coupled tank-piping system. Hence, the model is calibrated against the HS experimental results in order to reach a sufficient degree of accuracy. Along this line, some comparisons are shown in Fig. 2.32 and Fig. 2.33.
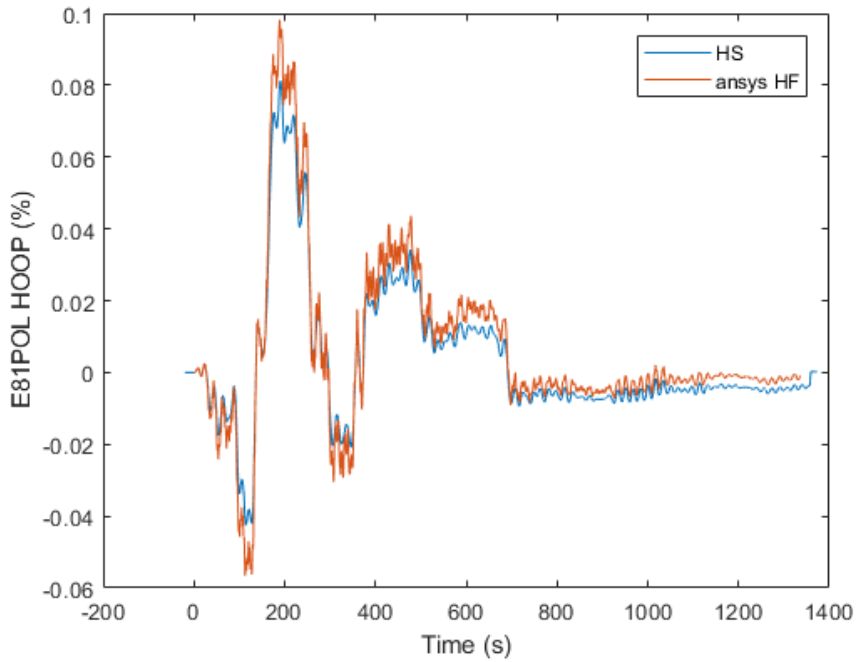
Figure. 2.32: Comparison between HS and HF model elbow E81 strain outputs - SLS seismic signal.
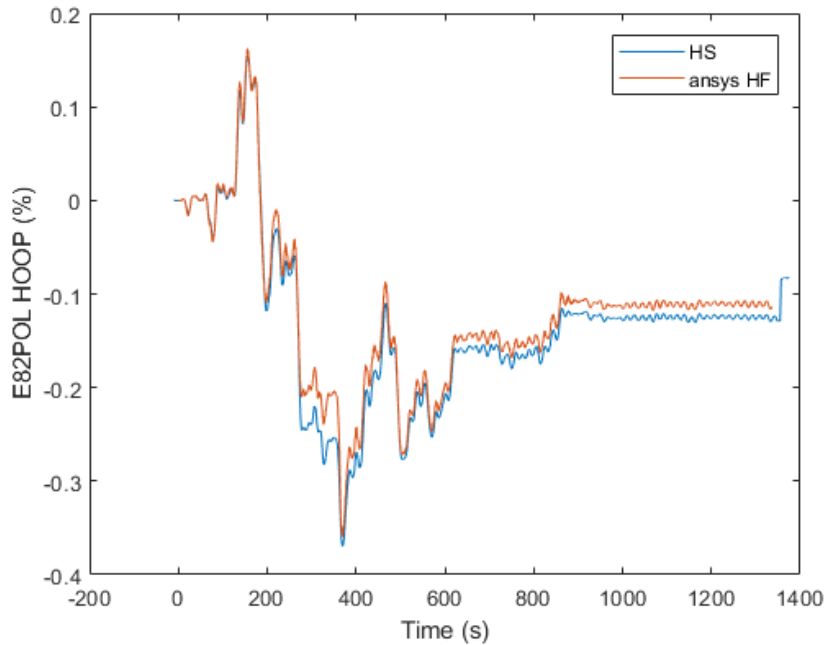
Figure. 2.33: Comparison between HS and HF model elbow E82 strain outputs – ULS seismic signal.

The comparison exhibits a satisfactory matching between the HS and the HF model confirming the value of the whole calibration process against experimental data. In detail, the HF model has a computational time of 300 seconds for each run.

2.4 Seismic fragility assessment based on surrogate modelling

In this section we present a procedure to perform a fragility assessment based on the seismic response of the coupled tank-piping system evaluated by means of a Hierarchical Kriging method, as described by Abbiati et al., 2018b. First, the analytical formulation of the Kriging method is discussed, thereafter we select a leakage limit state for piping elbows to be adopted in the fragility analysis.

2.4.1 Hierarchical Kriging surrogate of the tank-piping response

The Kriging method is a well-known technique to build surrogate model considering the output of a generic simulator as a realization of a Gaussian process, see for reference Santner et al., 2013:

$$y = \mathcal{M}(x) \approx \boldsymbol{\beta}^T \boldsymbol{f}(x) + \sigma_y^2 Z(x, \omega) \tag{2.28}$$

where $\boldsymbol{f}(x) = [f_1(x), \dots, f_p(x)]$ encompasses regression functions of a generic point x of the input parameter space $\mathcal{D}_X$ and $\boldsymbol{\beta}$ is a column vector of coefficients. Their product gives as result the trend of a Gaussian process of variance σ_y^2; $Z(x, \omega)$, which can be described by an autocorrelation function $R(|x - x'|; \boldsymbol{\rho})$ and its hyper-parameters $\boldsymbol{\rho}$. The Kriging surrogate is trained with a set of realizations $X = \{x^{(i)}, i = 1, \dots, N_t\}$ on the input parameter space $\mathcal{D}_X$ and their relevant responses of the computational mode $Y = \{y^{(i)} = \mathcal{M}(x^{(i)}), i = 1, \dots, N_t\}$l. which together form the so-called Experimental Design (ED) $\{X, Y\}$.

In our case the input and output parameters would be, $X = \{I_a, \omega_{mid}, \zeta\}$ and $Y = \{elbows\ strain\ intensity\}$ In detail the abovementioned Kriging parameters can be evaluated by the following generalized least-squared solution:

$$\boldsymbol{\beta}(\boldsymbol{\rho}) = (\mathbf{F}^T \mathbf{R}^{-1} \mathbf{F})^{-1} \mathbf{F}^T \mathbf{R}^{-1} Y \tag{2.29}$$

$$\sigma_y^2(\boldsymbol{\rho}) = \frac{1}{N_t} (Y - \mathbf{F}\boldsymbol{\beta})^T \mathbf{R}^{-1} (Y - \mathbf{F}\boldsymbol{\beta}) \tag{2.30}$$

where $[\mathbf{R}]_{ij} = R(|x^{(i)} - x^{(j)}|; \boldsymbol{\rho})$ represents the correlation matrix while $[\mathbf{F}]_{ij} = f_j(x^{(i)})$ is a matrix that gathers the values of all regression functions evaluated on X.

At this point, the prediction value of the simulator output at a generic point $x \in \mathcal{D}_X$ can be expressed as a Gaussian variable with mean value and variance given as follows:

$$\mu_{\hat{Y}}(x) = \boldsymbol{f}(x)^T \boldsymbol{\beta} + \boldsymbol{r}(x)^T \mathbf{R}^{-1} (Y - \mathbf{F}\boldsymbol{\beta}) \tag{2.31}$$

$$\sigma_{\hat{Y}}(x) = \sigma_y^2 (1 - \boldsymbol{r}(x)^T \mathbf{R}^{-1} \boldsymbol{r}(x) + \boldsymbol{u}(x)^T (\mathbf{F}^T \mathbf{R}^{-1} \mathbf{F})^{-1} \boldsymbol{u}(x)) \tag{2.32}$$

where $r_i(x) = R(|x - x^{(i)}|; \boldsymbol{\rho})$ and $\boldsymbol{u}(x) = \mathbf{F}^T \mathbf{R}^{-1} \boldsymbol{r}(x) - \boldsymbol{f}(x)$.

The Hierarchical Kriging method is capable of including several simulators with increasing level of accuracy and computational cost. Along this line, given l as the number of different simulators and y_s as the output of the most accurate simulator, for any $1 \leq l \leq s$, it is possible to define $\boldsymbol{x}$ as:

$$\mu_{\hat{Y}_l}(\boldsymbol{x}) = \mu_{\hat{Y}_{l-1}}(\boldsymbol{x})^T \beta + \boldsymbol{r}(\boldsymbol{x})^T \mathbf{R}^{-1}(\boldsymbol{Y}_l - \mathbf{F}\beta) \tag{2.33}$$

$$\sigma_{\hat{Y}_l}(\boldsymbol{x}) = \sigma_y^2 (1 - \boldsymbol{r}(\boldsymbol{x})^T \mathbf{R}^{-1} \boldsymbol{r}(\boldsymbol{x}) + u(\boldsymbol{x})^T (\mathbf{F}^T \mathbf{R}^{-1} \mathbf{F})^{-1} u(\boldsymbol{x})) \tag{2.34}$$

where $r_i(\boldsymbol{x}) = R(|\boldsymbol{x} - \boldsymbol{x}^{(i)}|; \boldsymbol{\rho})$ and $u(\boldsymbol{x}) = \mathbf{F}^T \mathbf{R}^{-1} \boldsymbol{r}(\boldsymbol{x}) - \mu_{\hat{Y}_{l-1}}(\boldsymbol{x})$ with $[\mathbf{F}]_i = \mu_{\hat{Y}_{l-1}}(\boldsymbol{x}^{(i)})$; $\boldsymbol{Y}_l$ is the vector of simulator l outputs, β is a regression factor as the one defined by (2.29).

The Hybrid Computational Hierarchical Kriging (HC-HK) method developed by Abbiati et al., 2018b, allows to merge together experimental and FE outputs. The main hypothesis behind this methodology is that the CS is cheaper in terms of general resources when compared to the HS. This assumption is clearly verified in this case where both HF and LF analyses can be performed on a common desktop PC against the more demanding experimental procedure shown in this manuscript to carry out the HS.

Along this line, the HC-HK method also states that, even though CSs would exhibit a lower degree of accuracy when compared with HS, these computational simulators have to be properly calibrated on the basis of HS results. As a matter of fact, we show both a calibration process and adequate CSs performance in section 2.3.

At this point to apply the procedure to our case study we proceed with the following steps:

1. Sampling of the input parameters space $\mathcal{D}_X$ and evaluation of the CSs response. In particular, our input space is defined by the reduced space of stochastic ground motion model parameters alongside with the baseline noise, as described in subsection 2.2.2.
2. Evaluation of the LF ordinary Kriging surrogate $\widehat{\mathcal{M}}_{LF}(\boldsymbol{x})$ of the CS response based on the ED $\{\boldsymbol{X}_{LF}, \boldsymbol{Y}_{LF}\}$ by solving (2.31-2.32)
3. Calculation of the multi-fidelity (MF) hierarchical Kriging surrogate $\widehat{\mathcal{M}}_{MF}(\boldsymbol{x})$ of tank-piping system response based on the EDs $\{\boldsymbol{X}_{HS}, \boldsymbol{Y}_{HS}\}$ and $\{\boldsymbol{X}_{HF}, \boldsymbol{Y}_{HF}\}$ by means of. (2.33-2.34), considering the mean predictor $\mu_{\hat{Y}_{LF}}(\boldsymbol{x})$ of the LF ordinary Kriging surrogate $\widehat{\mathcal{M}}_{LF}(\boldsymbol{x})$ as trend function.

Finally, we will be able to obtain the following Kriging surrogate:

$$elbow\ strain\ intensity = \widehat{\mathcal{M}}_{MF}(I_a, \omega_{mid}, \zeta) \tag{2.35}$$

The surrogate model defined by Eq. (2.35) will allow for a fast calculation of the tank-piping system seismic response, i.e. elbow stain levels, generated by synthetic ground motions generated on the basis of the stochastic ground motion model parameters.

2.4.2 Derivation of fragility curves

Fragility curves can express the probability of exceedance of an engineering demand parameter (EDP) given - conditional- an intensity measure (IM), see in this respect Baker, 2015. Nevertheless, it is important to define a proper capacity limit state, C_{LS}, for the chosen demand parameter, D, and an adequate IM. Along this line we can write the abovementioned probability as follows:

$$
\begin{aligned}
P(edp) &= \int_{im} P(EDP > edp|im)|d\lambda(im)| \\
&= \int_{im} P(D > C_{LS}|IM = im)|\lambda(im)dim|
\end{aligned}
\tag{2.36}
$$

As stated before, we decided to focus on leakage limit state for pipe bends of our coupled tank-piping system. Along this line, the selected EDP, as suggested by Bursi et al., 2018, is the tensile hoop strain. However, in order to describe C_{LS} as a random variable to take into account the uncertainty associated to material's resistance, we need to introduce a relevant probability distribution according to the work of Pedot et al., 2018.

In detail, a set of relevant strain limit states is drawn from literature and international codes. Specifically, as recalled by Vathi et al., 2015, Liu et al., 2009, and based on the recommendations of international codes (DNV, 2000 and ASCE, 2005), CLS can read 2%. Conversely it can be considered equal to 2.5% according to CSA, 2007, and 3% according to EN1998-4-8, 2006. As a result, we assume an average value of 2.5% in the interval between 2% and 3%. This value is also corroborated by Liu et al., 2009, which shows a correlation between the tensile strain resistance and the ratio of yield stress over ultimate stress of piping components.

Once the average value is set, it is necessary to define which kind of probability distribution can describe the variability of CLS. According to Fullwood, 1989, the resistance of piping elements follows a Gaussian distribution and the same approximation is made by Myers et al., 2009, where the low cycle fatigue resistance of steel specimens is assumed as normally distributed. Thus, in this study we assume CLS, as leakage threshold for tensile hoop strain of piping elbows, normally distributed with an average value of 2.5% and a standard deviation of 0.25%. The relevant parameters and the pdf are shown in Table 2.10 and Figure 2.34, respectively.

Table 2.10: Normal distribution parameters for the tensile hoop strain related to the leakage threshold after Pedot et al., 2018.

μ	2.5%
σ	0.25%
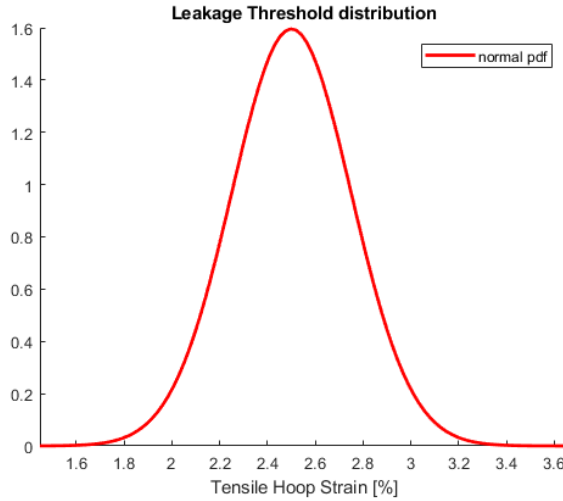
Figure. 2.34: Probability density function for leakage threshold after Pedot et al. 2018

On the other hand, the definition of a proper IM can be made based on the input parameters of our surrogate model, as defined in Eq. (2.35). In particular we will focus on the parameter I_a, which is, among the others, the one with the greatest influence on the system seismic response, as shown in the GSA results reported in Fig. 2.8. Hence, Eq (2.36) can be rewritten as:

$$P(leakage) = \int_{I_a} P(D > C_{LS}|IM = I_a)|\lambda(I_a)dI_a|$$ (2.37)

where $\lambda(I_a)$ is described by a uniform distribution whose boundaries are reported in Table 2.3.

2.5 Conclusions

In this manuscript, we presented a rigorous methodology to derive seismic fragility curves for a realistic tank piping system, based on hybrid simulations and synthetic ground motions. In particular, we focused on loss of containment from vulnerable components of the piping network like pipe bends.

As a first step we define a seismic scenario associated to a geographical site by means of a probabilistic seismic hazard analysis. Then, based on this analysis we provide an adequate seismic input employing a stochastic ground motion model calibrated against coherent natural seismic records. Moreover, we carry out a global sensitivity analysis to reduce the space parameters of the stochastic model and we synthetize a large set of ground motions to be used in both experimental tests and finite element simulations.

Besides, two different finite element models, a refined high-fidelity and a faster low-fidelity model, are calibrated against both hybrid simulations of the whole system and cycling tests of vulnerable components, i.e. piping tee joints and bolted flange joints. Specifically, the main difference between the two models is represented by the pipe bends implementation.

As a matter of fact, while the low-fidelity model encompasses linear equivalent beam to describe piping elbows behavior, the high-fidelity model relies on shell elements to replicate pipe bends seismic response.

In addition, we show the procedure to build a hierarchical kriging surrogate model based on hybrid simulations, high and low-fidelity models. As a result, the surrogate model is able to evaluate the seismic response of the coupled system on the basis of the stochastic ground motion model parameters.

In the last part of the manuscript we define a leakage limit state for piping elbows and we present the methodology to derive fragility curves based on the surrogate model. Considering the novelty of the approach further investigations are required to assess the performances of the procedure and its reliability.

Chapter 3

3. Seismic performance and fragility functions of a 3d steel-concrete composite structure made of high-strength steel

Abstract

This manuscript provides insight into a probabilistic seismic demand analysis of a steel-concrete composite structure made of a novel type of high-strength steel moment resisting frame, to be used either in a seismic risk assessment or a fully probabilistic Performance-Based Earthquake Engineering (PBEE) framework. The application of the PBEE methodology with a full probabilistic character is able to rigorously evaluate the seismic risk to which a structure may be exposed, as well as to quantify economic losses, including both direct -repair, reconstruction costs, etc.- and indirect costs -downtimes, etc.-. In this respect, the knowledge of seismic fragility function is paramount. Moreover, due to the dynamic complexity of the examined structure caused by irregularity in elevation and different lateral-force resisting systems in the two main directions -moment resisting frames and concrete shear walls- the seismic behaviour is not straightforward to foresee. Therefore, two separate 2D analyses along the building main directions may not suffice to identify the actual dynamic response and, consequently, a 3D comprehensive probabilistic seismic demand analysis was performed by taking into account the earthquake incident angle. In order to exploit the inherent overstrength of non-dissipative members, consistently with the capacity design philosophy, the structure, that is a representative example of a real office building, is characterised by a newly-conceived type of moment resisting frame made of high-strength steel circular columns filled of concrete and of mild steel beams. In this respect, a nonlinear 3D FE model was developed and calibrated on experimental tests performed on both beam-to-column and column-base joints that formed moment-resisting frames. A multiple incremental dynamic analysis was then performed with two groups of bespoke accelerograms characterized, on one hand, by large magnitude and large distance and, on the other hand, by near-source effects. The earthquake incidence angle was also considered and, to decrease the number of simulations, the accelerogram-incident angle pairs were selected by means of the Latin hypercube sampling (LHS) method. The relevant seismic analyses highlighted the need to include the incident angle to better characterise its dynamic behaviour. Hence, the seismic fragility functions were built both for damage and collapse limit states considering both the maximum interstorey drift ratio as engineering demand parameter and different intensity measures as well as the incident angle randomness. The

results showed that peak ground displacement entails a more efficient probabilistic model because the dominant structural dynamic behaviour was governed by moment resisting frames characterised by fairly long periods.

3.1 Introduction

3.1.1   Background and Motivation

In the last years, there has been a growing trend in the use of high-strength steel (HSS) in tubular structures thanks to the publication of EN1993-1-12, 2007, that extended the use of structural steel up to grades S690Q/S700MC. Nonetheless, EN1993-1-12 imposes many limitations at the material, structural and design level due to the limited knowledge of its actual behaviour. The use of HSS can be advantageous in seismic design when employing the capacity design philosophy for non-dissipative elements owing to its inherent overstrength. Thus, columns in moment-resisting frames (MRFs) designed in HSS and beams in mild steel can represent an effective solution for structures located in moderate seismic prone zones, when the limitation of lateral displacements is not dominant. For this purpose, in order to promote the use of HSS circular sections in buildings, the Research Fund of Coal and Steel (RFCS) project called ATTEL was funded, with the aim to investigate both seismic and fire behaviour (Jaspert et al. 2012, and Tondini et al., 2013). To exploit the inherent overstrength of non-dissipative members within the project, a novel type of moment resisting frame with HSS column filled with concrete and mild steel beams was conceived. Both cost savings of the proposed solution and the capability of beam-to-column and column-base joints to exhibit a favourable seismic behaviour for a medium ductility class was demonstrated in Pucinotti et al., 2015. The relevant reference structure is representative of a realistic office building.

In the last fifteen years, the adoption of the probabilistic PBEE methodology has become popular (Cornell et al., 2000) and the availability of seismic fragility functions of a particular structural typology or components is fundamental both for risk assessment and/or a probabilistic PBEE application (Cornell and Krawinkler, 2000). For instance, a fragility curve can express the probability of exceedance of an engineering demand parameter (EDP) given - conditional- an intensity measure (IM). Thus, the choice of interstorey drift ratio as global EDP can directly be assumed as a damage measure (DM), see Cornell and Krawinkler, 2000. In this respect, the Hazus database, FEMA 2013, already contains a number of fragility functions for various structural typologies and components. However, if the structural typology/component is new, they have to be determined. The computation of seismic fragility curves typically requires several nonlinear dynamic analyses with seismic input representative of the structure site. Due to the aleatory nature of ground motions a set of accelerograms has to be selected among: (1) artificial waveforms; (2) simulated accelerograms; and (3) natural records (Iervolino et al, 2008, and Bommer, 2004). Natural accelerograms are the most direct representation of ground motion; in fact, they contain amplitude characteristics, frequency content, energy and duration of actual events. Therefore, the use of natural accelerograms is spreading as input to the nonlinear structural dynamics. This happens due to easy availability of online Strong Motion Databases, like

PEER and ITACA, but also because it is possible to get an accurate, statistically correct estimate of seismic demand.

Generally, in design practice when plan regularity criteria are met, simplified 2D structural analyses are performed, as stated in EN1998-1, 2004. In that case, the structure is analysed with seismic loading acting along two orthogonal directions, typically the two axes of symmetry or two orthogonal directions along the main building directions. Conversely, when a non-symmetric irregular structure is examined, the dynamic behaviour becomes more complex and coupling between the two main directions owing to torsional effects is likely to occur; as a result, a more complex 3D model is required (Iervolino et al, 2008) Moreover, when a structure is made of two different lateral-force resisting systems in the two main directions, due to sensitive differences in dynamic properties the dynamic response of the whole system is less straightforward to predict. In fact, an increased dynamic complexity reduces considerably the intuitive understanding of structural response. For instance, this can occur for structures composed of a steel moment resisting frame (MRF) in one direction and concrete shear walls in the other (Pucinotti et al. 2002), a solution conceived to limit column strength and reduce complexity of beam-to-column joints. As a result, for structures with a certain degree of irregularity or characterised by different lateral resisting systems in both directions, as composite structures, a separate analysis along the two main building directions may not suffice to accurately capture the dynamic behaviour; thus, a 3D analysis is needed.

The application of two horizontal components along the main building directions may not lead to the most unfavourable case, because the influence of the incidence angle of a seismic event can be significant. However, the analysis is rarely performed considering a variation of the incident angle of seismic motion. Works related to this topic were carried out by a few researchers, in particular, Wilson et al., 1995, investigated the suitability of the 100%-30% and 100%-40% combination rules. Rigato and Medina examined the seismic behaviour of asymmetric and symmetric inelastic structures characterised by different periods of vibration. They showed that ductility demands are, in general, underestimated when horizontal components are applied along the principal directions of a structure. Athanatopoulou et al., 2005, proposed a formula valid for elastic structures to determine the critical incidence angle. MacRae and Mattheis, 2000, analysed the inelastic response of a 3D steel structure subject to near-fault motions by varying the incidence angle with negligible torsional effects. Lopez et al., 2000, proposed a method to determine the critical angle of seismic incidence and the corresponding peak response of discrete, linear structures subjected to two horizontal components applied along arbitrary directions and to the vertical component of earthquake ground motion. Moreover, Lopez et al., 2001, presented an explicit formula to calculate critical value of structural response due to both principal horizontal components acting along any incident angle and the vertical component of ground motion. Skrekas and Giaralis, 2013, investigated the influence of both near-fault effects and incident angle of earthquake waves by means of an incremental dynamic analysis (IDA) on the seismic response of a typical jack-up offshore platform. They demonstrated that the "pulse-like" fault normal component poses much higher seismic demands compared to the fault

parallel component. More recent works reported in the literature on the seismic behaviour of structures that include incident angle were drawn up by Lagaros, 2010a and 2010b. However, they refer to reinforced concrete structures with the same lateral-resisting system, i.e. moment resisting frames, in both directions. In detail, Lagaros, 2010a, proposed a procedure for performing multicomponent incremental dynamic analysis (MIDA) by taking into account incident angle. In particular, in accordance with MIDA, a sample of N pairs of record-incident angles was generated through the LHS method. Along this line, Sozonov et al., 2014, performed a probabilistic seismic demand analysis that relied on the cloud analysis method; it entailed the selection of a ground motion scenario representative of the Italian territory sorted according to magnitude and distance from the epicentre. The incident angle of the seismic event was deterministically considered with variations between 0 and 180 degrees.

3.1.2   Scope

Even though numerous studies have dealt with the probabilistic seismic demand of structures subject to seismic loading, a few publications have been devoted to: i) analyses of representative realistic buildings characterized by different lateral-force resisting systems; ii) analyses that include input uncertainties, also in terms of earthquake incident angle. All together, they represent basic issues that are explored hereinafter. In detail, the aim of this manuscript is to provide seismic fragility functions to be used in a full PBEE framework of a 3D steel-concrete composite structure made of a novel type of high strength steel moment resisting frame in one direction and reinforced concrete shear walls in the other. They were set for the probability of exceeding an interstorey drift ratio equal to 1% -associated with the damage limit state (DLS)-, and the probability of exceeding an interstorey drift of 5% -associated with the collapse prevention limit state (CLS)- given different IMs, e.g. peak ground displacement. These fragility curves will serve as a means for practitioners to probabilistically assess/design structures made of this novel type of moment resisting frame. Moreover, it gives insight into the 3D dynamic performance and the influence of the earthquake incident angle on this structure that is representative of a realistic office building.

The remainder of the manuscript is organised as follows: initially, Section 2 describes the reference 3D structure in terms of lateral-force resisting systems, members and both beam-to-column and column-base joints. In Section 3 numerical modelling of structure carried out by means of the OpenSEES software (Mazzoni et al., 2007) is presented. Section 4 illustrates the results of probabilistic seismic demand analyses (PSDA) and relevant seismic fragility functions. Finally, main conclusions are drawn in Section 5 with future perspectives.

3.2 The reference 3d structure

Steel Moment-Resisting Frames (MRF) are structural systems that are suitable for seismic prone zones. Indeed, if properly designed according to the capacity design philosophy, they are capable of enabling highly dissipating global mechanisms. Nonetheless, their complexity in terms of joint design advises against solutions that foresee MRFs in both principal directions of the structure. For this reason, other lateral-force resisting solutions to be coupled with MRFs are generally preferred. For instance, a pinned steel frame that relies on

Reinforced Concrete (RC) shear walls for withstanding horizontal forces represents a typical choice. In order to check the benefit of HSS, a reference 5-storey steel-concrete composite structure was conceived as a case study with the aim to propose structural elements and realistic configurations of beam-to-column and column-base joints to be tested in laboratory (Pucinotti et al., 2010). In particular, the structural system was conceived to optimise the use of high-strength steel in moderate seismic-prone regions. In this respect, the columns were made of high-strength steel whereas the beams in mild steel. Thus, a likely office building was considered. In order to better satisfy design criteria for static, seismic and fire loadings, moment resisting frames along one principal direction were designed, whereas a steel pinned system was preferred in the other main direction by inserting RC shear walls. The choice of two different systems for withstanding lateral forces allowed for the optimisation of structural performance by avoiding MRFs in both principal directions; in fact, they could entail too severe column and joint designs. Hereinafter, only the main features of the reference structures are presented. For a comprehensive description of the structure, joint typology and experimental tests, the interested reader may refer to Pucinotti et al. 2010.

3.2.1 Description of the structure

The main features of the reference structure are the following: the plan dimensions are 32 m x 32 m and a central open space 16 m x 16 m was created for the first three storeys as shown in Figure 3.1a-1d. The structure was made up of five (4+1) moment resisting frames (red colour in Figure 1) placed at the distance of 8 m in one direction and of four concrete walls 0.3 m x 6 m along the other direction (blue colour in Figure 1). Moreover, two staircases, necessary to evacuate the building during fire, were located between the concrete walls. The interstorey height was 3.5 m. The design was carried out according to the relevant parts of the Eurocodes: EN1991, EN1992, EN1993, EN1994 and EN1998. The main seismic design parameters of the reference structure were: i) Medium Ductility class DCM in agreement with EN1998-1; 2004, ii) peak ground acceleration (PGA) ag equal to 0.27g corresponding to a moderate-high seismic action in Europe.
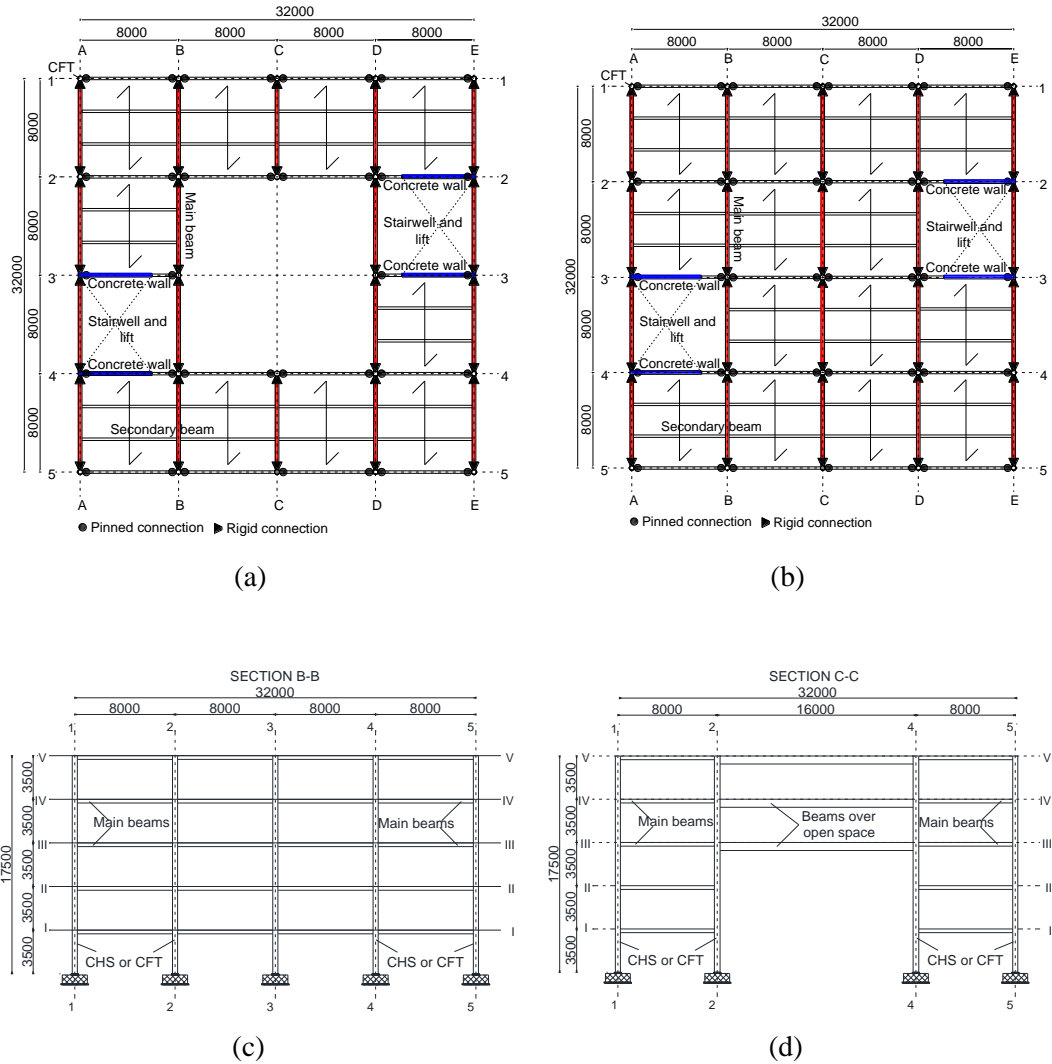
Figure. 3.1. Reference structure: a) plan of 1st and 2nd floor; b) plan of 3th, 4th and 5th floor; c) B-B cross section; d) C-C cross section. Dimensions in mm.

Concrete Filled Tubes (CFTs) columns made of steel S590 and steel composite H-beam profiles made of steel S275 constitute the MRFs. In detail, circular columns of diameter 355.6 mm and thickness 12 mm were filled with concrete C30/37 and with a reinforcement cage composed of 8 Φ18 longitudinal bars and Φ8@150-mm stirrups; the composite beams were composed of S275 HEB 280 steel profiles, fully connected to a C30/37 concrete slab 110mm thick by means of Nelson 19-mm stud connectors whose height, spacing and ultimate tensile strength f_u were 100 mm, 140mm and 450MPa respectively. B450C steel grade was adopted for 3 + 3Φ12 additional longitudinal reinforcing steel bars that were

85

arranged in such a way to satisfy recommendations proposed in EN1998-1, 2004, for the design of slabs of steel–concrete composite beams at beam-to-column joints in MRFs.

The shear wall dimensions are 6 m x 0.3 m x 17 m and concrete is of class C30/37. Beam-to-column joints and column-base joints belonging to the MRF were then tested under monotonic and cyclic loading in the Laboratory of Materials and Structural Testing of the University of Trento.

3.2.2 Characteristics of beam-to-column and column-base joints

A welded/bolted solution was proposed for beam-to-column joints, see Fig. 3.2, and was conceived in order to guarantee easiness of assembly and limited problems related to onsite welding.

(a)   (b)
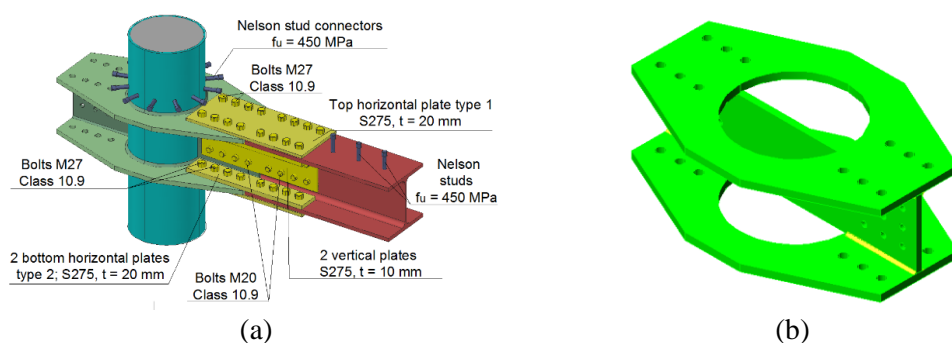
Figure 3.2. Beam-to-column joint; a) 3D view; b) detail of the vertical through-in plate.

The seismic design of the composite beam-to-column joint depicted in Figure 3.2 was devised to provide non-dissipative components, i.e. columns and connections with adequate overstrength and stiffness with respect to connected dissipative members, i.e. beams. The joint was designed to be Category B -slip-resistant at serviceability limit state-, rigid and partial strength in agreement with 1993-1-8, 2007. In order to directly transfer shear to the concrete core, a vertical steel plate - of thickness 10 mm and of the same height of the steel beam web - passing through the column was provided as shown in Fig. 3.2b. Then, in order to enable the development of the seismic slab-to-column transfer mechanism, an additional steel mesh φ10@100x100 mm was placed in the slab (Pucinotti et al., 2010). In fact, a steel mesh was needed to activate Strut & Tie Mechanism 1 and 2 as foreseen in EN 1998-1, 2004 and detailed in Pucinotti et al, 2011. Differently from this, Nelson stud connectors were interrupted close to the joints, as shown in Fig. 3.2.

With reference to column-base joints, two different solutions both rigid and full strength were designed: i) a standard solution with a base plate, anchor bolts and vertical stiffeners and ii) an innovative solution with the column embedded in the foundation, as depicted in Fig. 3.3. The latter is surely more performing for CFT columns because of an increase in strength owing to the tube embedded in the foundation as well as a higher easiness in construction that does not entail stiffeners welded to the base plate. Both solutions were designed to meet capacity design criteria. The innovative base joint was selected for the structure and numerically analyzed through the MIDA.
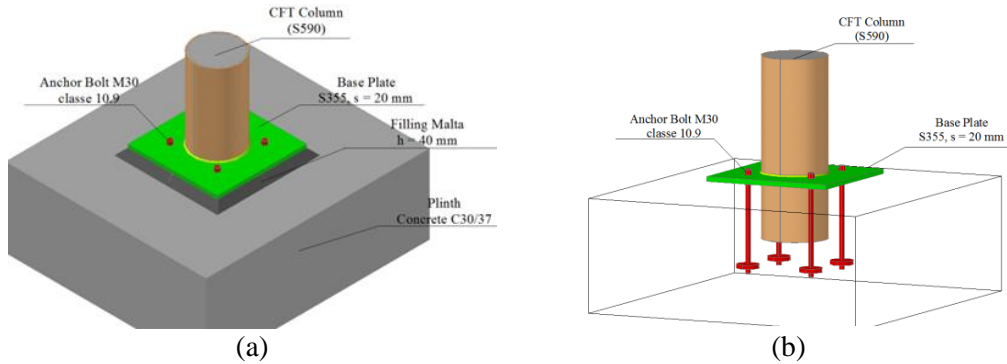
Figure 3.3. Innovative column-base joint: a) details with plinth and b) details of the embedded part.

3.2.3 Characteristics of RC shear walls

The shear walls were designed according to the EN1998-1, 2014, by allowing for ductile behaviour as they were classified as slender; in fact, the height to width ratio was about 3. The critical region of wall, i.e. where nonlinear behaviour is expected to occur, was identified at the base. Its height was found equal to that of the first storey and, as illustrated in Fig. 3.4, in order to account for a confined concrete behaviour in the edge zones of the shear wall cross section, an adequate reinforcement detailing was provided.
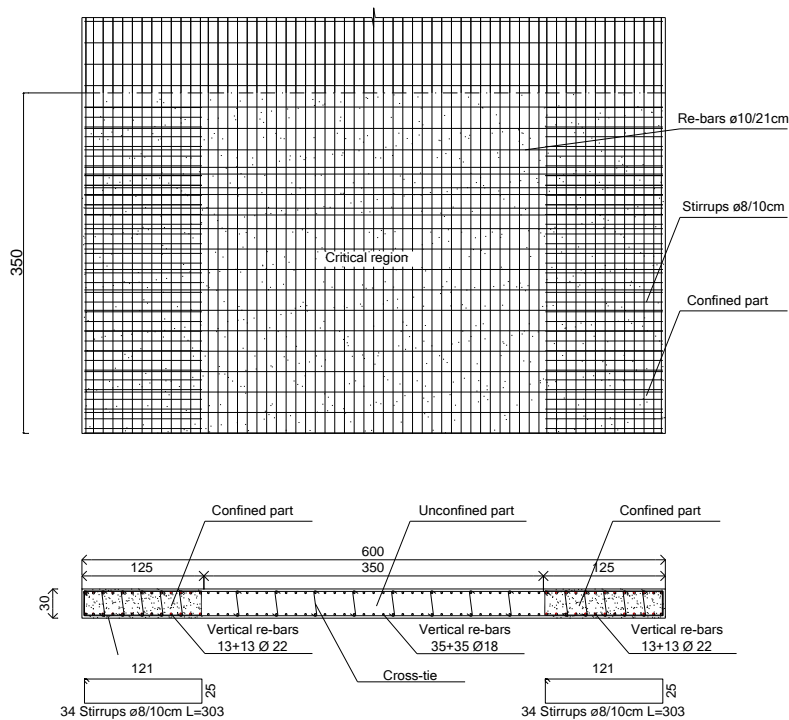
Figure 3.4. Rebar detailing of the shear wall within the critical region, with the characteristics of stirrups used for concrete confinement. Dimensions in cm.

3.3 Numerical modelling of the 3d structure

The numerical modelling of the structure was developed by means of the FE software OpenSEES (Mazzoni et al, 2007) by allowing for both material and geometric nonlinearities.

3.3.1   Steel-concrete composite moment resisting frames

Consistently with the capacity design philosophy, a lumped plasticity model was exploited to represent the seismic response of each moment resisting frame, as depicted in Fig. 3.5. In particular, the inelastic behaviour of joints was calibrated based on the experimental outcomes by means of a Bouc–Wen material model in parallel to a pinching hysteretic model. The Bouc–Wen model provided the main part of the actual inelastic behaviour, whereas the pinching model simulated slip owing to damaged concrete and consequent hardening; it also took into account the different behaviour between hogging and sagging moment, particularly in beam-to-column joints. Conversely, the calibration of the innovative column base joint was possible by only considering a Bouc–Wen model. As an example, the results of the joint calibration, i.e. beam-to-column joint (BTCJ) and innovative column-base joint (CBJ) subject to cyclic loading are shown in Fig. 3.6. For a comprehensive description of the joint calibration, the reader may refer to Pucinotti et al., 2010.

Conversely, the other parts of the frame were modelled with linear-elastic-displacement-based beam-column elements. For beams, the flexural stiffness (EI) of such elastic elements was assigned constant along their length and based on the average between the flexural stiffness under sagging moment, that is, no slab cracking, and the flexural stiffness under hogging moment, that is, by allowing for slab cracking. For columns, the effective flexural stiffness was computed according to EN1994-1-1, 2005.

BW Bouc-Wen model
P   Pinching model
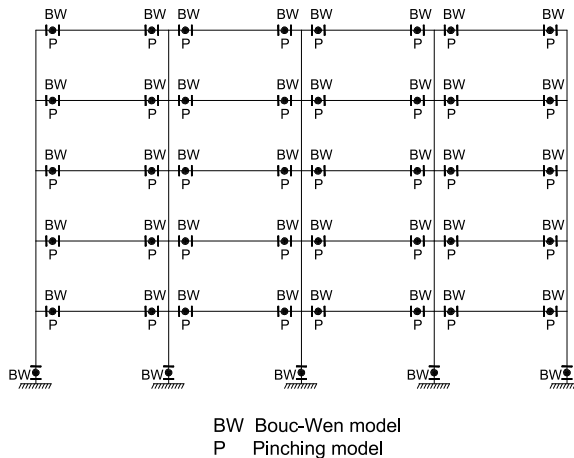
Figure 3.5. B-B MRF FE model with innovative column bases.

(a)

(b)

(c)
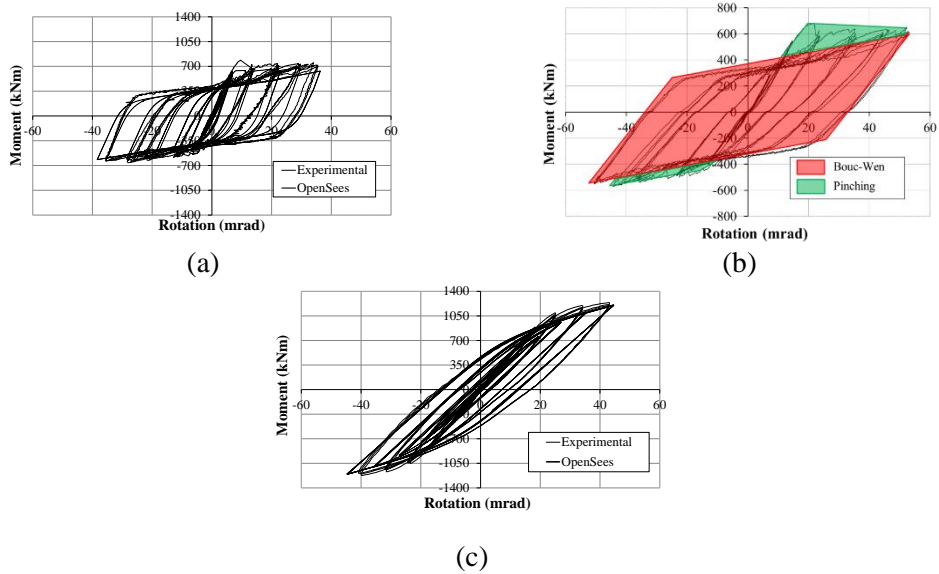
Figure 3.6. Hysteretic models of BTCJs and CBJs: a) Calibration of the BTCJ; b) effect of the hysteretic models on the BTCJ calibration; c) Calibration of the innovative CBJs.

3.3.2 Reinforced concrete shear walls

As mentioned above, the RC shear walls was endowed with a ductile behaviour and, therefore, only the flexural behaviour was allowed to exhibit nonlinearities; conversely, an elastic model was adopted for shear behaviour. In detail, each shear wall was modelled with 5 forced-based fibre-section beam-column elements (Taucer et al., 1991) - one for each storey - based on a distributed plasticity concept with 5 integration points, as shown in Figure 3.7. In this way, the properties of each fibre of the cross section relevant to: i) unconfined concrete; ii) confined concrete and iii) steel reinforcement could be assigned. Unconfined and confined concrete were modelled using the stress–strain relationship proposed by Mander et al. 1988. As a result, i) unconfined and confined concrete were modelled according to Concrete04, which is defined by a uniaxial Popovic's concrete material object with degraded linear unloading/reloading stiffness; ii) the longitudinal reinforcement was modelled using the Steel02 material, which is characterized by the Giuffrè–Menegotto–Pinto model with isotropic strain hardening. Relevant masses were lumped at each storey level. Elastic shear stiffness was reduced to $0.1 \times G \times A$, where G defines the shear modulus and A is the wall gross area, see for reference Lowes et al., 2012. Torsional response was modelled with an elastic-perfectly plastic model by following elasticity theory; in particular, "yield" strength was given by the Tresca criterion and torsional stiffness by $G \times J_w$, where J_w defines torsion constant of the wall section. Section Aggregator command was used to add shear and torsional properties to the section of shear walls. Once the shear wall was modelled, it was then incorporated in the relevant frames orthogonal to the MRF, i.e. in 2-2, 3-3 and 4-4 frames of Figure 3.1. The beam elements composing the remainder part of the frame were elastic with pinned constraints.

Finally, the numerical model of the 3D structure was assembled with MRFs and the frames that incorporate the shear walls by connecting them through rigid diaphragms, which represent the composite slab at each floor, by means of node constraints.
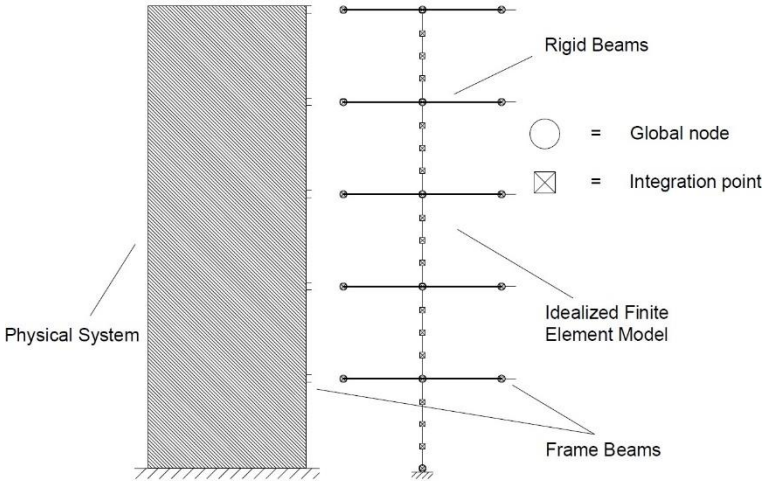
Figure 3.7. Shear wall modelling.

3.3.3 Dynamic properties of the reference structure

Once the modelling was completed, the dynamic properties were obtained through modal analysis and, relevant results, are reported in Table 3.1. They reveal that the 3D reference structure is characterised by a fairly long fundamental period in the direction of MRFs, as expected for steel-concrete composite frames. This hints that: i) the influence of higher modes associated with higher spectral ordinates can be significant; and ii) vertical loads tend to govern design because composite MRFs are required to resist lower base shears.

Table 3.1. Dynamic properties.

Mode	T (s)	Description
1	2.45	Translational in the MRF direction
2	1.02	Torsional
3	0.67	Translational in the MRF direction
4	0.43	Translational in the shear wall direction

3.4 Seismic performance and fragility functions

3.4.1 Selection of ground motions, intensity measures and engineering demand parameters

Near-field and far-field earthquake ground motion records were considered in this manuscript. The effect of directivity is more significant in near-field ground motions because the two horizontal components, i.e. fault-parallel and fault-normal, may exhibit quite

different shaking; whereas this effect is evened out at large distance from the epicentre [Yun, 2002]. The ground motions were selected using the magnitude-distance bin approach as explained in Shome and Cornell, 1997. This approach was developed to represent earthquake characteristics that crucially affect the engineering demand on structures by a small set of ground motions. In this study two bins composed of 20 ground motions each, to be used in an MIDA, were obtained from the ITACA Strong Motion Database. They are presented in Table 3.2 and 3.3 and they were carefully selected to represent two specific magnitude and distance scenarios: (i) Near Field (NF) and (ii) Large Magnitude and Large Distance (LMLD). In greater detail, ground motions with distance R<10 km were grouped into the NF bin whilst ground motions with distance R ranging between 30 km and 60 km and magnitude between 4.5 and 6 were classified as the LMLD bin. The ground motions were selected in order to be representative of the Italian territory. The soil was classified as type C according to EN1998-1 [13] and it is consistent with the one used to design the reference structure of Subsection 3.2.1.

Table 3.2. Near field ground motion bin.

Station Code	Event Name	Event ID	M (ML)	R (km)	Station name	Soil	Focal Mechanism*	Duration (s)	PGA (g) x	PGA (g) y	PGA (g) z	Sa(T) (g) x	Sa(T) (g) y	Sa(T) (g) z	PGD (cm) x	PGD (cm) y	PGD (cm) z
AQU	L'Aquila	IT-2009-0009	5.9	2.4	Aquila Castello	C	NF	90.00	0.260	0.308	0.312	0.109	0.137	0.100	3.3	8.1	6.3
AQU	L'Aquila	IT-2009-0102	5.4	8.9	Aquila Castello	C	NF	80.00	0.062	0.072	0.027	0.024	0.008	0.007	1.1	0.5	0.3
CLC	App. Umbro Marchigiano	IT-1997-0091	5.4	3.5	Colfiorito Casermette	C	NF	19.99	0.184	0.228	0.203	0.008	0.015	0.004	0.8	1.2	0.4
FIVI	NoName	IT-2013-0005	5.2	9.6	Fivizzano	C	NF	276.51	0.141	0.117	0.149	0.011	0.005	0.010	0.7	0.6	0.8
MI02	L'Aquila	IT-2009-0102	5.4	5.8	Paganica	C	NF	74.99	0.161	0.209	0.083	0.015	0.009	0.005	0.9	0.9	0.3
MIR01	Emilia 2nd	IT-2012-0011	5.8	1.4	Medolla	C	TF	150.00	0.419	0.380	0.369	0.201	0.399	0.077	8.3	21.0	5.1
MIR02	Emilia 2nd	IT-2012-0011	5.8	4.1	Mirandola	C	TF	150.00	0.217	0.237	0.461	0.299	0.390	0.057	12.0	15.5	5.1
MIR03	Emilia 2nd	IT-2012-0011	5.8	9.8	Quarantoli 1	C	TF	90.00	0.208	0.329	0.007	0.093	0.131	0.031	3.8	7.5	2.6
MIR08	Emilia 2nd	IT-2012-0011	5.8	7.3	Quarantoli 2	C	TF	170.00	0.223	0.248	0.313	0.144	0.302	0.108	3.4	10.0	4.2
MRN	Emilia 2nd	IT-2012-0011	5.8	4.1	Mirandola	C	TF	100.00	0.222	0.294	0.857	0.152	0.319	0.041	9.2	14.2	5.8
MRN	Emilia A.S.	IT-2012-0010	5.5	5.1	Mirandola	C	TF	119.85	0.134	0.202	0.127	0.017	0.018	0.006	1.4	1.2	0.4
MRN	NoName	IT-2012-0032	5.2	10.0	Mirandola	C	TF	82.85	0.257	0.218	0.115	0.009	0.011	0.003	0.7	0.7	0.2
NCB	App. Umbro Marchigiano	IT-1997-0091	5.4	9.6	Nocera Umbra Bisc.	C	NF	25.60	0.370	0.278	0.112	0.012	0.011	0.0125	1.3	0.7	1.1
SANO	Emilia 2nd	IT-2012-0011	5.8	4.7	San Felice sul Panaro	C	TF	170.00	0.175	0.220	0.314	0.215	0.264	0.045	7.7	10.7	3.0
T0802	Emilia 2nd	IT-2012-0011	5.8	8.0	T0802	C	TF	70.00	0.260	0.294	0.178	0.168	0.130	0.043	6.8	7.4	1.9
T0813	Emilia 2nd	IT-2012-0011	5.8	9.4	T0813	C	TF	150.00	0.368	0.338	0.174	0.163	0.125	0.044	5.6	5.8	2.1
T0814	NoName	IT-2012-0032	5.2	9.7	T0814	C	-	70.00	0.197	0.093	0.128	0.014	0.022	0.018	08	1.6	0.4
T0818	Emilia A.S.	IT-2012-0010	5.3	5.5	T0818	C	TF	100.00	0.113	0.161	0.103	0.021	0.092	0.056	1.6	2.5	0.9
T0819	Emilia A.S.	IT-2012-0010	5.3	8.6	Novi di Modena	C	TF	60.00	0.259	0.252	0.374	0.128	0.214	0.022	8.8	11.8	2.2
T0819	NoName	IT-2012-0032	5.2	3.9	Novi di Modena	C	TF	70.00	0.118	0.145	0.084	0.011	0.006	0.004	0.9	0.6	0.2

*normal faulting, NF; strike-slip SS; thrust faulting TF; unknown stress regime U

Table 3.3. Large magnitude large distance ground motion bin.

Station Code	Event Name	Event ID	M (ML)	R (km)	Station name	Soil	Focal Mechanism*	Duration (s)	PGA (g) x	PGA (g) y	PGA (g) z	Sa(T) (g) x	Sa(T) (g) y	Sa(T) (g) z	PGD (cm) x	PGD (cm) y	PGD (cm) z
AVZ	L'Aquila	IT-2009-009	5.9	34.9	Avezzano	C	TF	120	0.056	0.067	0.027	0.087	0.034	0.040	3.41	1.6	1.6
CDR	Friuli	IT-1976-0030	6.0	40.7	Codroipo	C	TF	29.6	0.030	0.039	0.011	0.020	0.021	0.034	1.2	0.7	0.8
GBP	Umbria-Marche	IT-1997-0006	5.8	38.4	Gubbio-Piana	C	NF	100	0.097	0.095	0.011	0.244	0.153	0.166	5.9	5.0	4.0
GBP	Umbro-Marchegiano	IT-1997-0091	5.4	38.6	Gubbio-Piana	C	NF	72.95	0.105	0.125	0.080	0.044	0.026	0.018	1.4	1.7	0.6
GBP	Umbro-Marchegiano	IT-1997-0062	5.0	37.2	Gubbio-Piana	C	NF	72.94	0.047	0.050	0.023	0.220	0.030	0.013	0.6	0.6	0.3
GBP	Umbria-Marche	IT-1997-0004	5.6	40.6	Gubbio-Piana	C	NF	75.49	0.034	0.034	0.017	0.031	0.036	0.023	0.9	1.0	0.7
GRG1	Val Comino	IT-1984-004	5.9	49.1	Garigliano	C	NF	26.09	0.061	0.060	0.017	0.017	0.010	0.015	1.0	1.1	0.6
GRM	Potenza	IT-1990-0001	5.2	36.7	Grumento Nova	C	SS	33.33	0.029	0.028	0.016	0.018	0.011	0.011	0.5	0.3	0.1
LNS	Umbria-Marche	IT-1997-0137	5.5	40.7	Leonessa	C	NF	34.92	0.044	0.038	0.022	0.007	0.005	0.004	0.1	0.2	0.1
GRG2	Val Comino	IT-1984-004	5.9	49.1	Garigliano	C	NF	26.19	0.058	0.059	0.016	0.003	0.003	0.002	0.9	1.0	0.4
LNS	Umbria-Marche	IT-1997-0006	5.8	52.7	Leonessa	C	NF	36.80	0.022	0.033	0.013	0.004	0.003	0.001	0.1	0.1	0.08
LNS	Umbria-Marche	IT-1997-0004	5.6	51.4	Leonessa	C	NF	40.75	0.024	0.027	0.014	0.011	0.004	0.008	0.3	0.2	0.2
LPD1	Val Comino	IT-1984-004	5.9	43.7	Lama dei Peligni	C	NF	44.12	0.077	0.073	0.053	0.014	0.008	0.010	1.3	0.6	1.2
LPD1	Val Comino	IT-1984-005	5.7	35.2	Lama dei Peligni	C	NF	34.26	0.041	0.040	0.22	0.003	0.002	0.002	0.1	0.1	0.1
LNS	Garzano	IT-1995-003	5.4	46.3	Garzano	C	TF	29.37	0.112	0.088	0.034	0.002	0.003	0.001	0.2	0.4	0.1
LSN	Molise 1st	IT-2002-045	5.4	41.8	Lesina	C	SS	43.41	0.059	0.065	0.018	0.005	0.008	0.003	0.1	0.2	0.1
ORT	Val Comino	IT-1984-004	5.9	33.6	Ortuchio	C	NF	37.23	0.087	0.058	0.028	0.006	0.009	0.007	0.3	0.7	0.3
PLL	Ferruzzano	IT-1978-0002	5.3	46.8	Pellaro	C	NF	19.14	0.042	0.036	0.021	0.003	0.005	0.003	0.2	0.3	0.1
SCL	App. Lucano	IT-1998-0103	5.6	34.1	Scalea	C	U	25.16	0.037	0.044	0.017	0.019	0.030	0.013	0.7	1.2	0.5
SUL	L'Aquila	IT-2009-0009	5.9	53.6	Sulmona	C	TF	104.00	0.034	0.028	0.024	0.032	0.033	0.023	1.0	1.2	0.9

*normal faulting: NF; strike-slip SS; thrust faulting TF; unknown stress regime U

The appropriateness of the aforementioned bins was verified by using both attenuation relations of Campbell, 1997, and Sabetta & Pugliese, 1987, in terms of Peak Ground Acceleration (PGA) and Peak Ground Velocity (PGV). In fact, it is well known that attenuation relations allow to obtain value of a seismic parameter (PGA, PGV, etc.) as a function of other seismic parameters, e.g. magnitude and epicentral distance. Moreover, they were selected such that the median spectral shapes and dispersions of the two bins were similar when scaled to a common spectral value, see for reference Grupta and Krawinkler, 2000.

Many different ground motion Intensity Measures (IMs) can be selected to characterise a ground motion for a MIDA (Tothong, 2007, and Luco, 2007b). In this manuscript the spectral acceleration at the first period Sa(T1;5%) and the peak ground displacement (PGD) were employed. The Sa(T1;5%) is commonly used as structure-dependent IM in design practice. The PGD is expected to be an effective structure-independent IM for structures with long vibration periods as the maximum displacement approaches PGD in the long-period range. Due to the dynamic properties of the building described in Section 3.3.3, it was deemed a suitable IM.

The employed Engineering Demand Parameter (EDP) was the maximum interstorey drift ratio, defined as the ratio between the horizontal relative displacement between two consecutive storeys and the storey height. It is a widely recognised EDP in design practice to represent both damage and collapse limit states of civil structural systems such as buildings and bridges (EN1998-1, 2004, and FEMA-356, 2000).

3.4.2 Seismic performance of the 3D structure

The first step consisted in analysing the seismic response of the 3D structure as a function of the incident angle. This analysis also allowed for understanding if the incidence angle represents a significant parameter to be included in fragility functions. Therefore, before performing MIDA, five accelerograms were randomly selected from the LMLD bin and, a series of nonlinear time-histories analyses was performed by varying the incident angle from 0° to 180°, with steps of 15°. The incident angle was not extended beyond 180° because the lateral-resisting force system depicted in Fig. 3.1a is anti-symmetric in plan. In addition, the horizontal component with higher PGA was applied along the MRF direction corresponding to incident angle equal to 0°. In order to induce significant nonlinearity in the structure to hand, all accelerograms were scaled by a factor of 15. Looking at the dynamic properties of the structural system characterised by long natural periods, see Table 3.1 in Subsection 3.3.3, such a scaling magnitude was foreseeable for exciting the structure in the nonlinear range. This is in line with Tothong and Luco , 2007b, for which scaling earthquake records are often needed because a few rare earthquake events have been recorded by seismometers and are considered in structural assessment/design. As a result, Fig. 3.8 clearly shows that the maximum interstorey drift is not attained at the same incident angle and, in particular, not always at angles 0° or 90°, which correspond to building main horizontal directions. Thus, it confirms that incident angle has a substantial influence on the seismic response of structure

and proves that the proposed analysis of the whole 3D building comprising several lateral-resisting systems in both directions can better characterise its seismic behaviour.
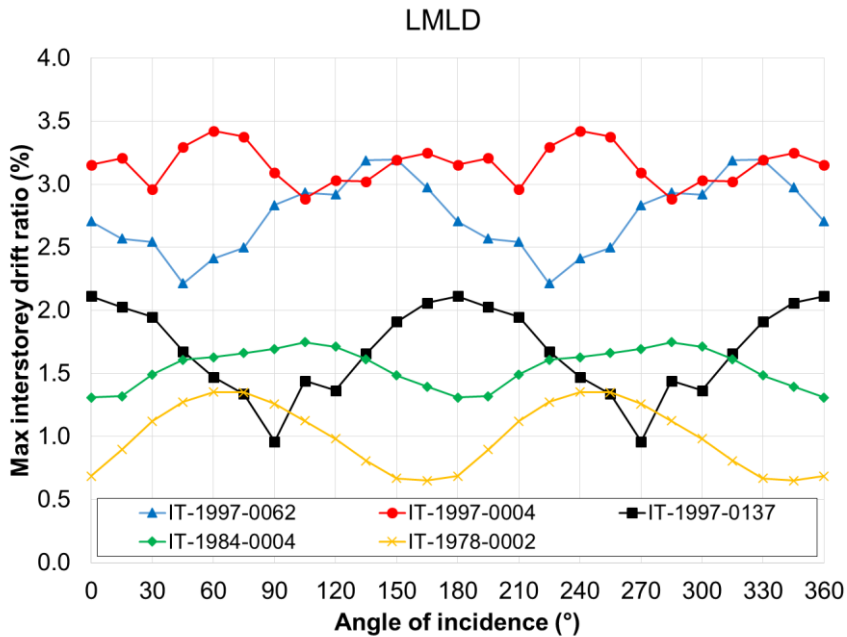
Figure 3.8. Maximum interstorey drift ratio as a function of incidence angle for five LMLD accelerograms scaled by a factor of 15.

3.4.3 Probabilistic seismic demand analysis through MIDA

In order to obtain a meaningful sample of seismic actions that includes the incidence angle at several levels of IMs, the PSDA was preceded by the association of random incident angles with accelerogram triplets. In this respect, firstly we assumed that the two input parameters, i.e. the incidence angle and the accelerogram triplet, behave as independent variables. Then, for each bin, we adopted the LHS method considering a continuous uniform probability distribution of the incident angle. Likewise, we considered each bin of accelerograms as a discrete uniform probability distribution composed of 20 elements. The goal was to create a meaningful sample of the bivariate distribution based on both incident angles and earthquake ground motions, both of them taken with their own probability distribution. The generated output was a set of 100 sets of seismic records and the relevant number of analyses was reckoned sufficient based on Lagaros, 2010a and 2010b.

The earthquake records were scaled up at different intensity levels based on the spectral acceleration at the first period with 5% equivalent damping ratio. Scaling factors were applied so as either to achieve maximum interstorey drift ratio of 5% (Pucinotti et al., 2010 and FEMA-356, 2000) which can be conventionally associated with a collapse limit state (CLS), or to experience numerical divergence. If the numerical collapse was exhibited before attaining 5%, the results given by such EDP-IM pairs were excluded. Such an occurrence happened for only four records out of hundred for each bin. The results of the MIDA are

95

presented in Fig. 3.9 where the 16%, 50% and 84% percentile are highlighted. From Fig. 3.9 an attentive reader can clearly observe that the dispersion associated to PGD is lower. This trend hints that the PGD-interstorey drift ratio pair be more efficient than the spectral acceleration Sa(T1;5%).

(a)

7

(b)

(c)

(d)
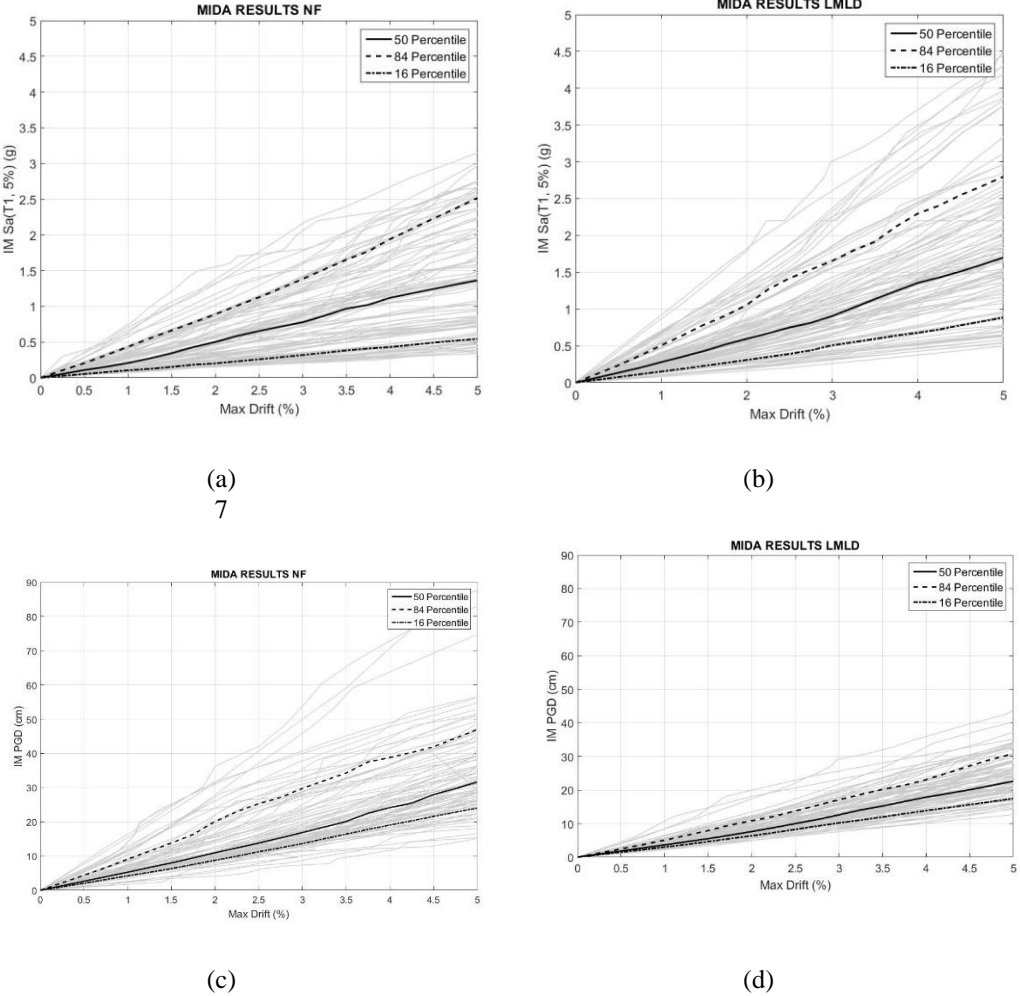
Figure 3.9. MIDA curves for each earthquake record set and according to different IMs: a) NF-Sa(T1;5%); b) LMLD- Sa(T1;5%); c) NF-PGD; d) LMLD-PGD.

As a result, the MIDA allowed to determine fragility functions for two specific limit states: i) DLS corresponding to an interstorey drift ratio equal to 1% as defined in EN1998-1, 2004, and adopted in Pucinotti et al, 2010; CLS with an interstorey drift ratio equal to 5% (Pucinotti et al., 2010 and FEMA-356, 2000). The main underlying assumption was a lognormal distribution of the IM-EDP pair. In fact, EDP data were assumed to obey to a lognormal distribution when conditioned on IM. Therefore, the conditional mean of EDP given IM was linear in a log-log plane and the conditional dispersion of EDP given IM was assumed constant. The fragility functions related to the different limit states were computed by means

of the lognormal cumulative probability function as reported in Eq. 3.1. The maximum log-likelihood method, see Eq. 3.2 as in Baker, 2015, was applied to estimate the parameters distribution, collected in Table 3.4.

$$P\left(C \mid IM = x\right) = \phi\left(\frac{lnx - \mu}{\sigma}\right) \tag{3.1}$$

$$\{\hat{\mu}, \hat{\sigma}\} = max_{\mu,\sigma} \sum_{i=1}^{m} \left\{ ln\binom{n_i}{z_i} + z_i ln\phi\left(\frac{lnx - \mu}{\sigma}\right) + \left(n_i - z_i\right) ln\left(1 - \phi\left(\frac{lnx - \mu}{\sigma}\right)\right) \right\} \tag{3.2}$$

Where n represents the number of input accelerograms, z the limit state exceedances, m the number of the IM values. As anticipated, Table 3.4 confirms that the PGD-interstorey drift ratio represents a more efficient EDP-IM pair because the dispersion is about 0.3-0.4 for both sets. In fact, the structure is characterised by fairly long periods and the spectral acceleration Sa(T1;5%) is less efficient in representing the demand model of flexible structures.

Table 3.4. IMs lognormal distribution parameters for both DLS and CLS

Limit State DLS (1% drift)	Sa(T$_1$;5%)		PGD	
NF	$\hat{\mu}$	$\hat{\sigma}$	$\hat{\mu}$	$\hat{\sigma}$
	-1.26	0.588	1.98	0.448
LMLD	$\hat{\mu}$	$\hat{\sigma}$	$\hat{\mu}$	$\hat{\sigma}$
	-0.96	0.504	1.65	0.332
Limit State CLS (5% drift)	Sa(T$_1$;5%)		PGD	
NF	$\hat{\mu}$	$\hat{\sigma}$	$\hat{\mu}$	$\hat{\sigma}$
	0.24	0.633	3.53	0.346
LMLD	$\hat{\mu}$	$\hat{\sigma}$	$\hat{\mu}$	$\hat{\sigma}$
	0.56	0.516	3.21	0.252

The seismic fragility functions that include incident angle randomness are shown in Fig. 3.10. Firstly, it is worth noting that the probability of exceeding of the assumed limit states given a Sa(T1;5%) value based on NF bin is higher than those of the LMLD bin. This was somehow expected since NF ground motions are generally characterised by higher PGDs compared to LMLD records at the same level of PGA and Sa(T1;5%) (see Table 3.2 and Table 3.3). In addition, due to the structure flexibility high scale factors had to be considered to reach intensity levels of Sa(T1;5%) that caused the exceeding of 5% interstorey drift ratio. Despite the variability of the drift response shown in Fig. 3.8 owing to the incident angle, the obtained probabilistic demand model resulted efficient when the PGD-interstorey drift ratio pair was considered. In sum, the seismic fragility curves depicted in Fig. 3.10, and

especially those related to PGD, can be effectively used in seismic risk assessment of realistic steel-concrete composite buildings or in a fully probabilistic PBEE analysis.
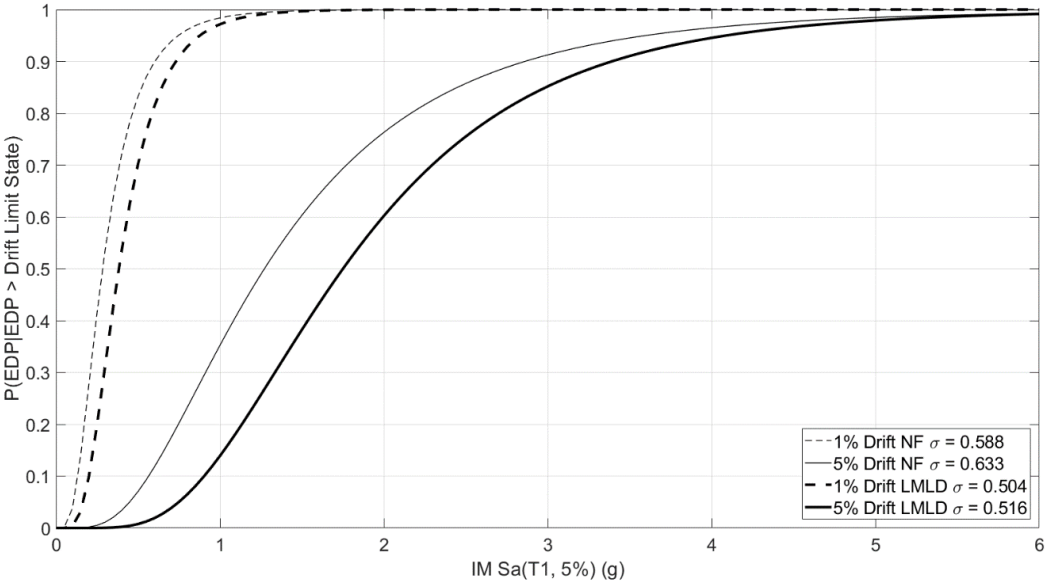
(a)
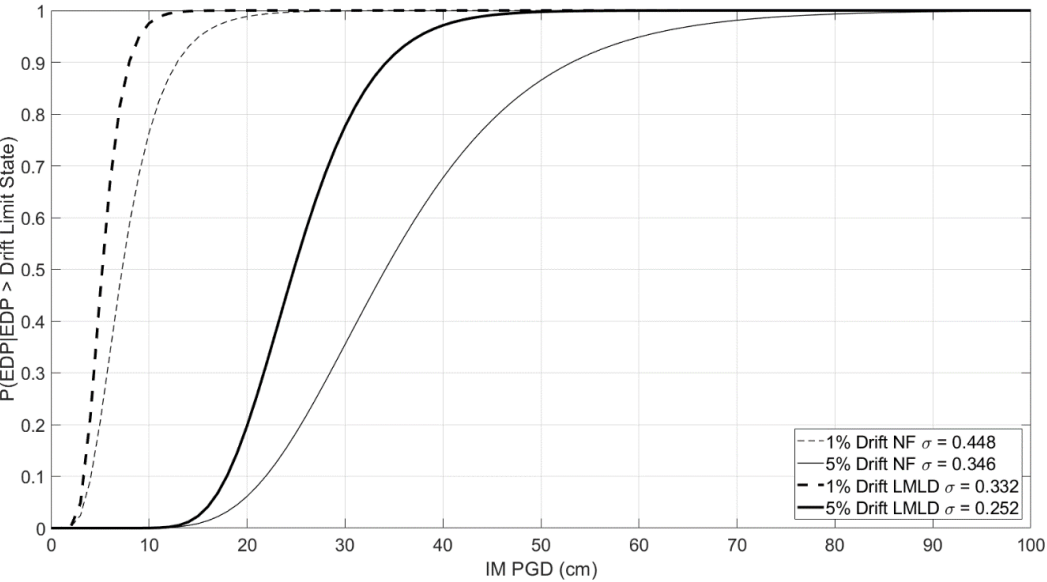
(b)

Figure 3.10. Fragility functions in terms of the probability of exceeding a drift limit state for different sets of ground motions and IMs: a) Sa(T$_1$;5%); b) PGD

3.5 Conclusions

The manuscript has presented a probabilistic seismic demand analysis of a 3D structure representative of a realistic office building made of a newly-conceived high strength steel moment resisting frame in one direction and concrete shear walls in the other main direction. In particular, the seismic performance of the whole structure was investigated by means of a nonlinear FE model set in OpenSEES and calibrated on experimental data. Time-history nonlinear dynamic analyses showed that the earthquake incidence angle significantly influenced the dynamic response in terms of maximum interstorey drift ratio. In fact, drift peaks occurred at different angles highlighting the dynamic complexity of structures characterised by different lateral-force resisting systems. Moreover, a probabilistic seismic demand analysis was performed through a multicomponent incremental dynamic analysis that allowed defining seismic fragility functions by including the incident angle randomness for both near source and far field scenarios as well as for two different limit states: damage and collapse. Different intensity measures were employed and the peak ground displacement-interstorey drift ratio pair resulted the more efficient in terms of low dispersion for flexible buildings and included variation of angle of incidence. Near-fault records entailed higher probability of exceedance of a drift limit state in terms of spectral acceleration at the first period $Sa(T1;5\%)$ with respect to LMLD records. This was due to the fact that NF ground motions were in general characterised by higher PGD for approximately the same levels of PGA and $Sa(T1;5\%)$. As a result, the determined fragility function portfolio can be enriched of this structural typology and these fragility curves can be then employed by analysts both in a seismic risk analysis and in a fully probabilistic performance-based earthquake engineering framework to quantify economic losses, including both direct -repair, reconstruction costs, etc.- and indirect costs -downtimes, etc.- .

Summary, conclusions and future perspectives

Summary

In order to prevent the serious consequences of NaTech events, the European directive Seveso-III (Directive 2012/18/EU) explicitly states that safety report for industrial plants involving hazardous substances should report "*detailed description of the possible major-accident scenarios and their probability or the conditions under which they occur*". The methodology of Performance-Based Earthquake Engineering (PBEE) can compute the probability of failure under seismic action and it is generally applied to quantify seismic risk of nuclear power plants. However, this framework is not so commonly adopted for petrochemical plants. This can be explained considering the several challenges that PBEE carries when applied to such facilities, such the high computational resources needed, several sources of uncertainties, the development of capable finite element models and the adoption of reliable experimental data. This thesis presents numerical and experimental methods to cope with the aforementioned issues alongside with their relevant application to realistic case studies.

The first part of the thesis analysed the seismic performance of a liquefied natural gas (LNG, ethylene) terminal, consisting in a series of process facilities connected by pipelines of various sizes, within the Performance-Based Earthquake Engineering (PBEE) framework. Particular attention was paid to component resistance to leakage and loss of containment, even though several different limit states were investigated. The LNG tank, support structures and pipework, including elbows and flanges, were analysed with a detailed 3D finite element model. For this purpose, a novel mechanical model to predict the leakage limit state of generic bolted flange joints (BFJs) was developed. Given the complexity of the FE model of the LNG plant, the Cloud method for probabilistic seismic demand analysis was selected, due to its advantages in terms of consistency in the seismic input and of computational savings. In particular, in order to develop fragility curves of critical components, such as elbows and BFJs, a set of 36 ground motions from a database of historic earthquake accelerations was selected and used for a series of nonlinear time history analyses.

In the second chapter a seismic reliability analysis of a coupled tank-piping system is presented. The novelty of this methodology lies in the implementation of artificial accelerograms, finite element models and experimental hybrid simulations to compute an accurate and fast surrogate meta-model of our coupled system. As the first step, a disaggregation analysis of the seismic hazard is performed to obtain the necessary input for a stochastic ground motion model able to generate synthetic ground motions coherent with the site-specific analysis. Hence, the space of parameters of the stochastic ground motion model is reduced by means of an extensive global sensitivity analysis upon the seismic response of our system, evaluated with a simplified Matlab FEM. Based on the reduced space of parameters, a large set of artificial waveforms is so generated and, among them, a

few signals to provide the input for experimental hybrid simulations are selected. In detail, the hybrid simulator is composed by a numerical substructure, able to predict the seismic sliding response of a steel tank, and a physical substructure made of a realistic piping network. Furthermore, these experimental results are used to calibrate a refined Ansys FEM with a special focus on the most vulnerable components, i.e. pipe bends More precisely, a special attention is given to tensile hoop strains in elbow pipes as a leading cause for leakage, monitoring them with conventional strain. Thus, a numerical Kriging model of the coupled system is evaluated based on both experimental and finite element model results. Finally, a seismic fragility analysis is carried out and, ultimately, the performance of the numerical surrogate model is assessed.

The last part of the thesis provides insight into a probabilistic seismic demand analysis of a steel-concrete composite structure made of a novel type of high-strength steel moment resisting frame, to be used either in a seismic risk assessment or a fully probabilistic PBEE framework. In this respect, the knowledge of seismic fragility function is paramount. Moreover, due to the dynamic complexity of the examined structure caused by irregularity in elevation and different lateral-force resisting systems in the two main directions -moment resisting frames and concrete shear walls- the seismic behaviour is not straightforward to foresee. Therefore, two separate 2D analyses along the building main directions may not suffice to identify the actual dynamic response and, consequently, a 3D comprehensive probabilistic seismic demand analysis was performed by taking into account the earthquake incident angle. In this respect, a nonlinear 3D FE model was developed and calibrated on experimental tests performed on both beam-to-column and column-base joints that formed moment-resisting frames. A multiple incremental dynamic analysis was then performed with two groups of bespoke accelerograms characterized, on one hand, by large magnitude and large distance and, on the other hand, by near-source effects. The earthquake incidence angle was also considered and, to decrease the number of simulations, the accelerogram-incident angle pairs were selected by means of the Latin hypercube sampling (LHS) method. Hence, the seismic fragility functions were built both for damage and collapse limit states considering both the maximum interstorey drift ratio as engineering demand parameter and different intensity measures as well as the incident angle randomness.

Conclusions

The main goal of this thesis is to present some innovative methodology to perform seismic risk evaluation of industrial or petrochemical plants and components. This work is essentially based on both numerical and experimental methods involving an extensive adoption of finite element models. It will appear clear that a significant part of the research activity showed in this thesis has been carried out in order to produce a "Digital Twin", i.e. an integrated multiphysics, multiscale, probabilistic simulator, of the different systems understudy. As predicted by Glaessigen and Stargel, 2012, the paradigm of a "Digital Twin", originally formulated for the aerospace applications, started to provide, in recent years, a significant support to the performance assessment of civil infrastructure and industrial plants. Along this line, the work of Patterson et al, 2015, proposes a framework to apply this

paradigm to nuclear power plants to reduce costs and increase reliability and safety. More recently, the work of Tsay et al., 2018, underline the importance of a "Digital Twin" in the optimization of design process in the petrochemical industry. However, in order to produce a reliable "Digital Twin" of industrial plants and components to be adopted for seismic risk assessment, both the systems response and the relevant seismic action need to be properly predicted. According to this, the thesis presents both finite element modelling based, where possible, on experimental results and the adoption of a seismic ground motion model calibrated to a seismic hazard analysis.

In the first part of the thesis, a probabilistic seismic demand analysis of an LNG plant following the Performance-Based Earthquake Engineering procedure was presented. First, the non-linear response of the whole LNG plant was evaluated. Then, the leakage risk of the most critical components of its pipeline network, i.e. elbows and bolted flange joints, was expressed by means of fragility functions. For this, a mechanical model of bolted flange joints for leakage prediction, was developed and calibrated by monotonic and cyclic joint testing. Regarding the seismic response of LNG plant components, the bolted flange joints were found relatively safe under seismic action, whilst elbows exhibited a significant degree of vulnerability. Due to the complexity of LNG plant and the high computation demand by the FE model, the Cloud method for probabilistic seismic demand analysis was used. With regard to elbow response, it was found that the maximum tensile hoop strain represents a suitable function for fragility analysis. Moreover, it was showed that fragility can be expressed as a function of peak ground acceleration of natural records. Nonetheless, the spectral acceleration evaluated at the period of the tank is more efficient due to the lower dispersion involved. The results of fragility functions of elbows, i.e. the probability of leakage over the reference life of the plant of about 1.4×10^{-3}, demonstrates that the examined plant characterized by a reference life of 100 years would be at risk. Therefore, an adequate pipework design for LNG plants subjected to strong earthquakes is needed, especially for piping components on top of tall tanks.

In the second part of the thesis, a rigorous methodology to derive seismic fragility curves for a realistic tank piping system, based on hybrid simulations and synthetic ground motions, is presented. In particular, the chapter focus on loss of containment from vulnerable components of the piping network like pipe bends. As a first step a seismic scenario associated to a geographical site is defined by means of a probabilistic seismic hazard analysis. Then, based on this analysis, an adequate seismic input employing a stochastic ground motion model calibrated against coherent natural seismic records, is presented. Moreover, a global sensitivity analysis is carried out to reduce the space parameters of the stochastic model and synthetize a large set of ground motions to be used in both experimental tests and finite element simulations. Besides, two different finite element models, a refined high-fidelity and a faster low-fidelity model, are calibrated against both hybrid simulations of the whole system and cycling tests of vulnerable components, i.e. piping tee joints and bolted flange joints. Specifically, the main difference between the two models is represented by the pipe bends implementation. As a matter of fact, while the low-fidelity model encompasses linear equivalent beam to describe piping elbows behaviour, the high-fidelity

model relies on shell elements to replicate pipe bends seismic response. In addition, the chapter presents a procedure to build a hierarchical kriging surrogate model based on hybrid simulations, high and low-fidelity models. As a result, the surrogate model is able to evaluate the seismic response of the coupled system on the basis of the stochastic ground motion model parameters. In the last part of the chapter w a leakage limit state for piping elbows is defined and the methodology to derive fragility curves based on the surrogate model is so presented. Considering the novelty of the approach further investigations are required to assess the performances of the procedure and its reliability.

The last part of this thesis has presented a probabilistic seismic demand analysis of a 3D structure representative of a realistic office building made of a newly-conceived high strength steel moment resisting frame in one direction and concrete shear walls in the other main direction. In particular, the seismic performance of the whole structure was investigated by means of a nonlinear FE model set in OpenSEES and calibrated on experimental data. Time-history nonlinear dynamic analyses showed that the earthquake incidence angle significantly influenced the dynamic response in terms of maximum interstorey drift ratio. In fact, drift peaks occurred at different angles highlighting the dynamic complexity of structures characterised by different lateral-force resisting systems. Moreover, a probabilistic seismic demand analysis was performed through a multicomponent incremental dynamic analysis that allowed defining seismic fragility functions by including the incident angle randomness for both near source and far field scenarios as well as for two different limit states: damage and collapse. Different intensity measures were employed and the peak ground displacement-interstorey drift ratio pair resulted the more efficient in terms of low dispersion for flexible buildings and included variation of angle of incidence. Near-fault records entailed higher probability of exceedance of a drift limit state in terms of spectral acceleration at the first period $Sa(T1;5\%)$ with respect to LMLD records. This was due to the fact that NF ground motions were in general characterised by higher PGD for approximately the same levels of PGA and $Sa(T1;5\%)$. As a result, the determined fragility function portfolio can be enriched of this structural typology and these fragility curves can be then employed by analysts both in a seismic risk analysis and in a fully probabilistic performance-based earthquake engineering framework to quantify economic losses, including both direct -repair, reconstruction costs, etc.- and indirect costs -downtimes, etc.-.

Future perspectives

With regard to the first part of the thesis, given the limited number of leakage data of elbows and the two unmodeled pipelines connected to the LNG pump columns, both the effects of uncertainty in leakage thresholds and the correlation among damage levels of critical elbows on fragility functions deserve further investigation. It is worthwhile to notice that methodologies generally adopted in nuclear power plants risk assessment, i.e. common cause failures (CCF) analyses, could be successfully implemented also in this case.

The procedure showed in the second part of the thesis needs to be finalized with the complete evaluation of the Kriging surrogate model. With respect to this, a large set of additional finite elements analyses have to be performed. Moreover, its performances must be assessed against standard seismic fragility evaluation methods. Furthermore, the possibility of an extension of the stochastic ground motion model can be investigated

According to the findings of the last part of the thesis, the incidence angle of the seismic action plays an important role in the response of 3D structures that cannot be neglected. In this respect, more structures should be investigated in order to better quantify the uncertainty in the seismic response evaluation associated to the incidence angle.

Bibliography

Abbiati G, Marelli S., Bursi O.S., Sudret B., Stojadinovic B., 2015 Uncertainty propagation and global sensitivity analysis in hybrid simulation using polynomial chaos expansion. The 15th International Conference on Civil, Structural and Environmental Engineering Computing CIVIL-SOFT-COMP (CSC2015) Prague, Czech Republic 1-4 September (2015), ISSN: 17593433, 2-s2.0-84966359045.

Abbiati G., Bursi O. S., Caracoglia L., di Filippo R., La Salandra V., 2016. Probabilistic Seismic Response of Coupled Tank-Piping Systems. Proceedings of the ASME 2016 Pressure Vessels & Piping Conference. PVP 2016, Vancouver, British Columbia, Canada, July 17-21, 2016.

Abbiati, Giuseppe, La Salandra, Vincenzo, Bursi Oreste S., & Caracoglia, Luca., 2018a. A composite experimental dynamic substructuring method based on partitioned algorithms and localized Lagrange multipliers. Mechanical Systems and Signal Processing. 100. 85-112. 10.1016/j.ymssp.2017.07.020.

Abbiati G., Abdallah I., Marelli S., Sudret B. and Stojadinovic B., 2018b, Hierarchical Kriging Surrogate of the Seismic Response of a Steel Piping Network Based on Multi-Fidelity Hybrid and Computational Simulators, Proceedings of the 7th International Conference on Advances in Experimental Structural Engineering (7AESE), September 6-8, EUCENTRE, Pavia, Italy (2018).

ANSYS Mechanical Software by ANSYS, Inc. 2015, Southpointe 2600 ANSYS Drive Canonsburg, PA 15317 USA

Antonioni G., Spadoni G., Cozzani V., 2007. A methodology for the quantitative risk assessment of major accidents triggered by seismic events. Journal of Hazardous Materials 147, 48–59.

ASME. Boiler and Pressure Vessel Code Section VIII. New York, USA: American Society for Mechanical Engineers; 2004.

ASCE, 2005, "Guidelines for the design of buried steel pipe (with addenda through February 2005)." ASCE, USA. 2005.

Athanatopoulou AM. Critical orientation of three seismic components. Eng Struct 2005;27:301–12.

Baesi S., Abdolhamidzadeh B., Hassan R., Hamid M. D., 2013. Application of a multi-plant QRA: A case study investigating the risk impact of the construction of a new plant on an existing chemical plant's risk levels J. Loss Prev. Process Ind., 26 (5), 924-935.

Baker J.W. (2008). "An Introduction to Probabilistic Seismic Hazard Analysis (PSHA)", Version 1.3.

Baker JW, 2015. Efficient Analytical Fragility Function Fitting Using Dynamic Structural Analysis. Earthquake Spectra. Vol. 31, No. 1, pp. 579-599.

Barros da Cunha S., 2016. A review of quantitative risk assessment of onshore pipelines. Journal of Loss Prevention in the Process Industries 44, 282-298.

Bommer, J. J., and Acevedo, A. B. [2004] The use of real earthquake accelerograms as input to dynamic analysis, Journal of Earthquake Engineering 8, Special Issue, 1, pp. 43–91.

Brinnel V., Schaffrath S., Münstermann S., Feldmann M., 2016. Validation of a Concept for Burst Pressure Prediction by Damage Mechanics. Proceedings of the ASME 2016 Pressure Vessels & Piping Conference PVP. PVP2016, Vancouver, British Columbia, Canada, July 17-21, 2016.

Bursi O. S., Reza Md S., Abbiati G., Paolacci F., 2015a. Performance-based earthquake evaluation of a full-scale petrochemical piping system. Journal of Loss Prevention in the Process Industries, 33, pp. 10-22.

Bursi O. S. et al. 2015b, Report on seismic hazard for seismic input selection, Deliverable 1.2, INDUSE-2-SAFETY, Grant No. RFSR-CT-2014-00025.

Bursi et al., 2016a, Report on mechanical characterization of selected steel for cyclic loading and temperature sensitivity, Deliverable 4.1, INDUSE-2-SAFETY, Grant No. RFSR-CT-2014-00025.

Bursi, O. S., Reza S. et al., 2016b, "Component Fragility Evaluation, Seismic Safety Assessment and Design of Petrochemical Plants Under Design-Basis and Beyond-Design-Basis Accident Conditions", Mid-Term Report, INDUSE-2-SAFETY Project, Contr. No: RFS-PR-13056, Research Fund for Coal and Steel.

Bursi, Oreste Salvatore, di Filippo, Rocco, La Salandra, Vincenzo, Pedot, Massimiliano and Reza, Md Shahin, 2018, "Probabilistic seismic analysis of an LNG subplant. Pages 45-60, Risk Analysis in Process Industries: State-of-the-art and the Future, Edited by Genserik Reniers, Ankur Pariyani, Volume 53, Pages 1-148 (May 2018)

Campbell K.W., 1997, Empirical Near-Source attenuation relationships for horizontal and vertica components of peak ground acceleration, peak ground velocity, and pseudo-absolute acceleration response spectra. Seismological Research Letters Vol. 68, n.1, 1997.

Campedel M., Cozzani V., Garcia-Agreda A., Salzano E., 2008. Analysis of major industrial accidents triggered by natural events reported in the principal available chemical accident databases. JRC Scientific and Technical Reports, EUR 23391 EN -2008.

Cozzani V, Antonioni G., Landucci G., Tugnoli A., Bonvicini S., Spadoni G., 2014. Quantitative assessment of domino and NaTech scenarios in complex industrial areas, Journal of Loss Prevention in the Process Industries 28, 10-22

Cornell CA, (1968). "Engineering seismic risk analysis." Bulletin of the Seismological Society of America, 58(5), 1583-1606

Cornell CA, Krawinkler H. 2000. Progress and challenges in seismic performance assessment. PEER Center News, http://peer.berkeley.edu.

Cornell CA, Jalayer, F, Hamburger, R.O, and Foutch, D.A. 2002. Probabilistic Basis for 2000 SAC Federal Emergency Management Agency Steel Moment Frame Guidelines. ASCE Journal of Structural Engineering, 128:4, 526-533.

Cruz A. M., Steinberg L. J., Ana Lisa Vetere-Arellano (2006) Emerging Issues for Natech Disaster Risk Management in Europe, Journal of Risk Research, 9:5, 483-501, DOI: 10.1080/13669870600717657

CSA-Z662-2007, "Canadian standards association. Oil and gas pipeline systems.". Exdale, Ontario, Canada. 2007

Der Kiureghian A. (2005). Non-ergodicity and PEER's framework formula, Earthquake Engng Struct. Dyn. 2005; 34:1643–1652

Der Kiureghian A., Ditlevsen O., 2009. Aleatory or epistemic? Does it matter?, Structural Safety, ISSN: 0167-4730, Vol: 31, Issue: 2, Page: 105-112, 2009.

Directive 2012/18/EU of the European Parliament and of the Council of 4 July 2012 on the control of major-accident hazards involving dangerous substances, amending and subsequently repealing Council Directive 96/82/EC

DNV-OS-F101, 2000, "Submarine Pipeline Systems.". HØvik Norway. 2000 [S].

Ebrahimian H., Jalayer F., Lucchini A., Mollaioli F., Manfredi G., 2015. Preliminary ranking of alternative scalar and vector intensity measures of ground shaking. Bull Earthquake Eng 13, 2805–2840.

ECCS TC1 TWG 1.3. (1986). Recommended testing procedure for assessing the behaviour of structural elements under cyclic loading. Brussels; European Convention for Constructional Steelwork.

Efron, B.; Hastie, T.; Johnstone, I. & Tibshirani, R., 2004, Least angle regression Annals of Statistics, 32, 407-499, 2004.

EN 1990 Eurocode – Basis of structural design. CEN 2002.

EN 1993-1-8. 2005. Eurocode 3: Design of steel structures – Part 1-8: Design of joints.

EN1993-1-8, "Eurocode 3 – Design of steel structures – Part 1-8: Design of joint"; EN 1993-1-8; CEN: Bruxelles, 2007.

EN1993-1-12. Eurocode 3 - Design of steel structures - Part 1-12: Additional rules for the extension of EN 1993 up to steel grades S 700, CEN: Bruxelles, 2007.

EN1994-1-1. Eurocode 4: Design of Composite Steel and Concrete Structures - Part 1-1: General Rules for Buildings, CEN: Bruxelles, 2005.

EN1998-1 2004, "Eurocode 8: Design of structures for earthquake resistance – Part 1: General rules, seismic actions and rules for buildings", CEN, Bruxelles, 2004.

EN 1998-4-8. 2006. Eurocode 8, "Design of steel structures – Part 4-8: Silos, tanks and pipelines.", CEN, Bruxelles, 2006

EN 1591-1. 2009. Flanges and their joints – Design rules for a gasketed circular flange connection – Part 1: Calculation method.

EN 1591-2. 2009. Flanges and their joints – Design rules for a gasketed circular flange connection – Part 2: Gasket parameters.

EN 1473. 2016. Installation and equipment for liquefied natural gas - Design of onshore installations.

Federal Emergency Management Agency, "Hazus®–MH 2.1 - Multi-hazard Loss Estimation Methodology -Earthquake Mode", Department of Homeland Security, Washington DC, 2013

FEMA-356. Prestandard and Commentary for the Seismic Rehabilitation of Buildings. FEMA: Washington, USA, 2000.

Firoozabad E. S., Jeon, B. G., Choi, H. S., & Kim, N. S. 2015. Seismic fragility analysis of seismically isolated nuclear power plants piping system. Nuclear Engineering and Design, 284, 264-279.

Fullwood, Ralph, 1989, "Review of pipe-break probability assessment methods and data for applicability to the advanced neutron source project for Oak Ridge National laboratory.", BNL 52187 (April 1989).

GIE LNG Map, 2015, Gas Infrastructure Europe. www.gie.eu.

Glaessgen, E. H., & Stargel, D. (2012). The digital twin paradigm for future NASA and US air force vehicles. AAIA 53rd Structures, Structural Dynamics, and Materials Conference, Honolulu, Hawaii.

Gorst, N. J. S., J., W. S., Pallett, P. F. & Clark, L. A. (2003): Friction in temporary works. Research report. Shool of Engineering, The University of Birmingham, Health and Safety Executive, Publication no. 071, Birmingham

Gupta, A. and Krawinkler, H,. "Behavior of ductile of SRMFs at various hazard levels," Journal of Structural Engineering, 126(ST1): 98-107, 2000.

Han, Z., Görtz, S. [2012] "Hierarchical Kriging Model for Variable-Fidelity Surrogate Modeling", AIAA Journal, 50(9), pp. 1885–1896.

Hoseyni, S.M., Yousefpour, S., Araei, A.A., Karimi, K., Hoseyni, S.M., 2014. Effects of soil-structure interaction on fragility and seismic risk; a case study of power plant containment. Journal of Loss Prevention in the Process Industries, 32, 276-285.

IAEA, 2009. Evaluation of Seismic Safety for Existing Nuclear Installation. IAEA Safety Guide NS-G-2.13. International Atomic Energy Agency, Vienna.

INDUSE Project, 2009-2012, "Structural safety of industrial steel tanks, pressure vessels and piping systems under strong seismic loading", RFS-CT-2009-00022

Iervolino I.,Maddaloni G., Cosenza E., Eurocode 8 Compliant Real Record Sets for Seismic Analysis of Structures, Journal of Earthquake Engineering, 12:54–90, 2008.

ITACA working group (2016), ITalian ACcelerometric Archive, version 2.1, DOI: 10.13127/ITACA/2.1.

I Y.T., Cheng Te-Lung, 2008. The development of a 3D risk analysis method. Journal of Hazardous Materials, 153, 600–608.

Jalayer F, Cornell CA, 2009. Alternative non-linear demand estimation methods for probability-based seismic assessments. Earthquake Engineering & Structural Dynamics, 38(8), 951-972.

Jaspart J-P., Demonceau J-F., Bursi O.S. et al., "Performance-based approaches for high strength tubular columns and connections under earthquake and fire loadings" Final Report, ATTEL Project, Contr. No: RFSR-CT-2008-00037, Research Fund for Coal and Steel, 2012.

JNES-NUPEC, 2008. Seismic Analysis of Large-Scale Piping Systems for the JNES-NUPEC Ultimate Strength Piping Test Program.

Karamanos S., 2016. Mechanical Behavior of Steel Pipe Bends: An Overview. J. Pressure Vessel Technology 138(4), Paper No: PVT-15-1165; doi: 10.1115/1.4031940.

Korndörfer J., Hoffmeister B., Feldmann M., 2016. Fragility Analysis of Horizontal Pressure Vessels in the Coupled and Uncoupled Case. Proceedings of the ASME 2016 Pressure Vessels & Piping Conference. PVP 2016, Vancouver, British Columbia, Canada, July 17-21, 2016.

Krausmann, E., Cruz, A. M., & Affeltranger, B., 2010. The impact of the 12 May 2008 Wenchuan Earthquake on Industrial Facilities. Journal of Loss Prevention in the Process Industries, 23, 2, 242-248.

La Salandra V.; di Filippo R.; Bursi O. S.; Paolacci F.; Alessandri S., 2016. Cyclic Response of Enhanced Bolted Flange Joints for Piping Systems. Proceedings of the ASME 2016 Pressure Vessels & Piping Conference PVP. PVP2016, Vancouver, British Columbia, Canada, July 17-21, 2016.

Lagaros N.D., "Multicomponent incremental dynamic analysis considering variable incident angle", Structure and Infrastructure Engineering, 6 (1-2), 77-94, 2010a.

Lagaros N.D., "The impact of the earthquake incident angle on the seismic loss estimation". Engineerign Structures, 32, 1577-1589, 2010b.

Lanzano G., de Magistris S. F., Fabbrocino G., Salzano E., 2015. Seismic damage to pipelines in the framework of Na-Tech risk assessment. Journal of Loss Prevention in the Process Industries 33 (2015) 159-172.

Li X., Koseki H., Sam Mannan M., 2015. Case study: Assessment on large scale LPG BLEVEs in the 2011 Tohoku earthquakes. Journal of Loss Prevention in the Process Industries, 35, 257-266.

Li H. and Mackenzie D., 2006. Characterising plastic collapse of pipe bend structures. International Journal of Journal of Pressure Vessels and Piping 83 (2006) 85–95.

Lipscy, Phillip; Kushida, Kenji; Incerti, Trevor (2013). "The Fukushima Disaster and Japan's Nuclear Plant Vulnerability in Comparative Perspective". Environmental Science & Technology. 47 (12): 6082–6088. doi:10.1021/es4004813.

Liu, Bing, Liu, X.J. and Zhang, Hong,2009, "Strain-based design criteria of pipelines.", Journal of Loss Prevention in the Process Industries, 22 (2009): pp. 884-888.

Lopez OA, Chopra AK, Hernandez JJ. "Critical response of structures to multicomponent earthquake excitation". Earthq. Eng. Struct. Dyn. 2000;29: 1759-78.

Lopez OA, Chopra AK, Hernandez JJ. "Evaluation of combination rules for maximum response calculation in multicomponent seismic analysis". Earthq Eng Struct Dyn 2001;30:1379_98.

Lowes L.N., Lehman D.E., Birely A.C., Kuchma D.A., Marley K.P., Hart C.R., Earthquake response of slender planar concrete walls with modern detailing, Engineering Structures, 43, 31-47, 2012.

Luco N, Bazzurro P., 2007a Does amplitude scaling of ground motion records result in biased nonlinear structural drift responses? Earthquake Engineering and Structural Dynamics 2007; 36:1813–1835.

Luco N., Cornell C.A., 2007b, "Structure-Specific Scalar Intensity Measures for Near-Source and Ordinary Earthquake Ground Motions", Earthquake Spectra, 23(2), 357-392, 2007.

Mackie K. and Stojadinović B., 2005. Comparison of Incremental Dynamic, Cloud, and Stripe Methods for Computing Probabilistic Seismic Demand Models. Structures Congress 2005: pp. 1-11.

MacRae GA, Mattheis J. Three-dimensional steel building response to near-fault motions. ASCE J Struct Eng 2000;126(1):117–26.

Malhotra P. K., Wenk. T., Wieland M., 2000. Simple Procedure for Seismic Analysis of Liquid-Storage Tanks. Structural Engineering International, 3/2000, pp. 197-201.

Myers, Andrew T., Deierlin, Gregory and Kanvinde, Amit, 2009, "Testing and probabilistic simulation of ductile fracture initiation in structural steel components and weldments", John A. Blume Earthquake Engineering Center, Stanford University, Report No. 170, May 2009.

Marelli, S. & Sudret, B. UQLab: A Framework for Uncertainty Quantification in Matlab 257 Vulnerability, Uncertainty, and Risk (Proc. 2nd Int. Conf. on Vulnerability, Risk Analysis and Management (ICVRAM2014), Liverpool, United Kingdom), 2014, 2554-2563.

Mander J.B., Priestley M.J.N.,. Park R, 1988, "Theoretical stress-strain model for confined concrete" Journal of Structural Engineering, 114(ST8), 1804–1826, 1988.

MATLAB and Statistics Toolbox Release 2015b, 2015, The MathWorks, Inc., Natick, Massachusetts, United States.

Mazzoni S., F. McKenna, M.H. Scott, G.L. Fenves, "OpenSees Command Language Manual" Pacific Earthquake Engineering Research Center, University of California, Berkeley, 2007.

Mostaghel, N. (1999). "Analytical description of pinching, degrading hysteretic systems." J. Eng. Mech., 125(2), 216,224.

Nie J., DeGrassi G., Hofmayer C., 2008. Seismic Analysis of Large-scale Piping Systems for the JNES-NUPEC Ultimate Strength Piping Test Program. U.S. NRC NUREG/CR-6983, BNL-NUREG-81548-2008.

Norme Tecniche, 2008, "Norme Tecniche per le costruzioni," DM Infrastrutture, 14 January 2008 (in Italian).

Otani et al.,2017, Seismic Qualification Of Piping System By Detailed Inelastic Response Analysis Part 2. A Guideline For Piping Seismic Inelastic Response Analysis. Proceedings of the ASME 2017 Pressure Vessels & Piping Conference PVP. PVP2017, Waikoloa, Hawaii, United States, July 16-20, 2017.

Park H.S., Lee T.H., 2015. Seismic Performance Evaluation of Boil-Off Gas Compressor in LNG Terminal. The Open Civil Engineering Journal, 2015, 9, 557-569.

Patterson Eann A.; Taylor Richard J.; Bankhead Mark, 2016, A framework for an integrated nuclear digital environment, Progress in Nuclear Energy, ISSN: 0149-1970, Vol: 87, Page: 97-103, 2016

PEER, PEER Strong motion Databse, http://ngawest2.berkeley.edu/, Pacific Earthquake Engineering Research Center.

Peng L.C., 1989. Treatment of Support Friction in Pipe Stress Analysis. Design and Analysis of Piping and Components, Vol. 169., Truong, O.N., Goodling, E.C., Bulashak, JR. J. J., Widera, G.E.O., Editors, PVP, ASME.

Pedot M., di Filippo R., Bursi O.S., A Seismic Vulnerability Analysis of a Liquefied Natural Gas Subplant, (2018), Proceedings of the ASME 2018 Pressure Vessels and Piping Conference, PVP2018, July 15-20, 2018, Prague, Czech Republic

Pucinotti R., Bursi O.S., Demonceau J.-F., 2011, "Post-eartquake Fire and Seismic Performance of Welded Steel-concrete Composite Beam-to-column Joints", Journal of Constructional Steel Research; 67(9):1358–1375, 2011.

Pucinotti R., Tondini N., Zanon G., Bursi O.S., 2015, Tests and Model Calibration of High-Strength Steel Tubular Beam-to-Column and Column-Base Composite Joints for Moment-Resisting Structures, Earthquake Engineering & Structural Dynamics, 2015, 44 (2) DOI: 10.1002/eqe.2547.

Rezaeian S., Der Kiureghian A. (2010). Simulation of synthetic ground motions for specified earthquake and site characteristics, Earthquake Engng Struct. Dyn. 2010; 39:1155–1180

Reza M.S., Bursi O.S., Paolacci F., Kumar A., 2014. Enhanced seismic performance of non-standard bolted flange joints for petrochemical piping systems. Journal of Loss Prevention in the Process Industries, pp. 124-136 (vol. 30).

Rigato AB and Median RA, Influence of angle of incidence on seismic demands for inelastic single-storey structures subjected to bi-directional ground motions, Engineering Structures, 29:2593-2601.

Sabetta F., Pugliese A., 1987, Attenuation of peak horizontal acceleration and velocity from Italian strong-motion records, Bull. Seism. Soc. Am. 77, 1491-1513, 1987

Santner, T. J., Williams, B.J., Notz, W.I., [2013] "The design and analysis of computer experiments", Springer Science & Business Media.

Sezen, Halil & Whittaker, Andrew. (2006). Seismic Performance of Industrial Facilities Affected by the 1999 Turkey Earthquake. Journal of Performance of Constructed Facilities - J PERFORM CONSTR FACIL. 20. 28-36. 10.1061/(ASCE)0887-3828(2006)20:1(28).

Singh P.K., Vaze K.K., Kushwaha H.S., Pukazhendi D.M., Seetharaman S., Murthy D.S.R., 2014. Experimental and Analytical Studies on Fatigue Crack Growth and Fracture Behaviour of Carbon Steel Elbows. 20th European Conference on Fracture, June-July 30-04, Trondheim-Norway.

Shome N., Cornell C.A., 1997, "Probabilistic seismic demand analysis of nonlinear structures", Stanford University, Dept. of Civil and Envir. Engineering: Reliability of Marine, Structures No. RMS-35, 1997.

Shome N., Cornell C. A., 1999. Probabilistic seismic demand analysis of nonlinear structures. Reliability of marine structures no. RMS-35, Stanford University, Department of Civil and Environmental Engineering

Skrekas, P. and Giaralis, A. (2013). "Influence of near-fault effects and of incident angle of earthquake waves on the seismic inelastic demands of a typical Jack-Up platform". 14th International Conference: The Jack-Up Platform Design, Construction & Operation, 17 - 18 September 2013, London

Sobol' IM. Sensitivity estimates for nonlinear mathematical models. Math Modeling Comput Exp;1:407–14. 1993.

Sozonov P., Pucinotti R., Tondini N., Bursi O.S., Zanon G., "Probabilistic Seismic Analysis of a Three-Dimensional Steel-Concrete Composite Structure", Proceedings of the Twelfth International Conference on Computational Structures Technology, B.H.V. Topping and P. Iványi, (Editors), Civil-Comp Press, Stirlingshire, Scotland, paper 168, 2014

Steinberg, Laura & Sengul, Hatice & Cruz, Ana. (2008). Natech Risk and Management: An Assessment of the State of the Art. Natural Hazards. 46. 143-152. 10.1007/s11069-007-9205-3.

T.-H. Lee, K.M Mosalam, "Probabilistic Seismic Evaluation of Reinforced Concrete Structural Components and Systems, Pacific Earthquake Engineering Research Center", PEER, Report n. 2006/04.

Taucer F., Spacone E., Filippou F.C., 1991, "A fiber beam-column element for seismic response analysis of reinforced concrete structures", Report No. 13 UCB/EERC-91/17. Earthquake Engineering Research Center, College of Engineering, University of California, Berkeley, 1991

Tondini N. and Stojadinoivc B., 2012. Probabilistic seismic demand model for curved reinforced concrete bridges. Bulletin of Earthquake Engineering, 10(5):1455-1479, 2012, doi 10.1007/s10518-012-9362-y.

Tondini N, Hoang VL, Demonceau J-F, Franssen J-M. Experimental and numerical investigation of high-strength steel circular columns subjected to fire. Journal of Constructional Steel Research 2013; 80:57–81.

Tondini N., Zanon G., Pucinotti R., di Filippo R., Bursi O.S., Seismic Performance And Fragility Functions Of A 3d Steel-Concrete Composite Structure Made Of High-Strength Steel, (2018), Engineering Structures, Volume 174, 1 November 2018, Pages 373-383.

Tothong P, Luco N, Probabilistic seismic demand analysis using advanced ground motion intensity measures. Earthq Eng Struct Dyn 36:1837–1860, 2007.

Tsay Calvin;.Pattison Richard C; Piana Michael R.; Baldea Michael, 2018 A survey of optimal process design capabilities and practices in the chemical and petrochemical industries, Computers & Chemical Engineering, ISSN: 0098-1354, Vol: 112, Page: 180-189

Vamvatsikos D, Cornell CA, 2004. Applied incremental dynamic analysis. Earthquake Spectra, 20(2), 523-553.

Vathi M., Karamanos S. A., Kapogiannis I. A, Spiliopoulos K. V., 2015. Performance Criteria for Liquid Storage Tanks and Piping Systems Subjected to Seismic Loading, Proceedings of the ASME 2015 Pressure Vessels & Piping Conference. PVP 2015, Boston, Massachusetts, USA, July 19-23, 2015.

Wilson EL, Suharwardy I. A clarification of the orthogonal effects in a three-dimensional seismic analysis. Earthq Spectra 1995;11(4):659–66.

Xie L. ,1998. The effect of multiple crack on the leak-before-break case of pipe. Int. J. Pressure Vessels and Piping. 75, 249-254.

Xiu, D., & Karniadakis, G. E.., 2002, The Wiener--Askey polynomial chaos for stochastic differential equations. SIAM Journal on Scientific Computing, 24(2), 619-644. 2002.

Yang TY, Mohele J, Stojadinovic B, Der Kiuregan A. 2009, Seismic Performance Evaluation of Facilities: Methodology and Implementation. Journal of Structural Engineering, Vol. 135, pp. 1146- 1154.

Young, S., Balluz, L., Malilay, J., 2005, Natural and technologic hazardous material releases during and after natural disasters: a review. Sci. Total Environ. 322, 3-20.

Zerres, H., & Guerout, Y., 2004. Present calculation methods dedicated to bolted flange connections. International Journal of Pressure Vessels and Piping, 81, 211216.